AD-A098 794 BELL HELICOPTER TEXTRON FORT WORTH TX F/G 1/3
FLIGHT TEST EVALUATION OF A NONLINEAR HUB SPRING ON A UH-1H HEL--ETC(U)
APR 81 P J HOLLIFIELD, L W DOOLEY DAAJ02-77-C-0064
UNCLASSIFIED USAAVRADCOM-TR-80-D-27 NL

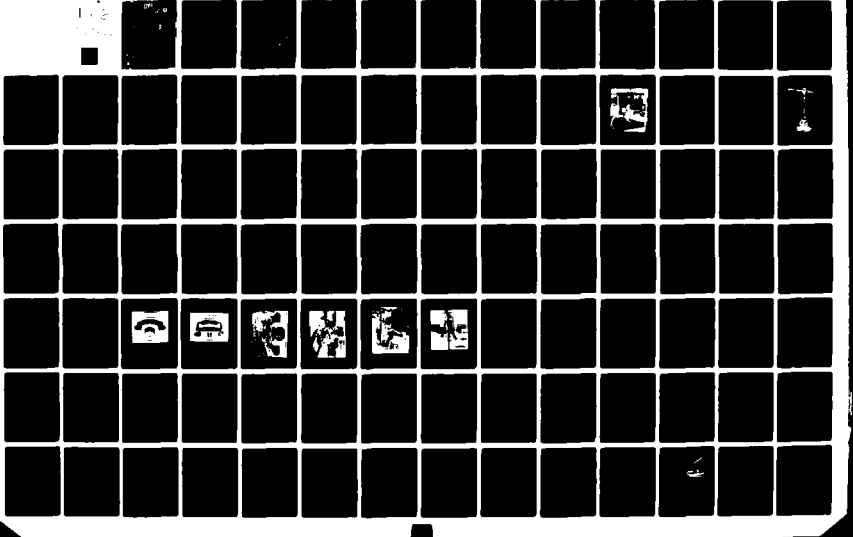

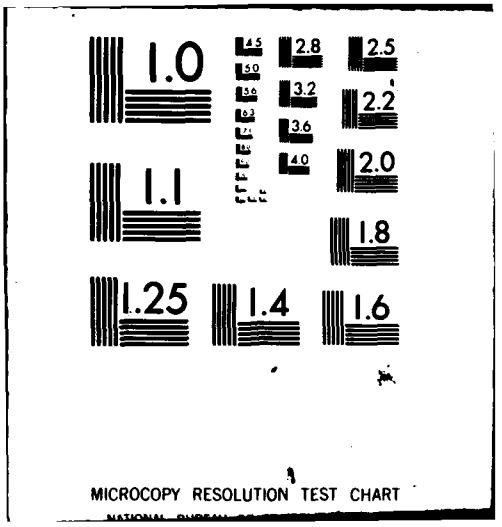
1.0
1.1
1.25
1.4
1.6
1.8
2.0
2.2
2.5
2.8
3.2
3.6
4.0
4.5
5.0
5.6
6.3
MICROCOPY RESOLUTION TEST CHART

LEVEL II

USAAVRADCOM-TR-80-D-27

AD A098794

FLIGHT TEST EVALUATION OF A NONLINEAR HUB SPRING ON A UH-1H HELICOPTER

P. J. Hollifield, L. W. Dooley, J. R. Van Gaasbeek
BELL HELICOPTER TEXTRON
P. O. Box 482
Fort Worth, Texas 76101

April 1981

Final Report

Prepared for

APPLIED TECHNOLOGY LABORATORY
U. S. ARMY RESEARCH AND TECHNOLOGY LABORATORIES (AVRADCOM)
Fort Eustis, Va. 23604

APPLIED TECHNOLOGY LABORATORY POSITION STATEMENT

This report documents the engineering analysis, development, and flight test of a nonlinear hub restraint mechanism for the UH-1H helicopter. The hub restraint consists of an elastomeric spring unit which imparts a restoring moment to the teetering rotor hub when deflected through the flapping angles. In all flight conditions tested the hub spring is shown to reduce the probability of teetering rotor hub contact with the rotor shaft or mast by reducing main rotor flapping.

The results contained in this report effectively support the nonlinear hub spring device as a means to reduce the levels of teetering rotor flapping that could lead to mast bumping and/or airframe blade strikes. The report further identifies a proposed mast design criterion to ensure that mast loads can be sustained and structural deformation made improbable during possible inflight flapping stop contact under operational or material failure conditions which the aircraft could otherwise be reasonably expected to survive.

Mr. G. T. White of the Aeromechanics Technical Area, Aeronautical Technology Division, served as project engineer for this effort.

UNCLASSIFIED

SECURITY CLASSIFICATION OF THIS PAGE (When Data Entered)

REPORT DOCUMENTATION PAGE

READ INSTRUCTIONS BEFORE COMPLETING FORM

(18) (19) 1. REPORT NUMBER: USAAVRADCOM TR-80-D-27

2. GOVT ACCESSION NO.: AD-A098794

3. RECIPIENT'S CATALOG NUMBER:

(6) 4. TITLE (and Subtitle): FLIGHT TEST EVALUATION OF A NONLINEAR HUB SPRING ON A UH-1H HELICOPTER.

(9) 5. TYPE OF REPORT & PERIOD COVERED: Final Report

6. PERFORMING ORG. REPORT NUMBER:

(10) 7. AUTHOR(s): P. J. Hollifield, L. W. Dooley, J. R. Van Gaasbeek, J. D. Honaker, J. Carr

(15) 8. CONTRACT OR GRANT NUMBER(s): DAAJ02-77-C-0064

9. PERFORMING ORGANIZATION NAME AND ADDRESS: Bell Helicopter Textron, P. O. Box 482, Fort Worth, Texas 76101

(16) (17) 10. PROGRAM ELEMENT, PROJECT, TASK AREA & WORK UNIT NUMBERS: 62209A 1L262209AH76 00 217 EK

11. CONTROLLING OFFICE NAME AND ADDRESS: Applied Technology Laboratory, U.S. Army Research & Technology Laboratories (AVRADCOM) Fort Eustis, Virginia 23604

(11) 12. REPORT DATE: April 1981 (12)

13. NUMBER OF PAGES: 158 (159)

14. MONITORING AGENCY NAME & ADDRESS (if different from Controlling Office):

15. SECURITY CLASS. (of this report): Unclassified

15a. DECLASSIFICATION/DOWNGRADING SCHEDULE:

16. DISTRIBUTION STATEMENT (of this Report)

Approved for public release; distribution unlimited.

17. DISTRIBUTION STATEMENT (of the abstract entered in Block 20, if different from Report)

DTIC ELECTE MAY 12 1981 C

18. SUPPLEMENTARY NOTES

19. KEY WORDS (Continue on reverse side if necessary and identify by block number)

Rotor Flapping, UH-1 Helicopter, Nonlinear Hub Spring, Main Rotor Restraint, Mast Loads Simulation, Helicopter Simulation, Flapping Spectrum, Flapping Stop Contact Loads

20. ABSTRACT (Continue on reverse side if necessary and identify by block number)

A nonlinear hub spring design and results of the subsequent flight testing as a concept to provide increased mast bumping safety margin for the UH-1H helicopter is presented. Although there is a need for additional testing, the hub spring is shown to provide an increased margin of safety by reducing main rotor flapping in all conditions tested. → next page

DD FORM 1 JAN 73 1473 EDITION OF 1 NOV 65 IS OBSOLETE

UNCLASSIFIED 054200

SECURITY CLASSIFICATION OF THIS PAGE (When Data Entered)

As a part of this effort, a hybrid computer program was verified as able to predict mast loads due to flapping stop contact. Using this program a parametric study of mast loads as a function of rotor flapping was performed in order to develop a design criteria to ensure that mast loads can be sustained during in-flight flapping stop contact.

In addition, a comparison of the main rotor flapping predicted by the hybrid computer and the digital computer C81 program using elastic blades is shown. Also, an evaluation of U. S. Army helicopter tactics to determine which NOE maneuvers are susceptible to high main rotor flapping is presented.

PREFACE

The work reported herein was performed by Bell Helicopter Textron (BHT) under Contract DAAJ02-77-C-0064, "Proposal for Criteria and Concept for Improved UH-1 Mast Bumping Safety Margin," awarded in September 1977 by the Applied Technology Laboratory (ATL) of the U.S. Army Research and Technology Laboratories (AVRADCOM).

Technical program direction was provided by Mr. G. T. White of the ATL. Principal Bell Helicopter Textron personnel associated with the program were Messrs. P. J. Hollifield, L. W. Dooley, J. R. Van Gaasbeek, J. D. Honaker, J. Carr, K. G. McEntire, and J. P. Norvell.

TABLE OF CONTENTS

TABLE OF CONTENTS (Continued)

TABLE OF CONTENTS (Concluded)

LIST OF ILLUSTRATIONS

LIST OF ILLUSTRATIONS (Continued)

LIST OF ILLUSTRATIONS (Continued)

LIST OF ILLUSTRATIONS (Continued)

LIST OF ILLUSTRATIONS (Concluded)

LIST OF TABLES

1. INTRODUCTION

Since 1972, when a mast bumping problem was identified by the U.S. Army, studies have been conducted to better define the problems of high main rotor flapping, to determine the effects of the operational envelope limits of flapping, and to design and test concepts to improve the mast bumping safety margin of UH-1 helicopters. In 1975, the U.S. Army awarded Bell Helicopter Textron (BHT) a contract (DAAJ02-75-C-0030) to investigate and define rotor blade flapping criteria. During this investigation, computer simulation was used to determine flight conditions, pilot control inputs, and helicopter characteristics influencing main rotor flapping. The findings and recommendations of this investigation are presented in Reference 1. A follow-up contract (DAAJ02-76-C-0043) was awarded to BHT by the U.S. Army in 1976 to study and report on the effect of operational envelope limits on teetering rotor flapping. This study was to verify the accuracy of flapping predictions given by computer simulation, to investigate the effect of operation outside the recommended flight envelope, and to investigate methods of extending this envelope. Reference 2 presents the findings and recommendations of this study. Following the recommendations of Reference 2, a third contract (DAAJ02-77-C-0064) was awarded to BHT by the U.S. Army in 1977. This study would seek to develop criteria and a concept for improving the UH-1 helicopter's mast bumping safety margin. The results of this work are presented in this report.

1.1 OBJECTIVES

The objectives of this contracted study were developed from the results of previous work on the subject of main rotor flapping. These objectives were:

- Verify, by comparison with rotor model tests, the ability to calculate loads due to flapping stop contact.

---

[1]Dooley, L. W., ROTOR BLADE FLAPPING CRITERIA INVESTIGATION, Bell Helicopter Textron, USAAMRDL Technical Report 76-33, Eustis Directorate, U.S. Army Air Mobility Research and Development Laboratory, Fort Eustis, Virginia, December 1976, AD A034459.

[2]Dooley, L. W., and Ferguson, S. W. III, EFFECT OF OPERATIONAL ENVELOPE LIMITS ON TEETERING ROTOR FLAPPING, Bell Helicopter Textron, USARTL Technical Report 78-9, Applied Technology Laboratory, U.S. Army Research and Technology Laboratories, Fort Eustis, Virginia, July 1978, AD A059187.

- Design and procure a nonlinear hub spring for the UH-1 helicopter.

- Formulate a design load criteria for flapping stop contact loads.

- Evaluate elastic rotor effects on flapping predicted by computer simulation.

- Evaluate current U.S. Army Nap-of-the-Earth (NOE) tactics for possible high flapping maneuvers.

- Verify by flight test the UH-1 nonlinear hub spring as a concept to improve the mast bumping safety margin by reducing main rotor flapping and increased flapping-stop-to-mast clearance.

1.2 TECHNICAL APPROACH

In order to define the load generated during flapping stop contact, the BHT rotor/pylon hybrid computer program (ARHM20) was modified and used to investigate the loads on both model and full-scale masts during simulated conditions of in-flight flapping stop contact. In order to obtain flapping and mast contact loads data at simulated flight conditions, aeroelastic model rotor whirl-stand tests were conducted. Correlation between the aeroelastic model rotor and the rotor/pylon hybrid computer program was demonstrated.

After establishing that the hybrid program could adequately correlate measured and predicted mast loads, it was used to conduct a parametric analysis of stiffness parameters in the U.S. Army UH-1H helicopter rotor and pylon system. From this analysis, a design load criterion reflecting inadvertent flapping stop contact was defined.

A nonlinear hub spring was subsequently designed for the UH-1H helicopter rotor system. Design considerations included flapping value for flapping stop snubber engagement, shape of the snubber, shear pad, snubber spring rates, and spring mounting arrangement. A structural analysis of the main rotor mast, hub, and blades, which included moments introduced by the nonlinear hub spring, followed to assure a positive structural margin of safety. After U.S. Government approval, the design was released for competitive procurement.

Prior to defining a flight test plan, the following tasks were accomplished. First, comparisons were made between the hub flapping predicted by the "rigid blade" hybrid version of the Rotorcraft Flight Simulation Computer Program (C81) and the

digital C81 with elastic blades in order to determine the effect of elastic blades on predicted main rotor blade flapping. Also, current Army helicopter tactical instruction manuals were analyzed to determine the impact of these tactics on excessive flapping. Finally, an observation flight in an Army UH-1H helicopter over the nap-of-the-earth course at Fort Rucker, Alabama, was made to determine if any typical UH-1H operational NOE maneuvers are susceptible to high flapping.

A flight test program was then developed that would determine the effectiveness of a nonlinear flapping restraint in improving the UH-1 mast bumping safety margin. The test aircraft was instrumented to measure main rotor mast, hub, and blade loads, handling qualities parameters, and vibration levels.

Results of the mast loads simulation are presented in Section 2, the hub spring design in Section 3, and the design load criteria in Section 4. The effects of the elastic rotor on main rotor hub flapping prediction are presented in Section 5 and the evaluation of NOE tactics in Section 6. The flight test program and the results of that program are presented in Section 7.

2. MAST LOADS SIMULATION

Calculation of mast loads due to rotor flapping stop contact requires a complex simulation model. An existing BHT hybrid computer program (ARHM20) was modified to the necessary degree of sophistication and was subsequently used to compute mast bending moment and transverse shear during flapping stop impact. The modified program (named ARHF01) simulates a helicopter in either hover or forward flight, and consists of elastic rotor, elastic fuselage, and elastic landing gear models, which are dynamically coupled. The models used in the program and an input guide are given in Reference 3.

Modeling Considerations

The rotor model in ARHF01 uses three-quarter radius aerodynamics and a maximum of three rotor elastic modes. The blade-element lift and drag coefficients are functions of angle of attack and are built into the program using limiter circuitry. These two relationships are presented in Figure 1.

Rotor dynamics are accounted for by using a rigid body flapping mode, a coning mode, and an inplane mode. The latter two are represented by a rigid blade articulated at separate, offset, coning, and inplane hinges. The natural frequency of these two modes is computed using the nonrotating frequency and the Southwell coefficient for each mode. All three modes are input as uncoupled modes (i.e., the out-of-plane mode has no inplane deflection) and are coupled in the equations of motion through the aerodynamics and inertia loads. Rotor elastic torsion is ignored. Coupling between the rotor and the pylon structure is also accounted for in the program. Undersling, precone, mast tilt, and δ_3 are included in the rotor model.

Up to six elastic modes can be used to represent the airframe. The airframe modes include five components of displacement at the hub so that coupled rotor-pylon dynamics are modeled (the yaw displacement at the hub is ignored). Mode shape components at selected points in the airframe can also be input so that fuselage vibration can be computed. Control coupling is included as is aerodynamic coupling arising from blade velocity components due to pylon motion. The landing gear modes are dynamically coupled with the airframe, and this model can be used for studying landing dynamics.

---

[3]VanGaasbeek, James R. and Landry, L. Matthew, Jr., HYBRID COMPUTER PROGRAM ARHF02, Technical Data Report 699-099-015, to be published by Bell Helicopter Textron, Fort Worth, Texas.

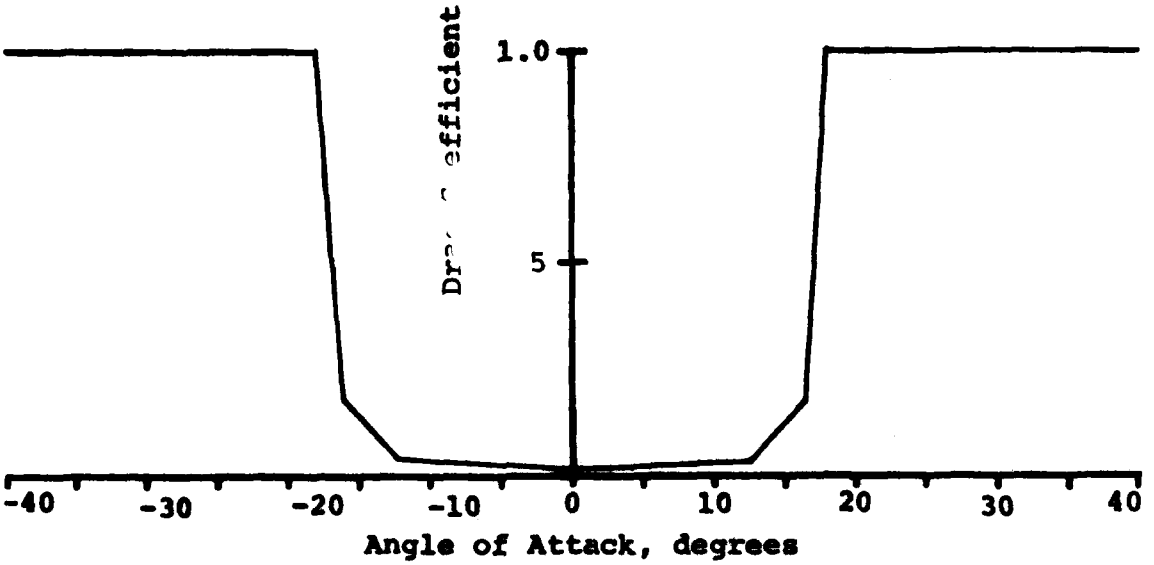

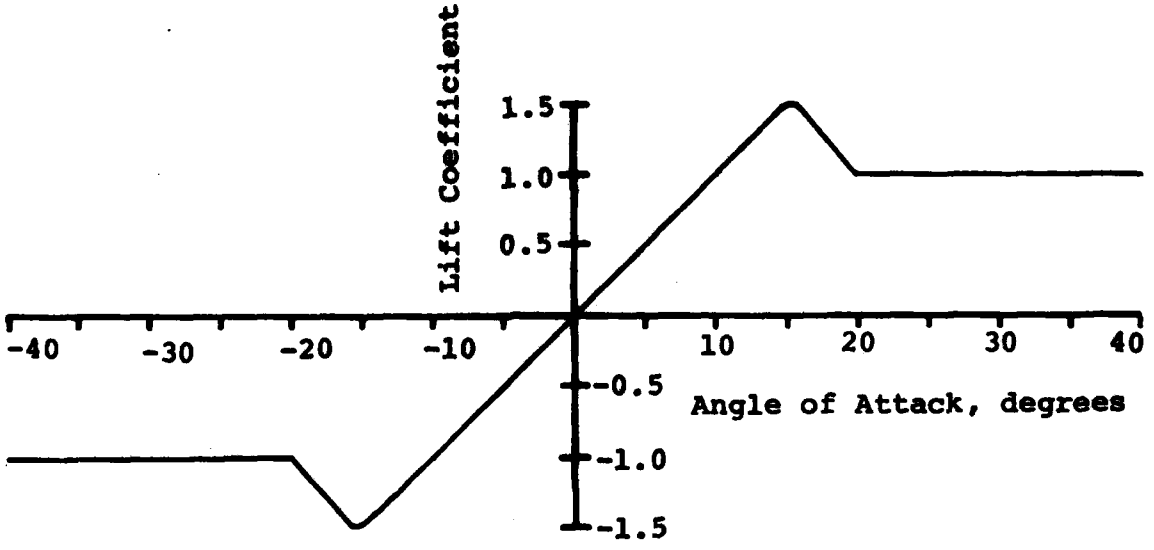

Figure 1. Rotor blade-element aerodynamic coefficients used in ARHF01.

2.1 PROGRAM MODIFICATIONS

Several modifications were made to the ARHM20 program to enhance the simulation model and to facilitate program utilization. In the former category, the ability to calculate mast loads at up to three points was incorporated, and a nonlinear flapping spring model was added. One of the three mast points for load calculations is the flapping stop contact point. The loads are:

$$S = (-H \cos \psi + Y \sin \psi) + \frac{M_{FS}}{XLFS} \tag{1a}$$

$$M = (-H \cos \psi + Y \sin \psi)\,(XLFS) - M_{TOT} - M_{FS} \tag{1b}$$

where S and M are the mast shear and bending moment in the rotating system. H and Y are the hub inplane shears, including inertia loads due to rotor hub accelerations, in the nonrotating system, and M_{TOT} is the externally applied hub flapping moment due to flapping restraint. XLFS is the distance from the teetering axis to the flapping stop contact point.

M_{FS} is the externally applied moment due to the flapping stop contact, which is modeled as a spring that is engaged when β (hub flapping) exceeds β_S (the flapping stop angle). The resulting moment is

$$M_{FS} = K_{FS}\ \beta^* \tag{2a}$$

where

$$\beta^* = \{\beta - \beta_S\}\ \text{sign}\ (\beta), \qquad \beta > \beta_S \tag{2b}$$

$$= 0 \qquad \beta < \beta_S \tag{2c}$$

In this model, the hub actually "penetrates" the mast by having $\beta > \beta_S$. Sign conventions and geometry are given in the following sketch.

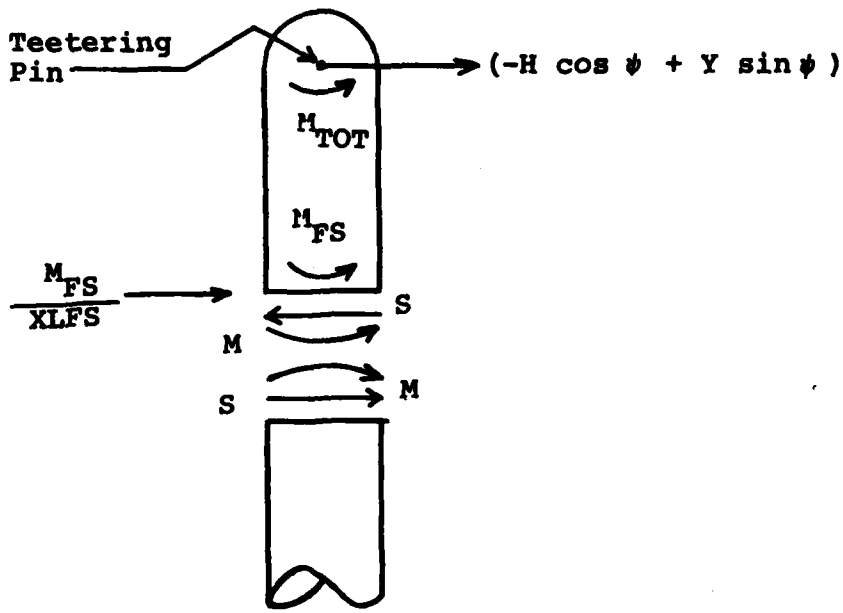

In like manner, the mast moment at any user-selected points below the flapping-stop contact point is computed as

$$M = M_{TOT} + M_{FS} + (-H \cos\psi + Y \sin\psi)\, X \qquad (3)$$

in which M_{TOT} and M_{FS} are as defined for Equations (1a) and (1b), and X is the distance from the teetering axis to the point at which the moment is computed.

The flapping spring model in the ARHF01 program was modified to add a nonlinear spring to the linear spring already in the program. The nonlinear model chosen was that in the digital version of the Rotorcraft Flight Simulation Program C81 (Reference 4). The total flapping spring moment is

$$M_{TOT} = K_L \beta \qquad |\beta| < |\beta_B| \qquad (4a)$$

$$= K_L \beta + K_{NL} (\beta \beta^{r-1} - \beta_B^{\,r}) \qquad |\beta| > |\beta_B| \qquad (4b)$$

---

[4]VanGaasbeek, James R., ROTORCRAFT FLIGHT SIMULATION COMPUTER PROGRAM C81, WITH DATAMAP INTERFACE, Volume I - User's Manual, to be published by the United States Army Research and Technology Laboratories, Applied Technology Laboratory, Fort Eustis, Virginia.

where

K_{NL} is the nonlinear spring rate

β_B is the flapping angle at which the nonlinear spring is engaged

r is the order of the nonlinearity

In addition to these analytical enhancements, the program was modified to improve its ability to run without saturating the analog amplifiers by allowing scaling changes to be made as inputs instead of requiring a recompilation of the FORTRAN program on the digital computer. The program was also modified to permit the user to specify a piecewise-linear or sinusoidal time history of the controls. Lastly, the ARHF01 program was modified to output certain time-history variables on a digital tape for tabulation or CALCOMP plotting at a later time.

2.2 PROGRAM VERIFICATION

A series of whirl-stand tests were conducted with a model rotor to provide data for verification of the ARHF01 program. As the model rotor was assembled from components fabricated for previous test programs, it was not an exact scale model of any particular production rotor. Certain components were modified to attempt to make the model representative of a UH-1-type rotor. The model characteristics are summarized in Table 1. Figure 2 shows the rotor mounted on the test stand.

The model rotor hub is fabricated from aluminum with a beamwise flexure, giving a coning virtual hinge offset of 1.35 inches. Feathering is accomplished through a spindle arrangement on the grip. The blade is constructed of a twisted tapering S-glass spar with the airfoil shape formed by balsa glued to the spar. A fiberglass skin has been applied to the leading edge and segments of music wire are embedded in the leading edge to provide mass balance.

The test stand consists of a focused, sprung pylon with an eight horsepower hydraulic motor and rise-and-fall swashplate. The mast was made from a section of drill rod.

Rotor structural properties were determined either experimentally or analytically. The rotor component masses were determined by weighing a blade and the entire rotor.

Figure 2. Rotor model on test stand.

TABLE 1. MODEL CHARACTERISTICS

Radius, inches	36.0
Rotational speed, rpm	800
Undersling, inches	0.65
Precone, degrees	2.5
Pitch-flap coupling, degrees	0.0
Blade chord, inches	2.62
Twist, degrees	-8, linear
Airfoil	NACA 0012
Coning frequency, per rev	1.06
First inplane frequency, cantilevered, per rev	1.39
Pylon longitudinal frequency, per rev	0.668
Pylon lateral frequency, per rev	0.679
Distance between teetering axis and flapping stop contact point, inches	1.6
Flapping stop angle, degrees	4.5

The mass of the hub plus pitch horn was derived from these measurements and assumed to be uniformly distributed. The hub was subjected to a load deflection test and a beam and chord stiffness were computed from the tests. The blade stiffness distributions were calculated using the dimensions and material properties of the spar and fiberglass nose cap. Due to its very low modulus, the contribution of the balsa to the blade stiffness was neglected. The Rotor Frequency Program DN9100 was used to find the rotor natural frequencies and mode shapes, with the latter used to locate the rotor inplane and virtual hinge location. The out-of-plane virtual hinge location was assumed to be at the center of the flexure, a supposition borne out by load-deflection data.

The pylon natural frequencies were determined by placing a longitudinal accelerometer at the top of the mast, plucking the mast longitudinally, and observing the resulting frequency in the accelerometer trace. An identical test was conducted for the lateral frequency. As only one component of the mode shape was measured, and six were needed for the mathematical model, a NASTRAN model of the pylon was constructed and an eigenvalue analysis performed. The computed frequencies were in good agreement with those measured. The computed mode shapes and measured frequencies were used in the simulation.

A flapping stop was constructed by attaching a machined aluminum block to the mast and attaching a block with setscrews to the rotor hub. The setscrews were adjusted to give a flapping stop angle of 4.5 degrees, and the flapping stop contact point was 1.6 inches below the teetering axis (see Figure 3).

The flapping stop spring rate was determined analytically using the previously constructed NASTRAN model of the pylon. Referring to Figure 4, two opposing shears (S) were applied, one at the teetering axis and one at the flapping stop location, in order to model the couple due to flapping stop impact. The spring rate was computed from the angular deflection (θ) of the shaft at the teetering axis. The resulting spring rate was found to be 71.68 feet-pound/radian.

The rotor hub was instrumented for critical beam and chord bending moments, which were monitored during the test to determine if stress allowables were being exceeded, and a potentiometer was installed to measure hub flapping. Tip-path-plane flapping was recorded on videotape. Strain gages were applied to the mast 2.8 and 11.8 inches below the teetering axis to measure mast bending moments. Pylon longitudinal and

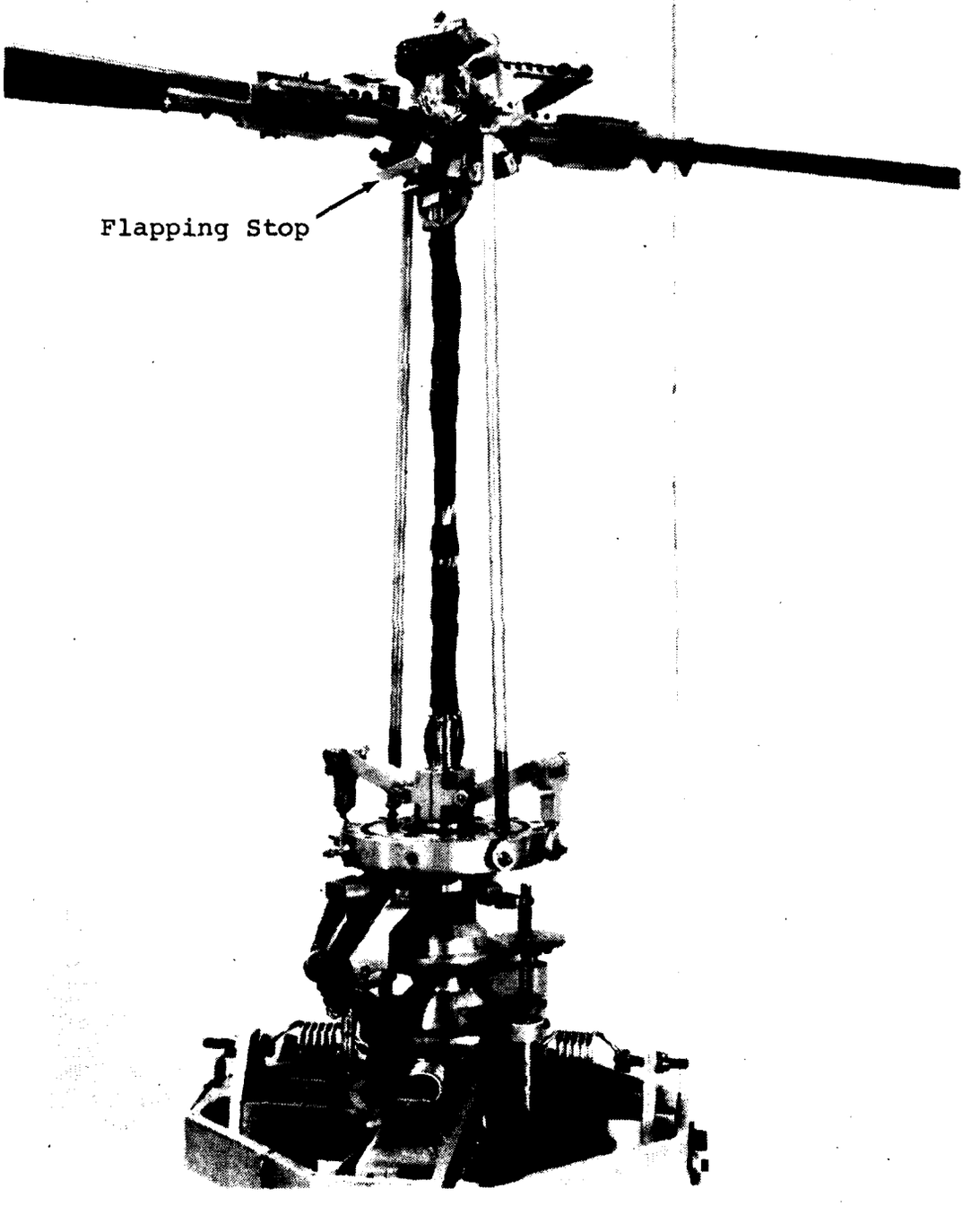

Figure 3. Rotor model and flapping stops.

lateral rocking angles were also measured. All eight quantities were recorded on an oscillograph for runs made at 800 rpm and θ_{75} = 0.0 and 3.0 degrees and values of B_1 (at the hub) between 0 and 8.25 degrees. Several cases of severe flapping stop impact were encountered.

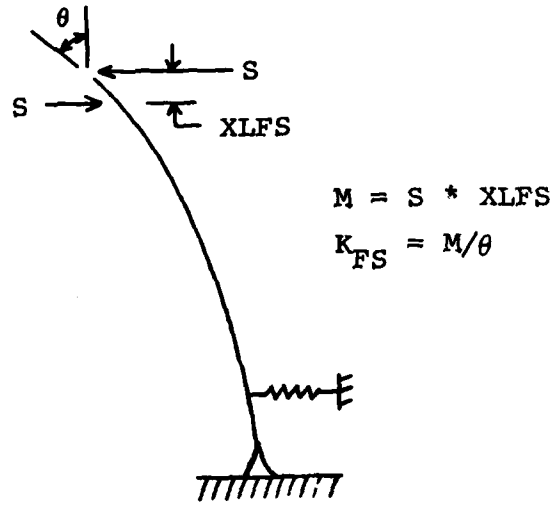

Figure 4. Analytical model for determination of flapping stop spring rate.

Hybrid computer simulations were run for the same cases in order that bending moment and shear time histories could be compared. Figures 5 and 6 present a comparison of the upper mast bending moment time histories for two cases with flapping stop contact. The measured and computed time histories are in good qualitative agreement, with almost identical oscillatory (one-half peak-to-peak) amplitudes. Adjusting the test data for the obvious zero shift (the steady moment should be zero), the measured and computed time histories then agree almost exactly, except for a slight phase difference. (This phase difference may be due to a slight misplacement of the azimuth event instrumentation in the test.) The lack of high frequency content in the computed time history is due to the program's allowance for only the flapping, coning, and first inplane modes, in conjunction with the three-quarter radius aerodynamics.

The predicted and measured overall oscillatory (one-half peak-to-peak) moments are plotted versus rotor cyclic in Figures 7 and 8, again with favorable agreement. The computer program underpredicts the moments at control angles, which result

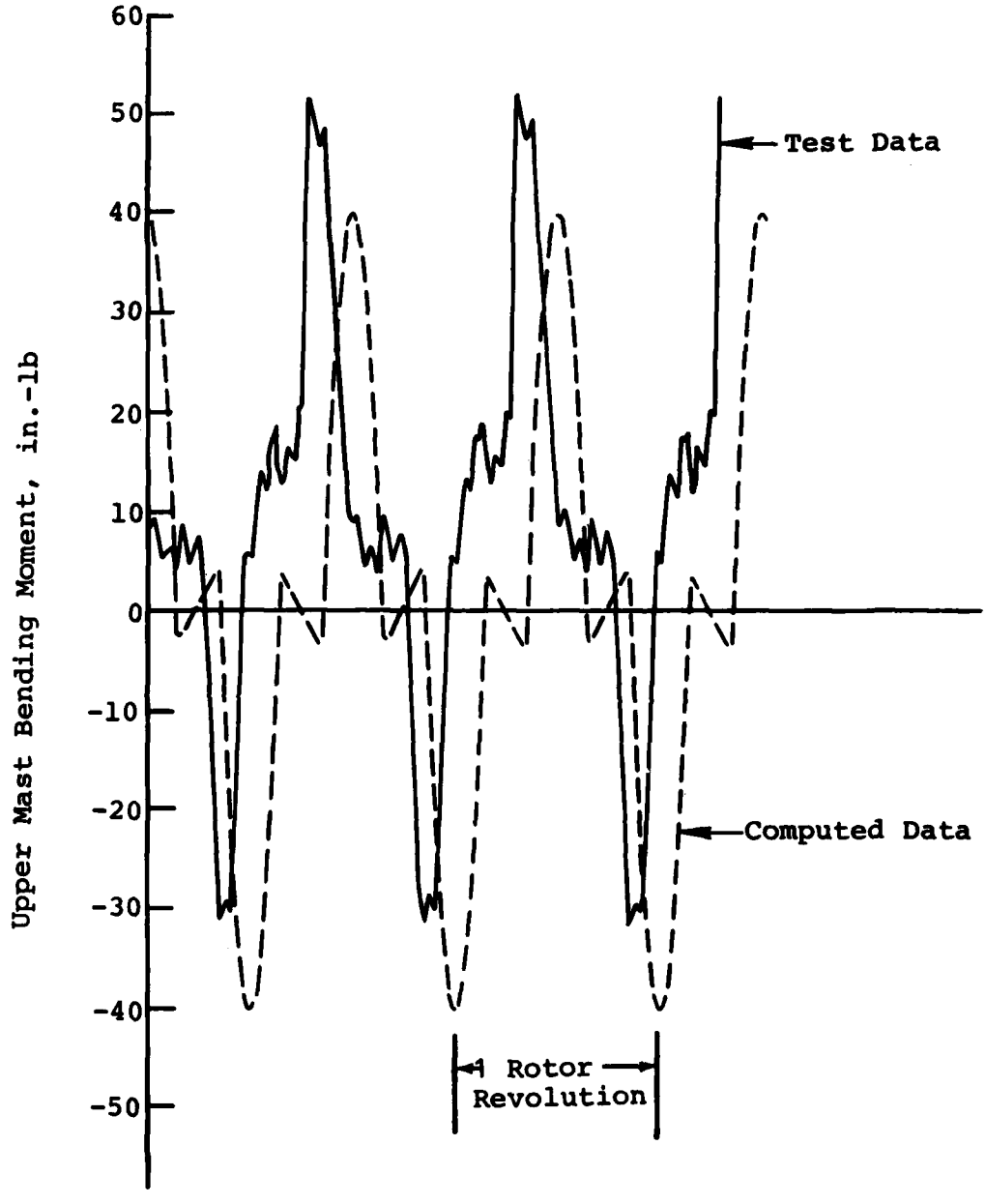

Figure 5. Comparison of measured and computed upper mast bending moment, model rotor, $\theta_{75}=0°$, $B_1=7.5°$.

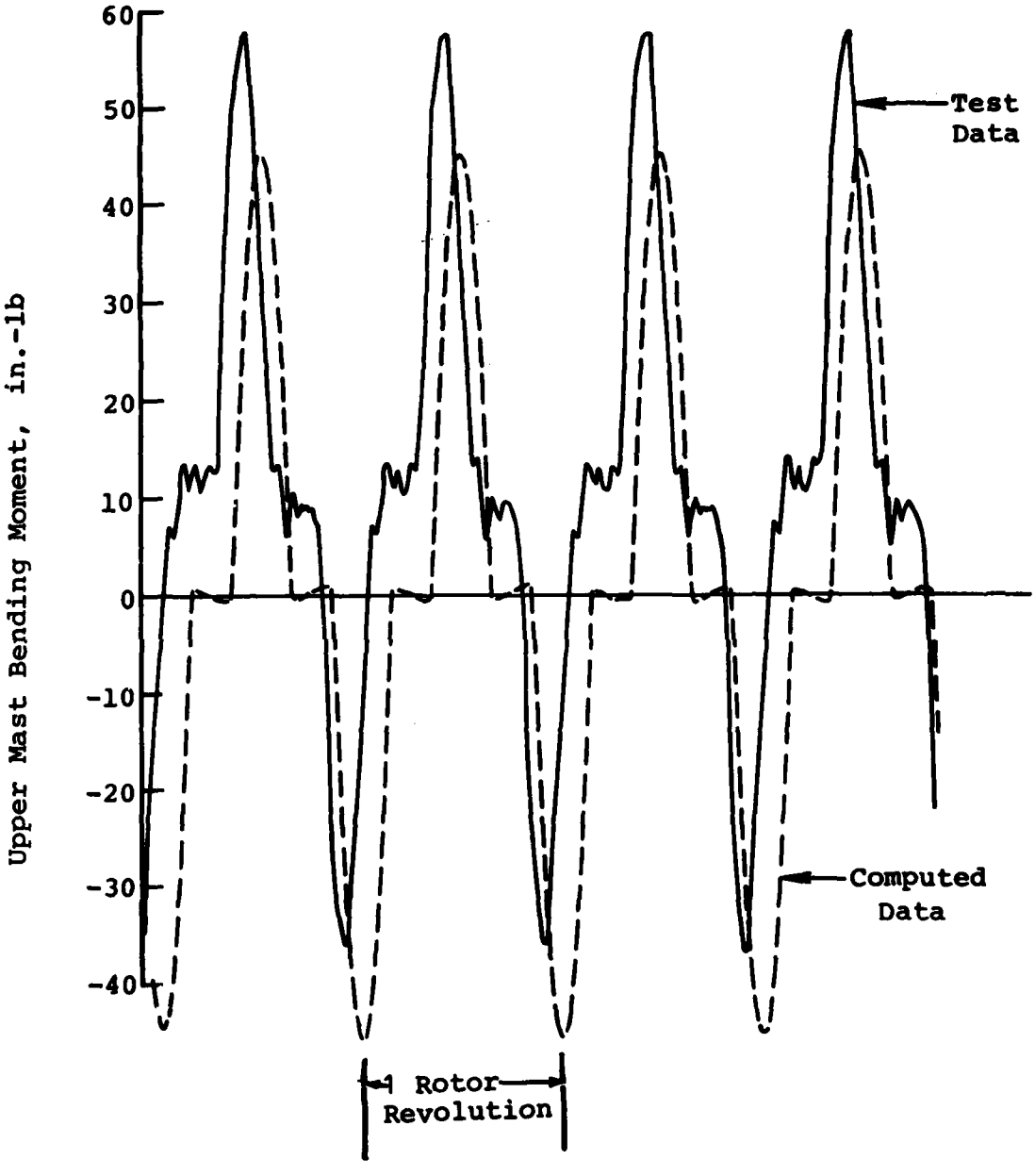

Figure 6. Comparison of measured and computed upper mast bending moment, model rotor, $\theta_{75}=3°$, $B_1=7.5°$.

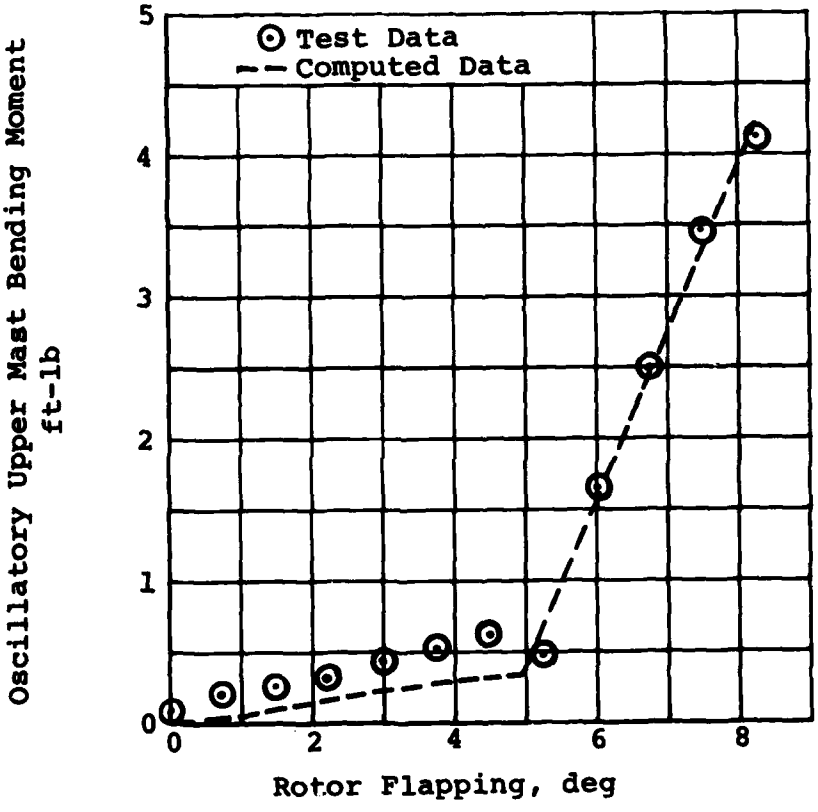

Figure 7. Comparison of measured and computed upper mast bending moment, model rotor, $\theta_{75}=0°$.

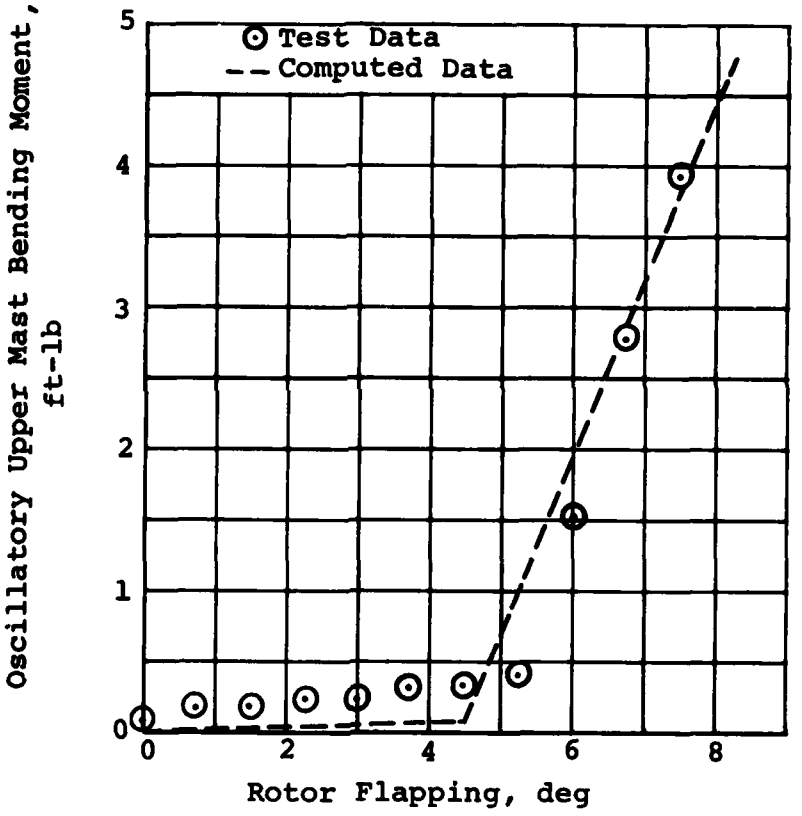

Figure 8. Comparison of measured and computed upper mast bending moment, model rotor, $\theta_{75}=3°$.

in hub flapping angles less than the flapping stop angle. An inspection of Equation (1b) indicates that at these low flapping angles, the only contribution to mast bending is the inplane hub shear, which is not a directly measureable quantity. Apparently, the ARHF01 program is underpredicting these shears. Since the interest in this study is in mast loads during flapping stop impact, it was thought that the data presented in Figures 5 through 8 demonstrate good agreement between theory and test.

2.3 UH-1H SIMULATION

Program verification was followed by a simulation of flapping stop impact for a full-scale UH-1H helicopter. Inputs for the UH-1H were developed and used first to conduct a preflight analytical investigation of mast loads due to flapping stop contact with and without the hub spring. The same inputs were later used for postflight correlation with data recorded during the flight test program.

2.3.1 UH-1H Model

The UH-1H inputs are listed in Table 2, and a detailed input data set listing is shown in Appendix A. The majority of the inputs were derived from the geometric description of the helicopter. A complete twenty-segment structural model of the UH-1H rotor blade was analyzed, using the Rotor Frequency Program DNAM05 (Reference 4, Section 10), to identify virtual hinge locations and natural frequencies. A NASTRAN model of a UH-1N helicopter was modified to yield a model of the UH-1H pylon, which was used to compute pylon frequencies and mode shapes and the flapping stop spring rate (130,000 feet-pound/radian). However, five items in the input data require further explanation.

First, the hub mass is input as zero because the NASTRAN model used to generate the fuselage elastic modes had a point mass at the center of rotation equal to the total rotor mass minus the mass of the blades outboard of the inplane virtual hinge. This ensures that the total rotor mass is properly accounted for in the pylon dynamic response.

Secondly, the coupled inplane natural frequency was checked before data runs were conducted. This test is performed by including only the inplane rotor mode and the pylon modes in the analysis and integrating the equation of motion. The inplane mode is excited impulsively and the coupled natural frequency determined from the transient response. The Southwell coefficient input for the inplane mode (KZEDAP) was set to yield the correct coupled inplane frequency.

TABLE 2. UH-1H CHARACTERISTICS

Radius, feet	24
Rotational speed, rpm	324
Undersling, inches	5.2
Precone, degrees	2.75
Pitch-flap coupling, degrees	0.0
Blade chord, inches	21.0
Twist, degrees	-10, linear
Airfoil	NACA 0012
Coning frequency, per rev	1.17
First inplane frequency, cantilevered, per rev	1.13
Pylon Longitudinal Frequency, per rev	0.594
Pylon lateral frequency, per rev	0.546
Distance between teetering axis and flapping stop contact point, inches	7.3
Flapping stop angle, degrees	11.5

Figure 9 gives the spring rate versus flapping angle for the nonlinear spring, as well as the best curve fit for Equations (4). In the nomenclature of that equation,

K_L = 300 (ft-lb)/deg/rotor

K_{NL} = 0.100 (ft-lb)/deg$^{4.71}$/rotor

β_B = 4 deg

r = 4.71

Fourth, since the landing gear model was not required for this analysis, no data were input for this part of the model. The landing gear data given in the appendix are the default values set by the program. Finally, fuselage aerodynamic data were also unnecessary for the analysis and were not input. The values printed are the internal defaults.

2.3.2 Preflight Simulation

The simulation performed prior to the flight test used this UH-1H model in the form of a rotor mounted on a pylon, without an elastic fuselage. The rotor longitudinal cyclic pitch was varied to compute mast loads for steady conditions at various flapping angles. The rotor was simulated at both 2500 and 8500 pounds thrust, with three levels of flapping restraint - no hub spring, a linear hub spring, and a full nonlinear hub spring. (The linear-spring cases were run with a spring rate of 330 feet-pound/degree/rotor, i.e., the spring rate in the linear range of the nonlinear spring.)

The oscillatory mast bending moment and shear are plotted in Figures 10 through 13 for the six different cases. Comparison of the 2500- and 8500-pound thrust cases show qualitative agreement, but lower mast loads were experienced for the 2500-pound cases because the inplane shear portion of the moment is significantly lower.

As to be expected, increasing the flapping restaint moment, by adding springs, increases the mast loads for a given flapping level. However, the additional control power provided by the spring will tend to reduce the flapping required for a given maneuver, thus alleviating some of this increased load. In addition, if the hub restaint is designed to spread these loads over a much larger bearing surface than that encountered during flapping stop impact with the standard rotor, the shear stresses in the mast will actually be lower.

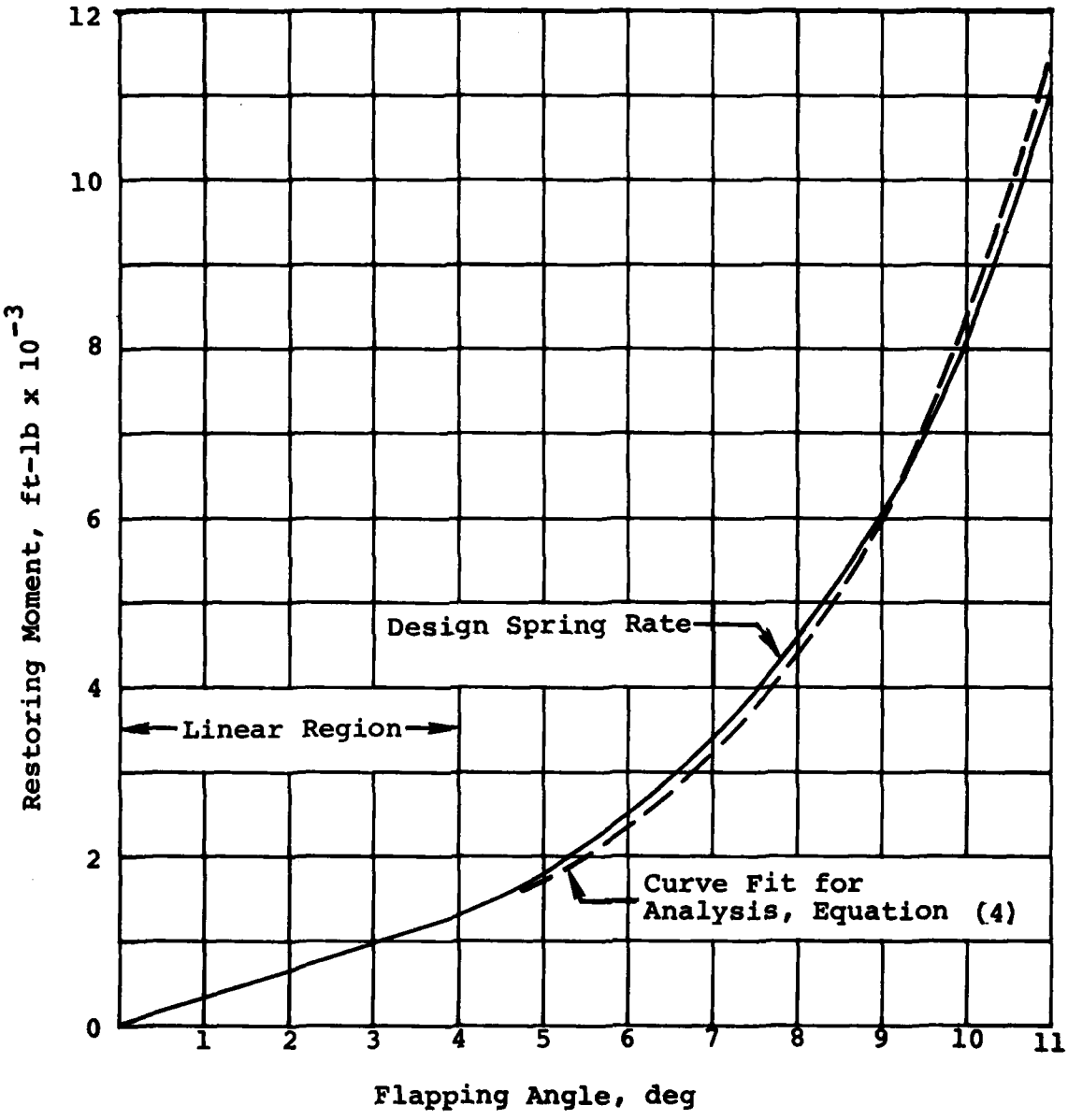

Figure 9. Total hub restoring moment due to hub spring.

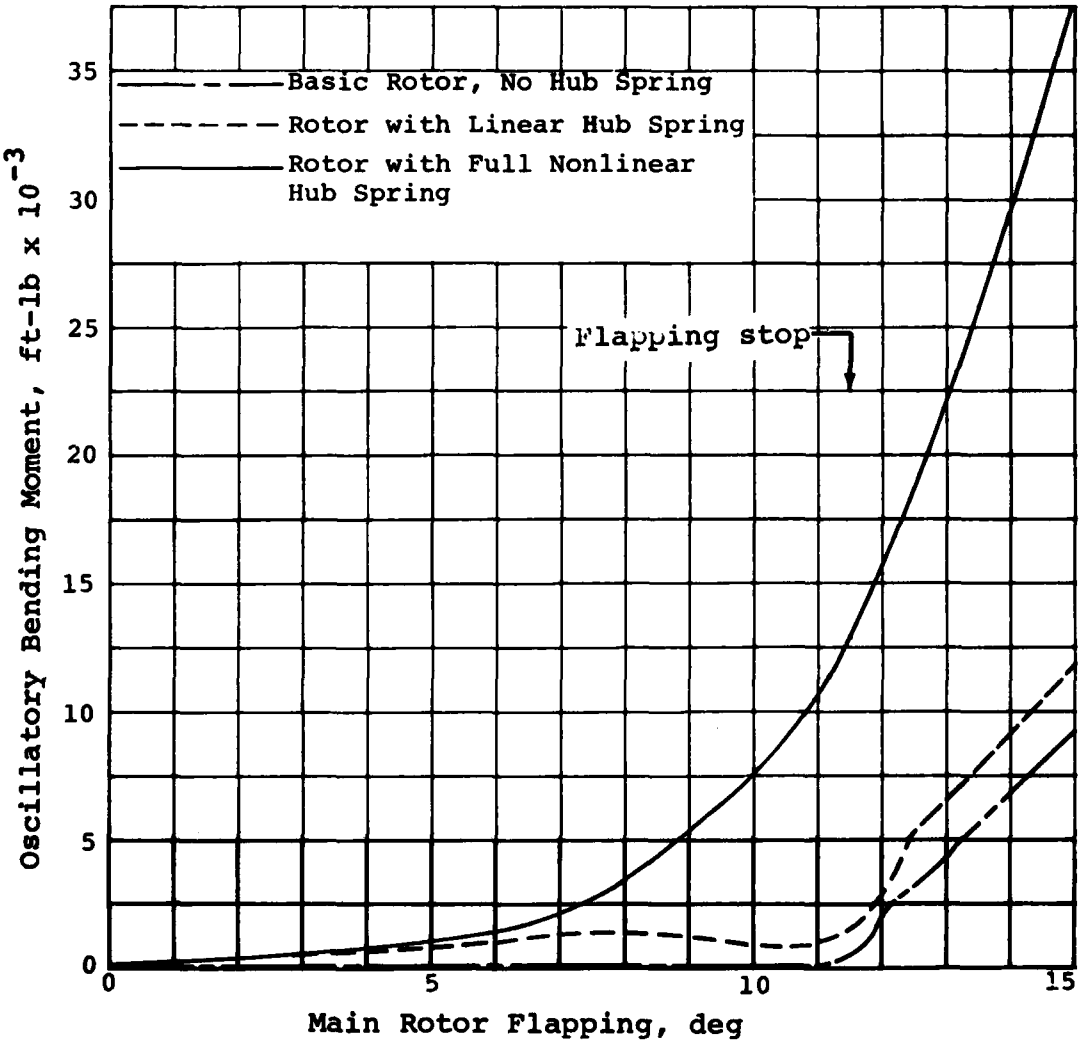

Figure 10. Computed oscillatory mast bending moment at flapping stop contact point, UH-1H main rotor, 2500-pound thrust, hover.

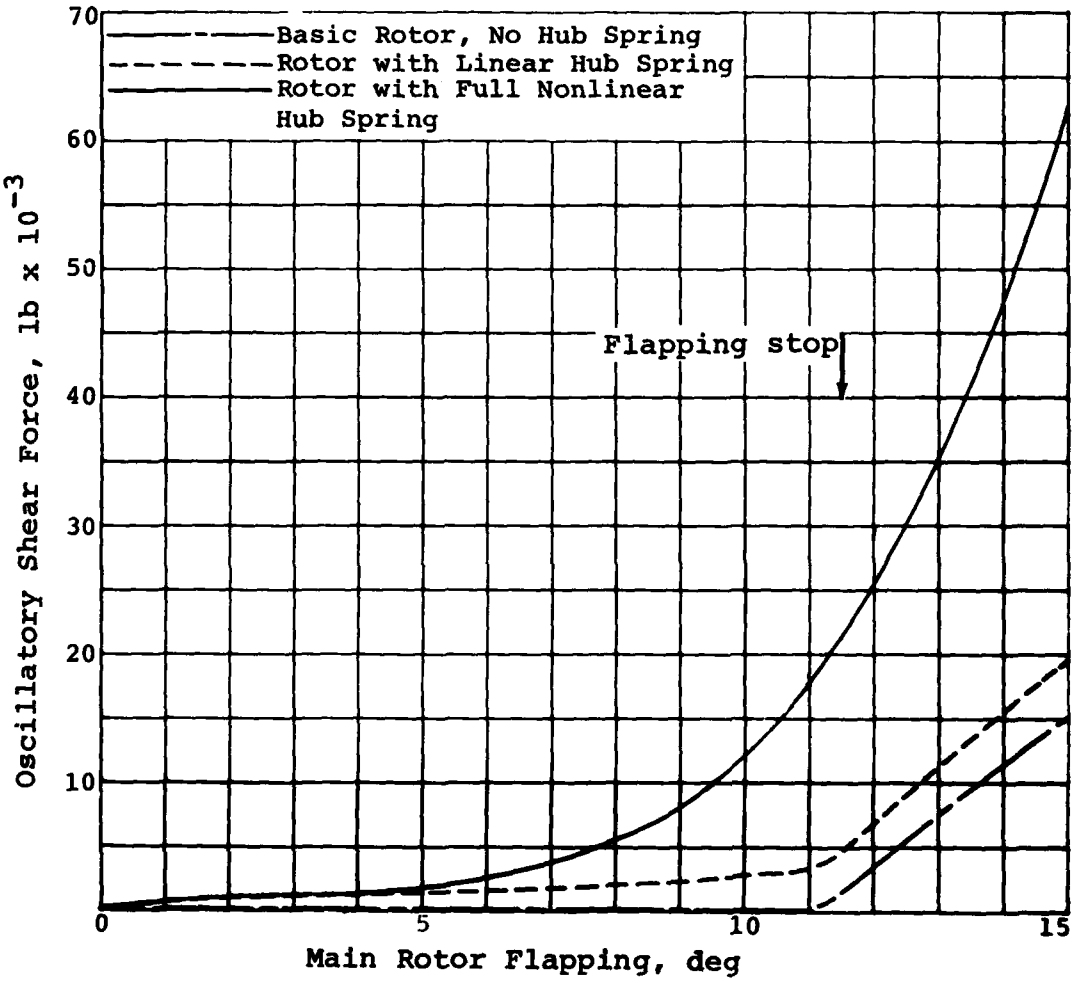

Figure 11. Computed oscillatory mast shear at flapping stop contact point, UH-1H main rotor, 2500-pound thrust, hover.

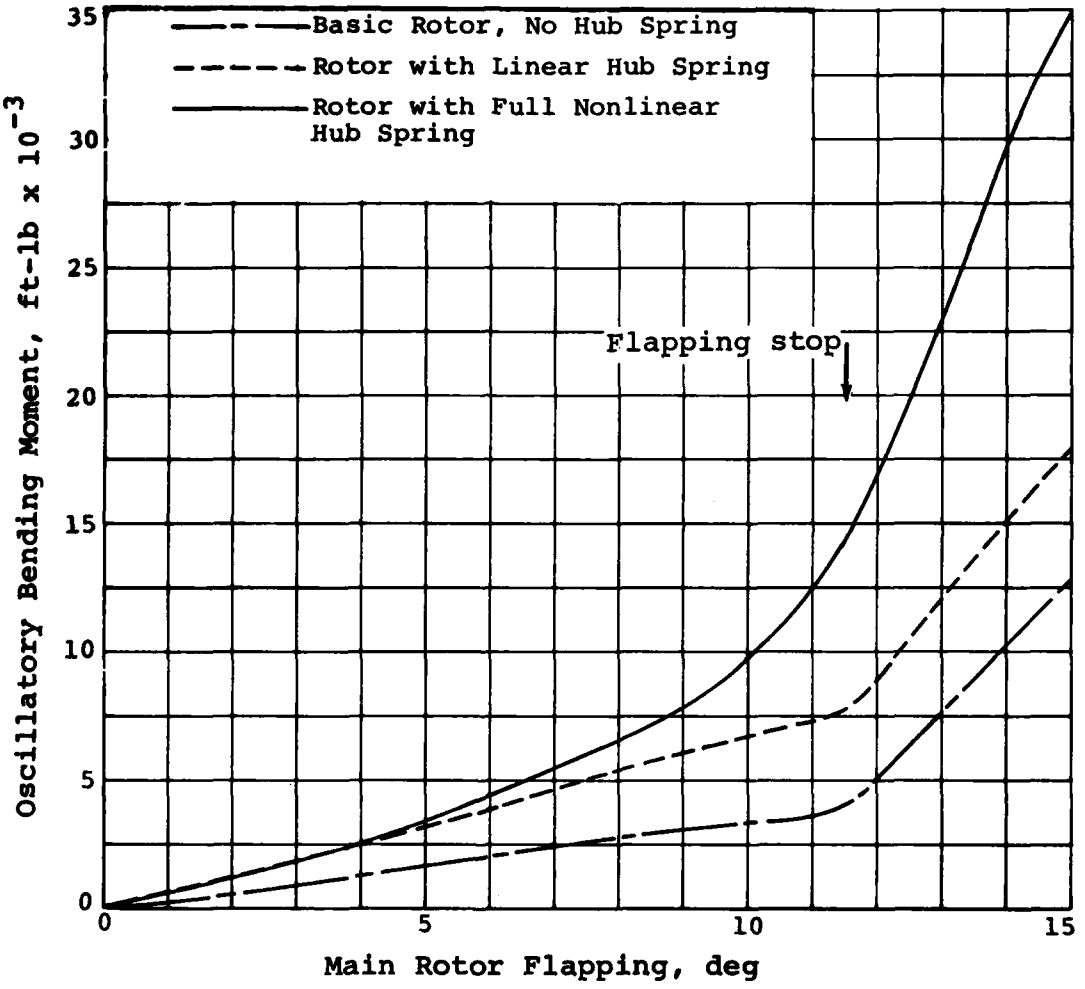

Figure 12. Computed oscillatory mast bending moment at flapping stop contact point, UH-1H main rotor, 8500-pound thrust, hover.

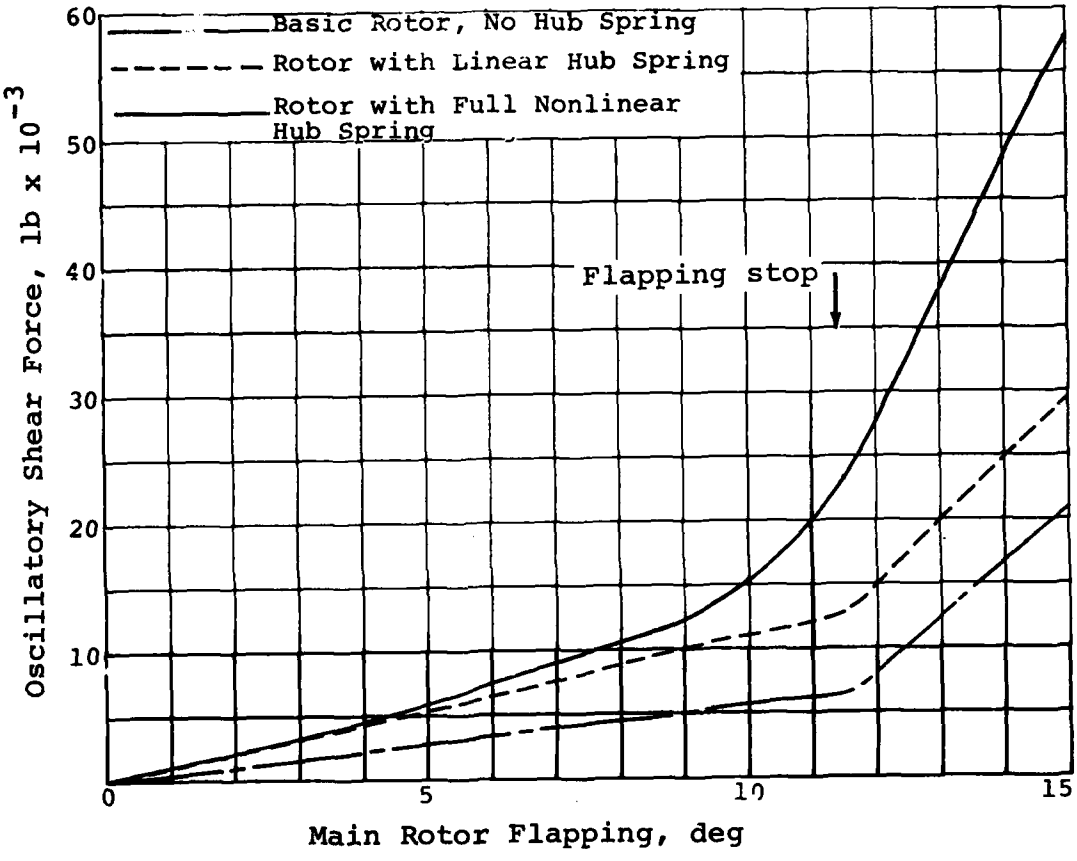

Figure 13. Computed oscillatory mast shear at flapping stop contact point, UH-1H main rotor, 8500-pound thrust, hover.

2.4 UH-1H HUB SPRING POSTFLIGHT ANALYSIS

The ARHF01 program was further verified through a postflight analysis of the full-scale UH-1H helicopter with the hub spring installed. Flight test data for two forward flight test points and one tie-down condition were simulated using the same inputs as discussed in Paragraph 2.3, with the addition of a 5-degree-of-freedom rigid-body fuselage.

The three test conditions that were simulated are listed in Table 3. The hub spring was installed for all three cases. The amount of thrust generated during the tie-down test (Counter 616 of Ground Run 17) is unknown. The hub flapping angles are based on a harmonic analysis of the hub flapping time history and are the coefficients in the positive Fourier series for flapping, i.e.,

$$\beta(t) = \beta_o + \beta_{1_s} \sin \Omega t + \beta_{1_c} \cos \Omega t + \ldots \qquad (6)$$

The tip-path-plane flapping assumes a different sign convention; e.g., positive longitudinal TPP flapping is indicated by a negative coefficient for the cosine term.

2.4.1 Definitions and Sign Conventions

Mast parallel and perpendicular bending moments were measured at points 16.0 and 46.75 inches below the teetering axis. The mast parallel bending moment is measured by strain gages mounted to the mast in a vertical plane parallel to the blade feathering axes, while mast perpendicular bending moments are measured in a vertical plane perpendicular to the blade feathering axes. These moments and their sign conventions are shown in Figure 14.

The equations for these two moments are

$$M_{\parallel} = M_{TOT} + (H \cos\psi - Y \sin\psi)x \qquad (7a)$$

$$M_{\perp} = -(H \sin\psi + Y \cos\psi)x \qquad (7b)$$

where

M_{TOT} is the moment applied at the top of the mast due to flapping restraint and flapping stop contact

TABLE 3. PARAMETERS OF TEST CONDITIONS SIMULATED

Flight Counter Flight Condition	GR17 616 Tie-Down	197A 746 Level Flight	197A 748 Level Flight
Gross weight, lb	*	8000	8000
Center of gravity, in.	--	144.5	144.5
Airspeed, KTAS	0	66.2	118.7
Euler pitch attitude, deg	0.3	4.73	1.46
β_{1_s}	1.136	-0.511	-0.746
β_{1_c}	-0.392	-2.625	-2.510
Density Ratio	0.9925	0.9391	0.9391

*The amount of thrust generated during the tie-down run is unknown.

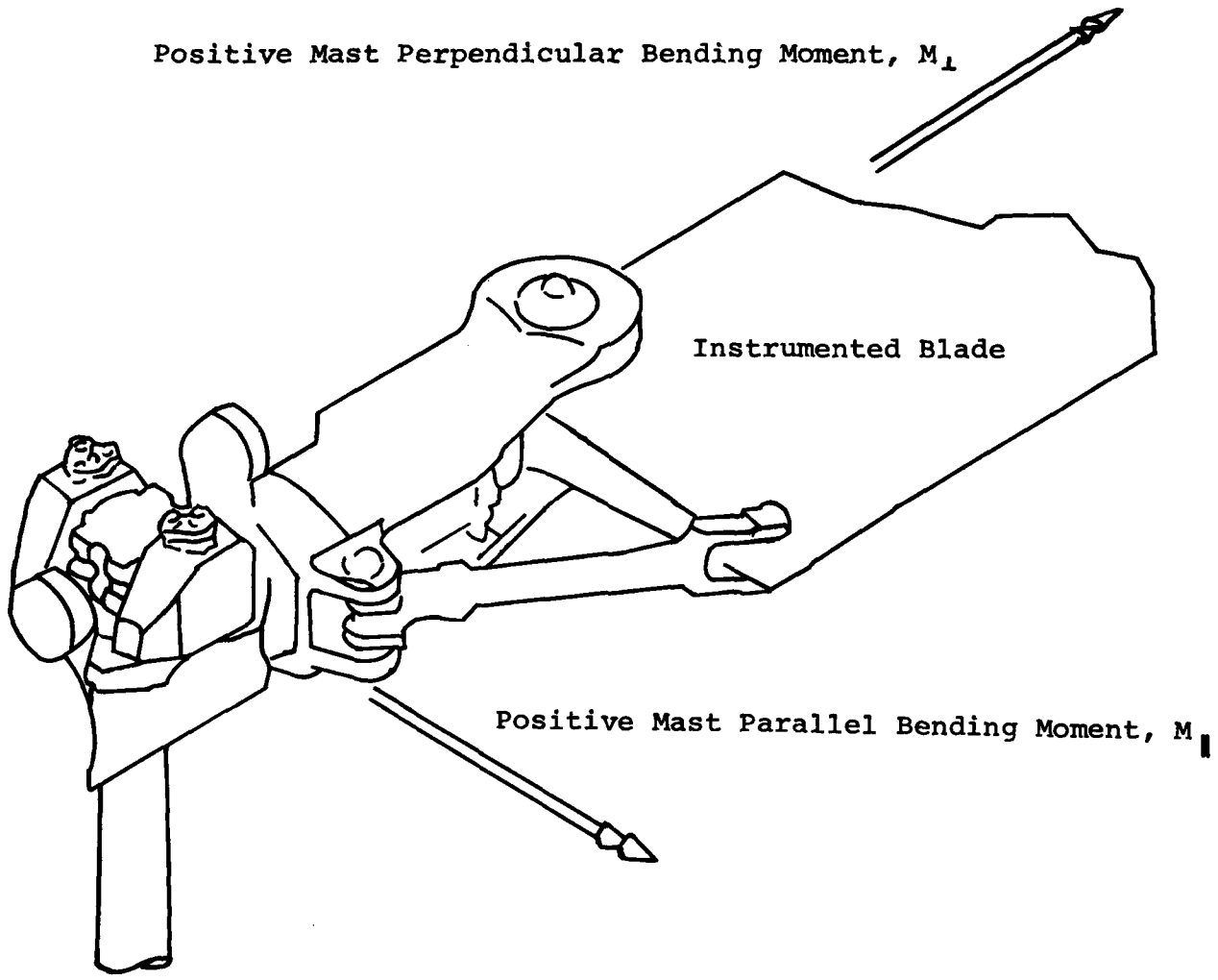

Figure 14. Main rotor mast bending moment sign convention.

H,Y are the longitudinal and lateral hub shears in the fixed system, positive forward and to starboard, respectively

x is the distance from the teetering axis to the point at which the moment is measured

In the rotating system, in the absence of a hub spring, a positive parallel bending moment at a point in the mast arises from a shear that is positive outward along the noninstrumented blade. The primary aerodynamic portion of this shear is $L\sin\beta$ (assuming that the lift is perpendicular to the tip-path plane). The remainder of this shear arises from the inertia loads in the blade spanwise direction.

In like manner, a positive mast perpendicular bending moment is generated in the mast due to a hub shear (in the rotating system) that is positive toward the trailing edge of the instrumented blade. The aerodynamic portion of this shear is the difference in the drag between the two blades ($D_1 - D_2$). The remainder of the shear is due to inertia loads in the blade chordwise direction.

Simulations of each of the three test conditions were performed by setting the airspeed and fuselage Euler pitch angle to the values measured during the test, setting collective and cyclic pitch angles, and recording data after the transient response damped out. The recorded thrust and flapping angle time histories were then harmonically analyzed to determine if the desired mean thrust and one-per-rev flapping had been achieved. If the difference between the desired and computed thrust was more than 200 pounds, or if the computed values of β_{1_s} and β_{1_c} differed individually from the measured values by more than 0.1 degree, the control position inputs were changed and the case was rerun.

2.4.2 Measured versus Computed Mast Bending Moments

Computed mast parallel and perpendicular bending moments have been compared with those measured in flight, for both mast Station 16.0 and mast Station 46.75. The computed mast parallel bending moments are in good agreement with the test data; the computed mast perpendicular bending moments are not in good agreement with the test data.

As was described in Paragraph 2.4.1, the mast parallel bending moment consists of a moment due to the hub spring and a moment due to the thrust vector and rotor flapping. Since the hub flapping angle and the thrust were being matched for the

forward flight cases, the moment due to the hub spring and the moment due to shear resulting from the thrust vector tilt should be an accurate representation of those portions of the measured mast parallel bending moment. For example, the cosine one-per-rev component of the Station 16 mast parallel bending moment measured at 118 KTAS was -12643 inch-pounds. The same term computed using just the hub spring moment and the thrust vector tilt is -15623 inch-pounds. The full ARHF01 analysis computes a cosine one-per-rev term of -22200 inch-pounds, indicating that the spanwise inplane inertial terms are probably overstated in the program, and of the opposite algebraic sign with respect to the inertia loads experienced during the test.

Inspection of the sources of the mast perpendicular bending moment has shown that it arises from an inplane aerodynamic shear, equal to the difference in the total drag of the two blades, and a shear due to the chordwise inertia loads. This can be restated in symbolic form as

$$\text{Shear} = D_1 - D_2 + IL_1 - IL_2 \qquad (8)$$

Where the shear is positive toward the trailing edge of blade 1, D_1 and D_2 are the drag forces of the two blades and IL_1 and IL_2 are the inplane shears at the root of blades 1 and 2 due to inplane inertia response. The aerodynamic representation of the rotor blade element drag is quite simple (Figure 1), so the $(D_1 - D_2)$ term will only be an approximation of the correct value. In like manner, the blade inplane motion is represented by a simple hinge-spring-rigid blade mode, so the $(IL_1 - IL_2)$ term is also only an approximation to the spanwise hub shear. The simplicity of the model results in incorrect or overestimated mast perpendicular bending moments. Therefore, there is a significant discrepancy between computed and measured mast perpendicular bending moments; the remainder of the discussion will consider only mast parallel bending moments.

Time histories of the computed and measured mast parallel bending moments are compared in Figures 15 and 16 for the tie-down test condition of Counter 616. Since the thrust actually developed by the rotor during the test is unknown, cases were run at thrusts from 4000 to 10,000 pounds with both one-per-rev components of the flapping angle being matched to within 0.1 degree. The computed mast parallel bending moment time histories plotted are for the two extreme cases.

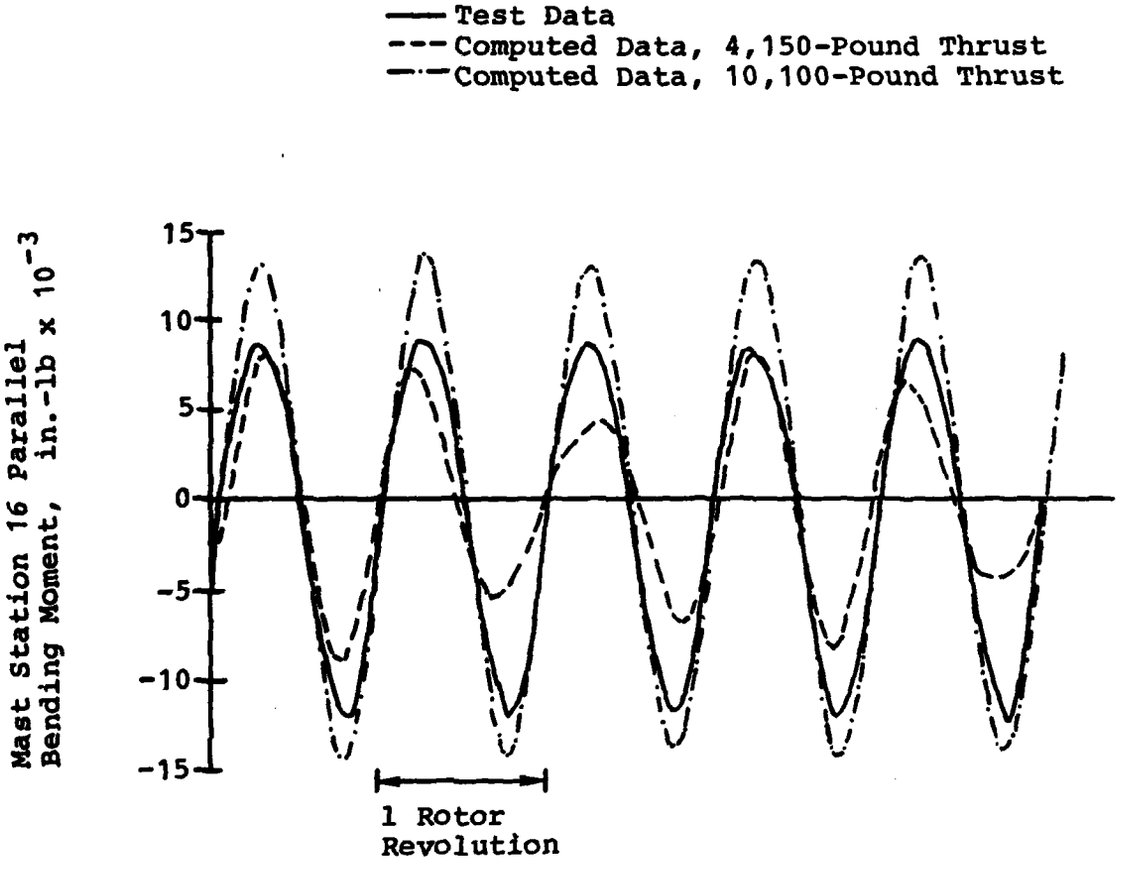

Figure 15. Measured and computed main rotor mast Station 16 parallel bending moments for the tie-down test.

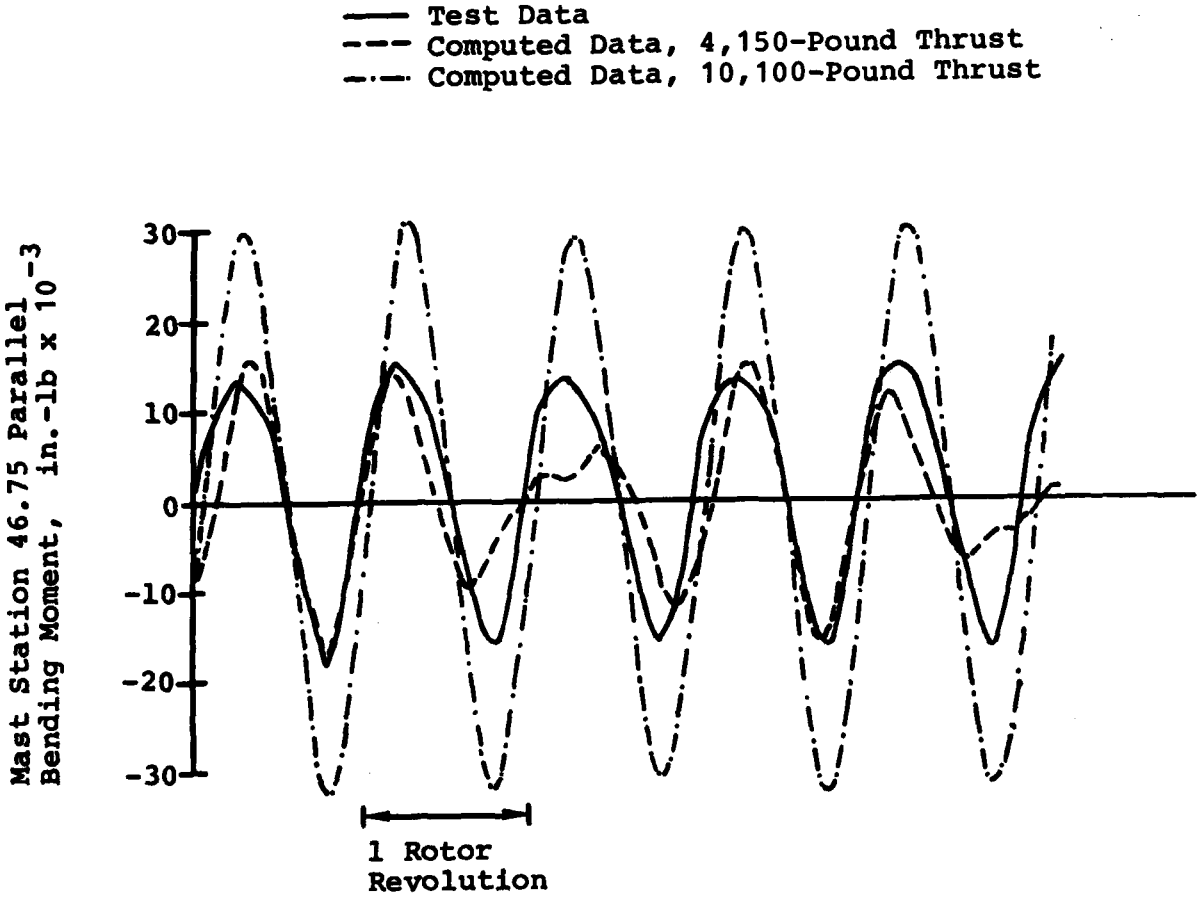

Figure 16. Measured and computed main rotor mast Station 46.75 parallel bending moments for the tie-down test.

The computed parallel bending moment time histories for mast Station 16 (Figure 15) are almost exactly in phase with the test data. The overall amplitude of the measured bending moment exceeds that computed at 4000 pounds thrust and is less than the amplitude predicted at 10,000 pounds thrust. (Note that there is a subharmonic response present in the computed results. This is due to a portion of the transient response having very low damping. The investigators were unable to entirely eliminate this response.)

The measured and computed mast parallel bending moment time histories for Station 46.75 are presented in Figure 16. Again, computed time histories are plotted for the two extreme thrust conditions simulated due to the uncertainty in the thrust generated during the test. The computed time histories exhibit the same phase, with respect to the azimuth event indicator, as the measured time history. The amplitude computed in the low thrust case is approximately the same as that measured, while the amplitude of the time history generated in the high thrust simulation is approximately double the measured quantity.

Figures 17 through 20 contain comparisons of the measured and computed mast parallel bending moment time histories at Stations 16.0 and 46.75 for the 66 and 118 KTAS test conditions (Counters 746 and 748). The computer-generated time histories are in excellent agreement with the test data with regard to phase angle. The overall amplitude of the computed Station 16 bending moment is approximately 30 to 50 percent greater than that measured, while the overall amplitude of the computed Station 46.75 bending moment is approximately double that recorded in flight. Since the contribution of the hub spring moment is the same at both stations and very close to that obtained in flight, these discrepancies must be due to differences between the inplane shear computed in ARHF01 and that actually experienced in flight. That portion of the shear due to the tilt of the thrust vector has been well-matched, so the spanwise inplane inertia loads must be suspected as the source of the difference between the measured and computed mast parallel bending moments.

Considering the simplicity of the mathematical model contained in hybrid computer program ARHF01, the results presented in this section of the report demonstrate acceptable correlation with flight test.

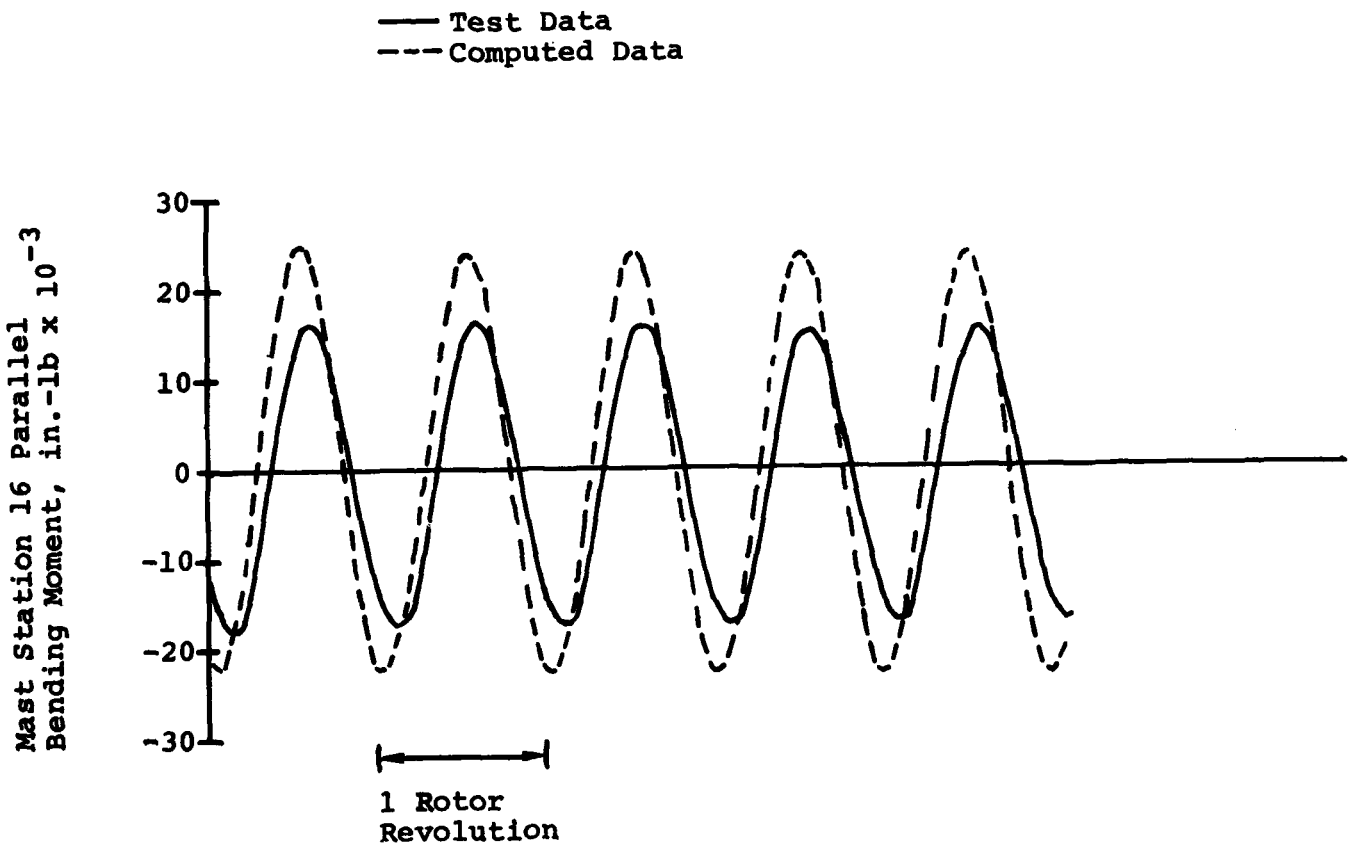

Figure 17. Measured and computed main rotor mast Station 16 parallel bending moments at 66 KTAS.

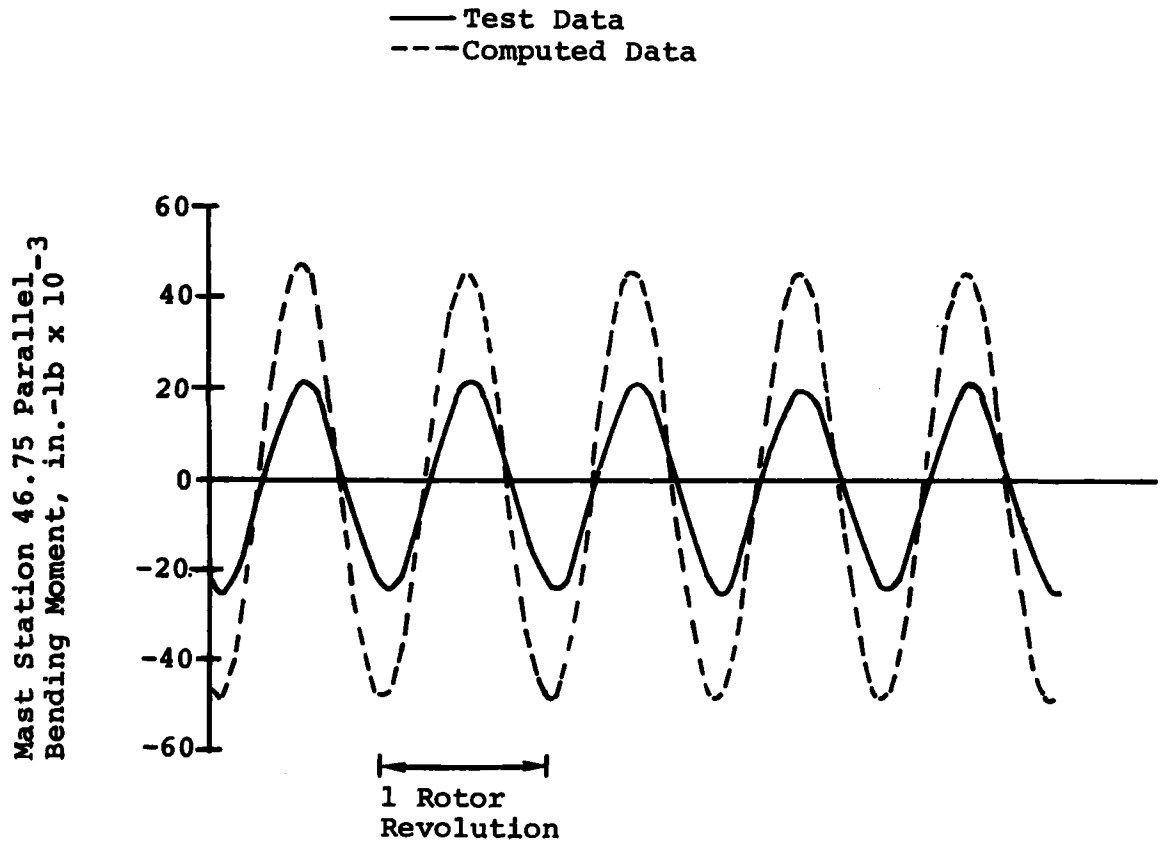

Figure 18. Measured and computed main rotor mast Station 46.75 parallel bending moments at 66 KTAS.

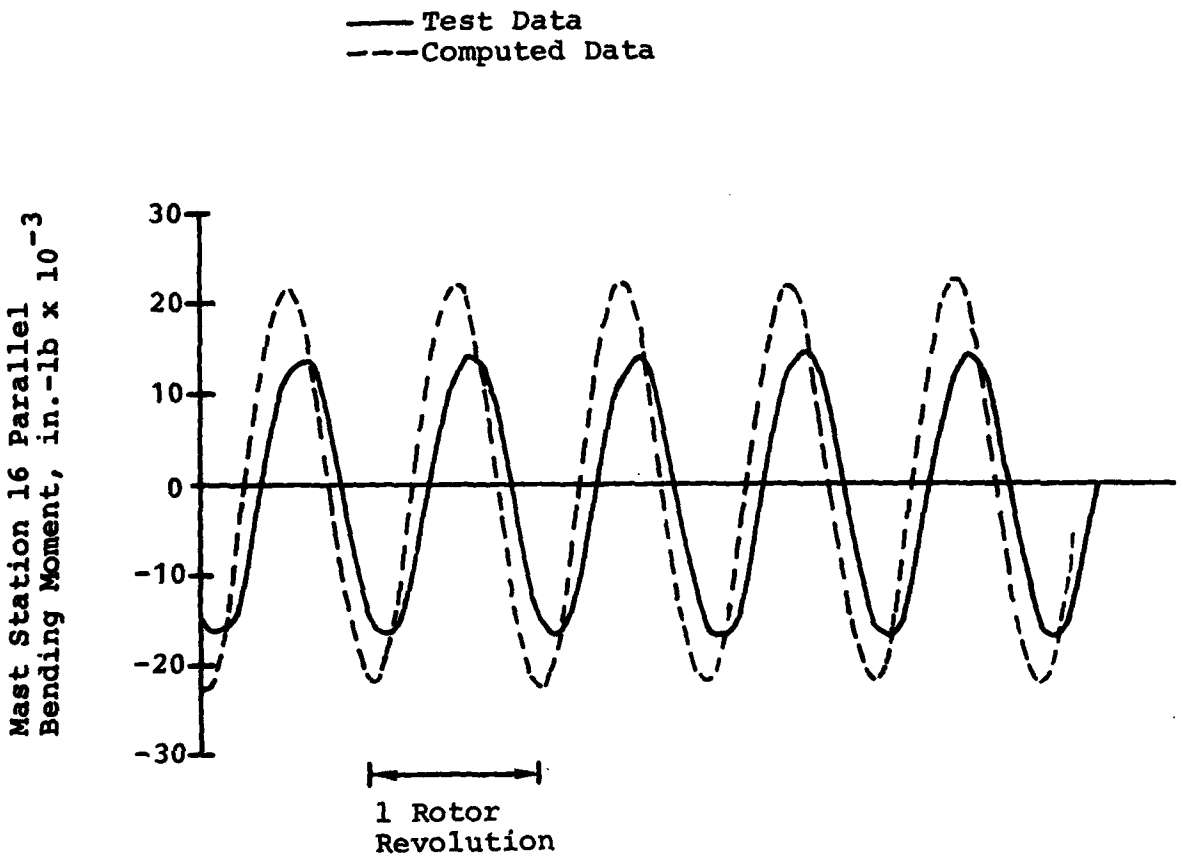

Figure 19. Measured and computed main rotor mast Station 16 parallel bending moments at 118 KTAS.

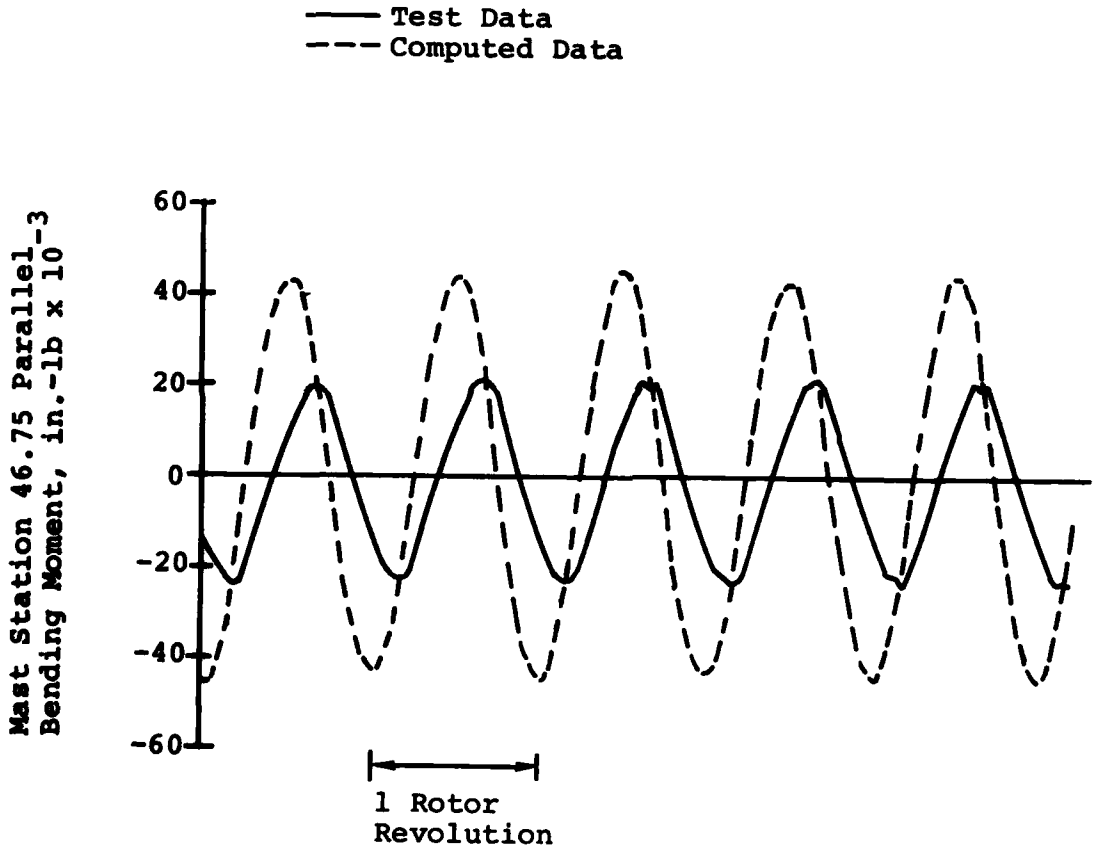

Figure 20. Measured and computed main rotor mast Station 46.75 parallel bending moments at 118 KTAS.

3. HUB SPRING DESIGN

The addition of a nonlinear hub spring to an existing helicopter design requires a compromise between the level of spring rates desired for handling qualities and the allowable loads that the new spring will add to the existing structure. And further, the craftsman-like nature rather than pure scientific control exercised in the composition of elastomeric properties necessitates that some variation in desirable characteristics be tolerated.

3.1 DESIGN CHARACTERISTICS

The nonlinear hub spring was designed for the UH-1D/H helicopter to provide increased control power for reduction of main rotor flapping in steady flight and maneuvers, and to eliminate metal to metal contact of the flapping stop and mast. Additional design objectives were a design that could be retrofitted with few modifications, a design that did not reduce the fatigue life of the UH-1 hub and mast assemblies, and a design that did not reduce the flapping limit.

The design of the hub spring is a trade-off between the control power obtained with high spring rates and the additional structural loads applied to the hub and mast by the hub spring that were not present in the current design of the UH-1D/H helicopter. The method used to achieve this compromise is to employ a flapping spring that provides a two-stage, linear/nonlinear, variation in hub moment with rotor flapping. Flapping in this case refers to the once per revolution teetering action of the main rotor hub.

A flapping spectrum was defined based on flapping data obtained during the UH-1D/H Load Level Survey tests and modified for the flapping reduction in steady flight provided by the hub spring. This spectrum is presented as Table 4. This spectrum was the basis for calculations of the fatigue loading of the rotor and spring components. The linear rate portion of the hub spring was chosen such that for over 90 percent of the service life of the helicopter, flapping would be less than 4 degrees which results in unlimited fatigue life of all existing UH-1D/H parts. The maximum load resulting from the hub spring moment at 11 degrees of flapping was chosen such that no parts of the mast, hub, and blade assemblies would have a negative margin of safety.

As previously stated, the constraints were that there be no reduction of fatigue life at low flapping angles and that maximum control power (i.e., hub moment) be applied to the

TABLE 4. DESIGN FLAPPING SPECTRUM

Condition	Oscillatory Angle (deg)	% of Time	Cumulative % Time
1	±0.8	1.48	1.48
2	±1.6	16.68	18.16
3	±2.4	21.57	39.73
4	±3.2	29.69	69.42
5	±4.0	21.05	90.47
6	±4.8	6.72	97.19
7	±5.6	1.57	98.76
8	±6.4	0.70	99.46
9	±8.0	0.44	99.90
10	±8.8	0.09	99.99

helicopter at high angles of flapping. A purely linear hub spring can only meet one, but not both, of these constraints; however, the nonlinear design was able to satisfy both constraints. A linear hub moment is provided throughout the flapping spectrum by four elastomeric shear pads. Hub moments at the rate of 330 ft-lb per degree of flapping are generated by the shear pads. At 4 degrees of flapping, an elastomeric snubber (compression spring) contacts a mast sleeve providing additional, nonlinear hub moment. The total, maximum hub moment at 11 degrees limit flapping is 13,000 ft-lb. The equation defining hub moment is given as Equation (4), Section 2.1. The additional control power provided by hub moment produced by main rotor flapping is characterized by Figure 21.

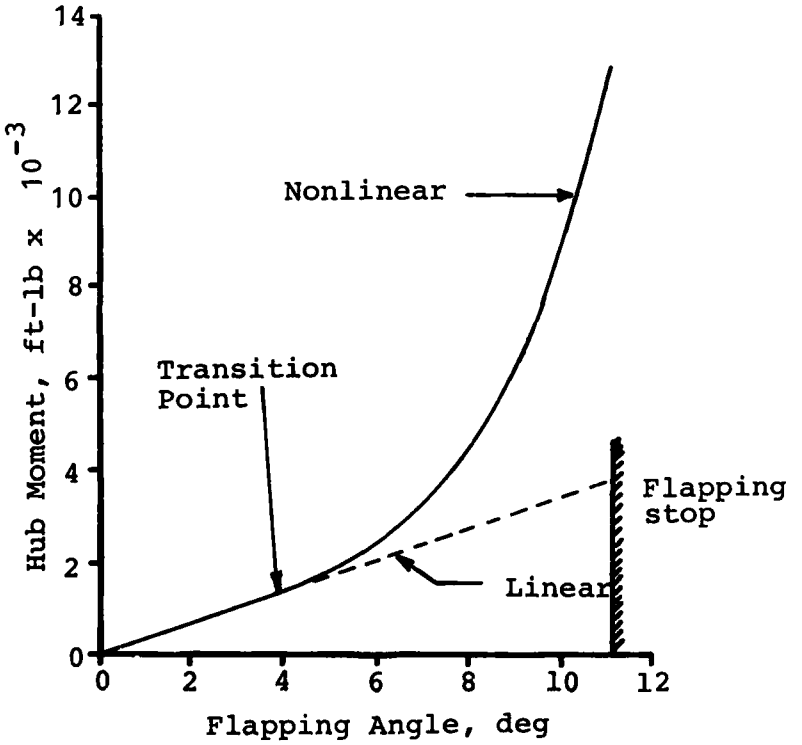

Figure 21. Hub moment provided by nonlinear hub spring.

The hazards associated with the metal-to-metal contact between the mast and the flapping stop at extreme flapping (greater than 11.5 degrees) are greatly reduced by the UH-1 hub spring. The contact between mast and hub is via the snubber, which greatly increases the area of load application during contact. In addition, the mode of load application is changed from a rapidly applied dynamic load to a more gradually applied load.

The UH-1 hub spring can be easily retrofitted to the UH-1D/H. In addition to the hub spring assembly, a sleeve set, a clamp, and stronger pillow block attachment bolts are required. Prior to installation, the thick wall mast (P/N 204-011-450-7) must be installed because of the higher loads produced by the hub spring. Hub spring installation requires removal of the main rotor and attachment of the hub spring to the yoke and the mast.

The hub spring bracket was designed to have an infinite life. The hub spring elastomeric components have minimum service life of 1500 hours. The Miner's damage coefficient has been calculated for the required minimum service life and was found to be 0.4832.

A postflight analysis to determine the effect of the hub spring on mast bearing lives also resulted in a determination that a positive margin of safety could not be calculated for the transmission case. This analysis used lower stress allowables and new casting factors for magnesium castings. Also, the maximum moment produced by the hub spring (13,000 ft-lb) was used in addition to the maximum loads measured during the structural demonstration program. This finding will require additional testing or an alternate material (aluminum) to be used for the transmission case (See Section 7.6.5).

A drawing of the UH-1H nonlinear hub spring is presented as Figure 22. Figure 23 pictures the hub spring itself. Not shown is this picture are the clamps that attach the hub spring to the main rotor yoke or the mast sleeve. Figure 24 pictures the hub spring attached to the main rotor yoke. Although the hub assembly is not attached to the mast in the picture, the mast sleeve and yoke clamp are clearly visible. The hub spring, as installed on the test aircraft, is pictured as Figure 25. Wiring bundles, which appear in Figures 23 through 25, are associated with the instrumentation used for this program.

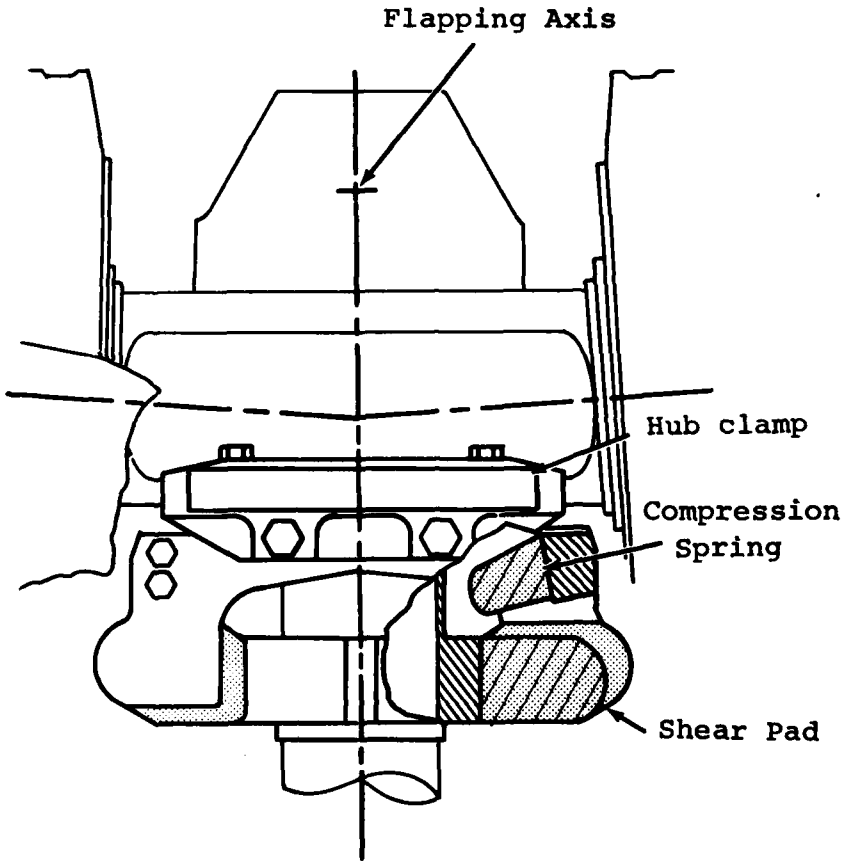

Figure 22. Drawing of UH-1H nonlinear hub spring.

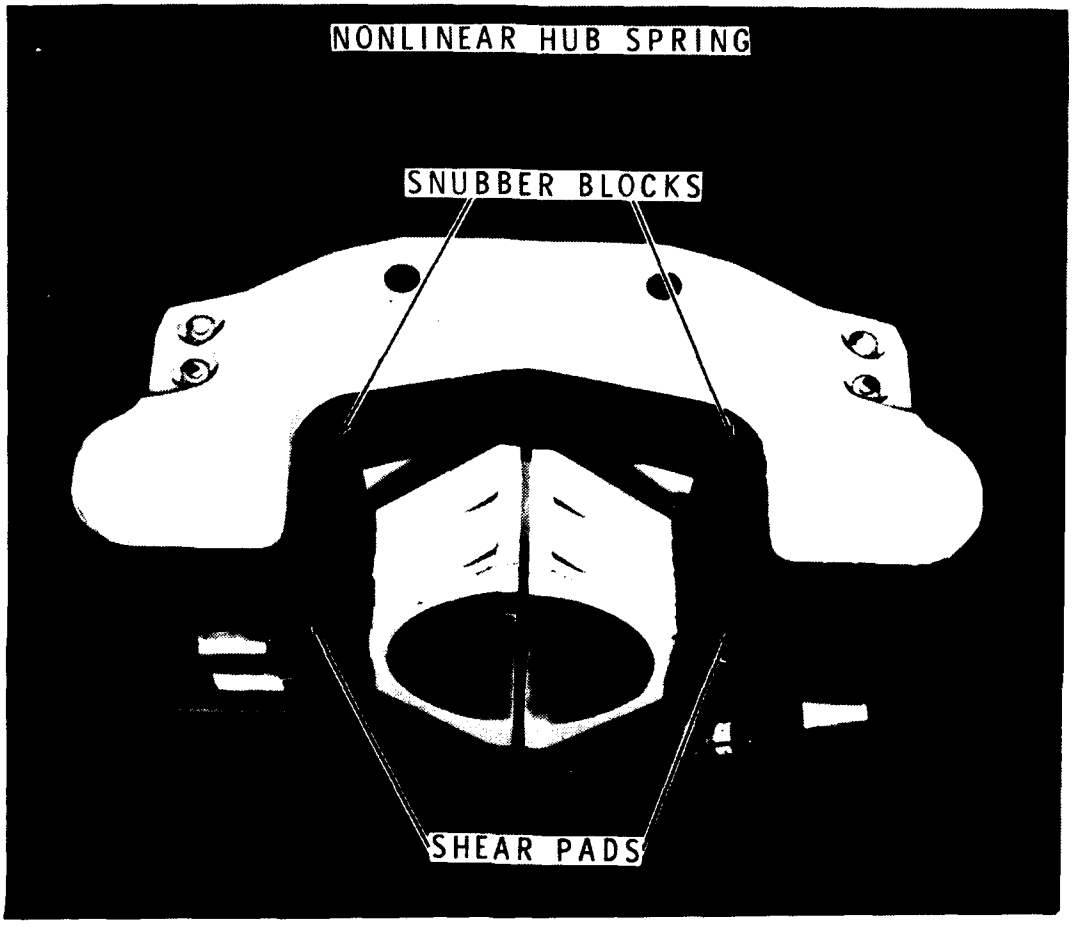

Figure 23. UH-1H nonlinear hub spring.

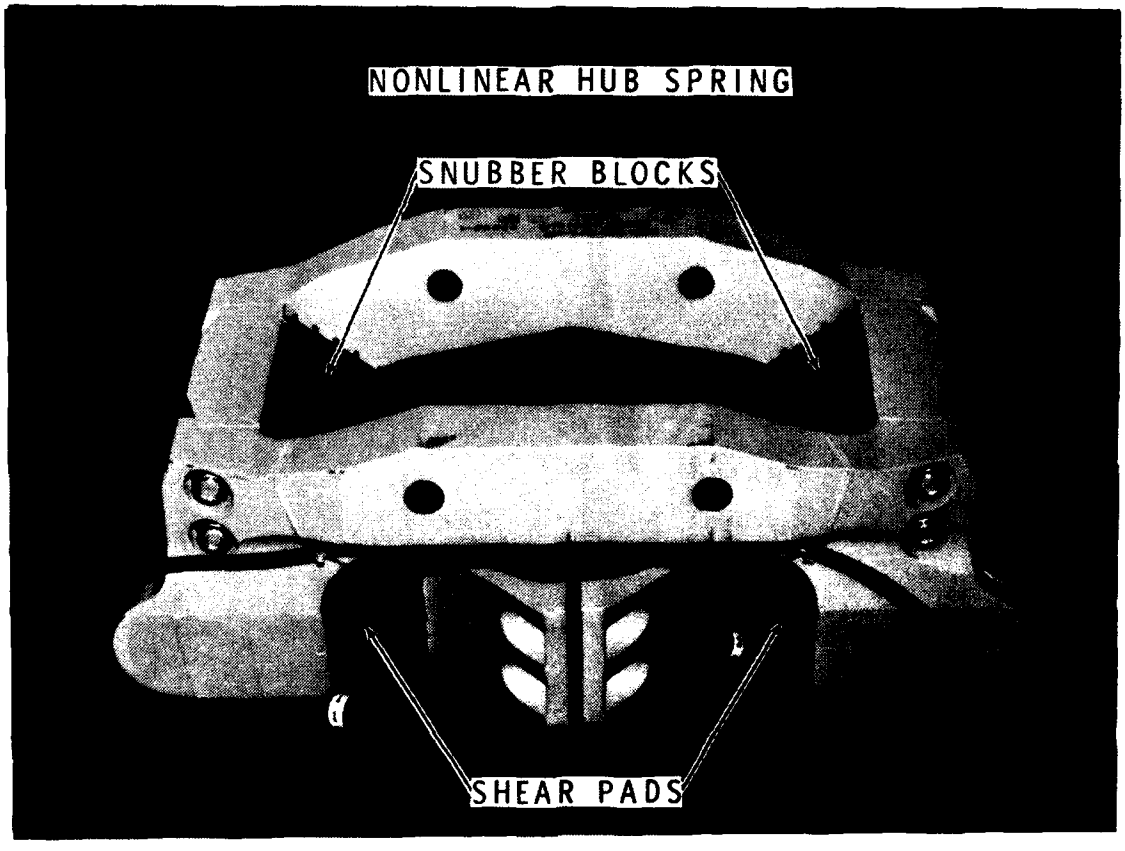

Figure 23. Concluded.

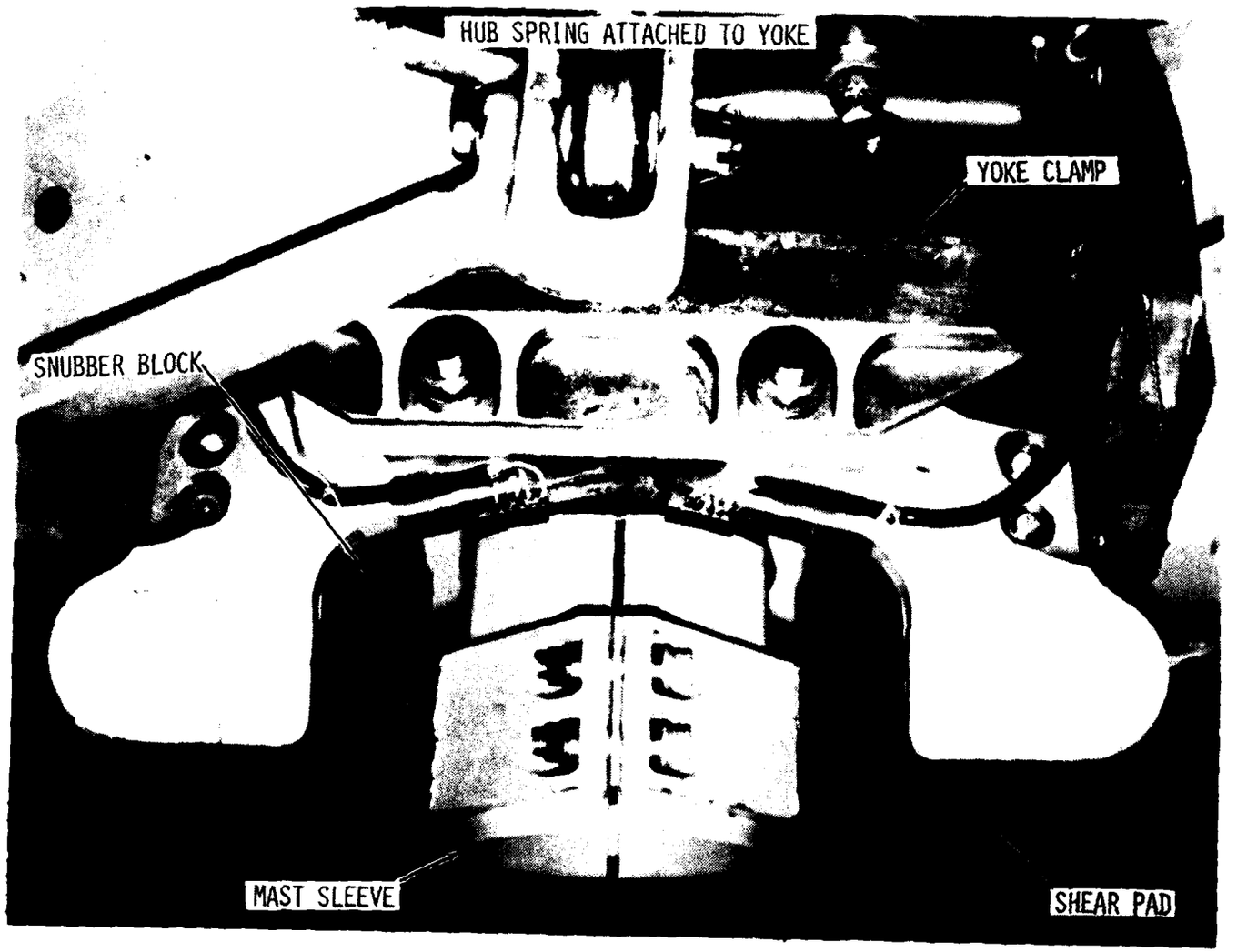

Figure 24. UH-1H nonlinear hub spring attached to main rotor yoke.

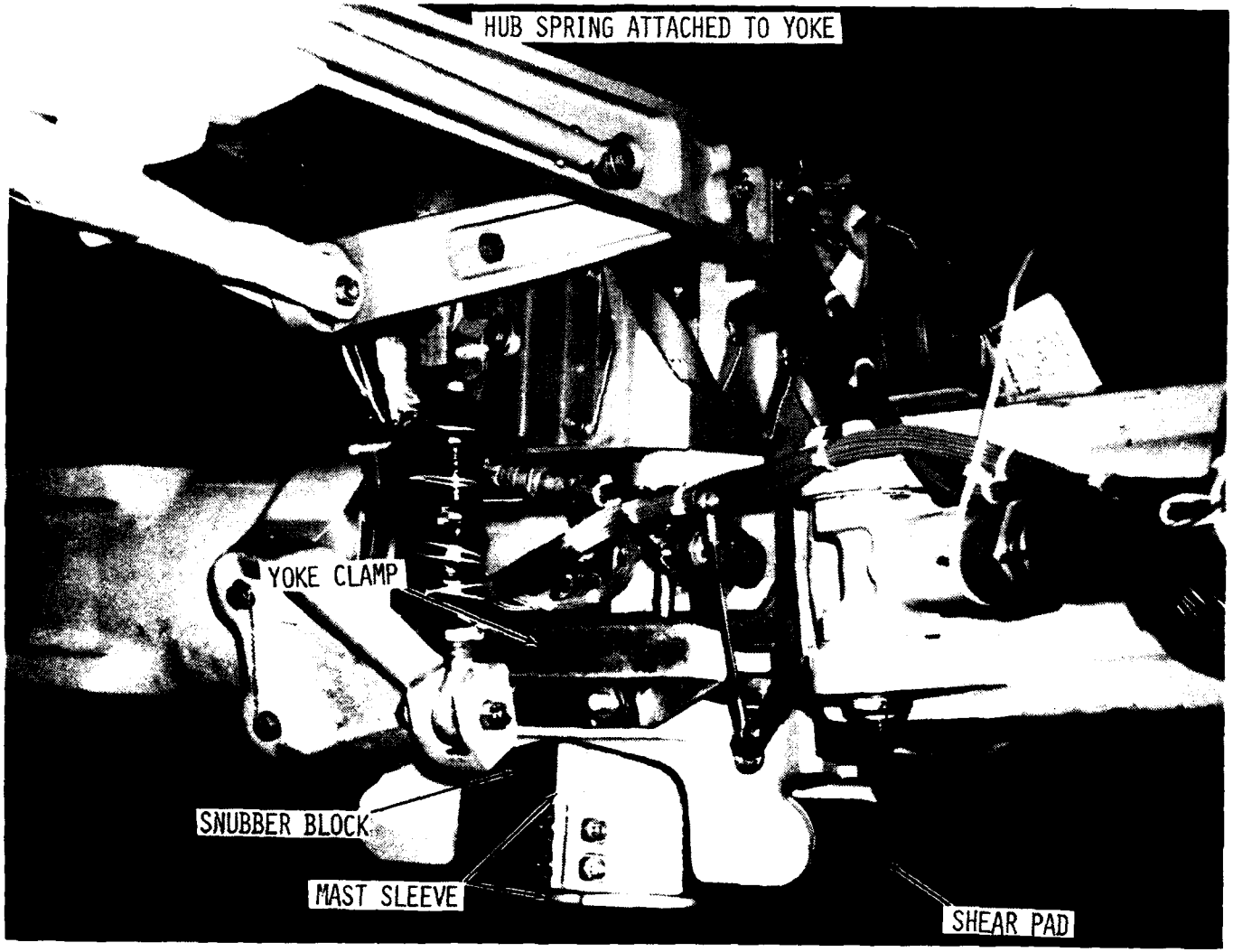

Figure 24. Concluded.

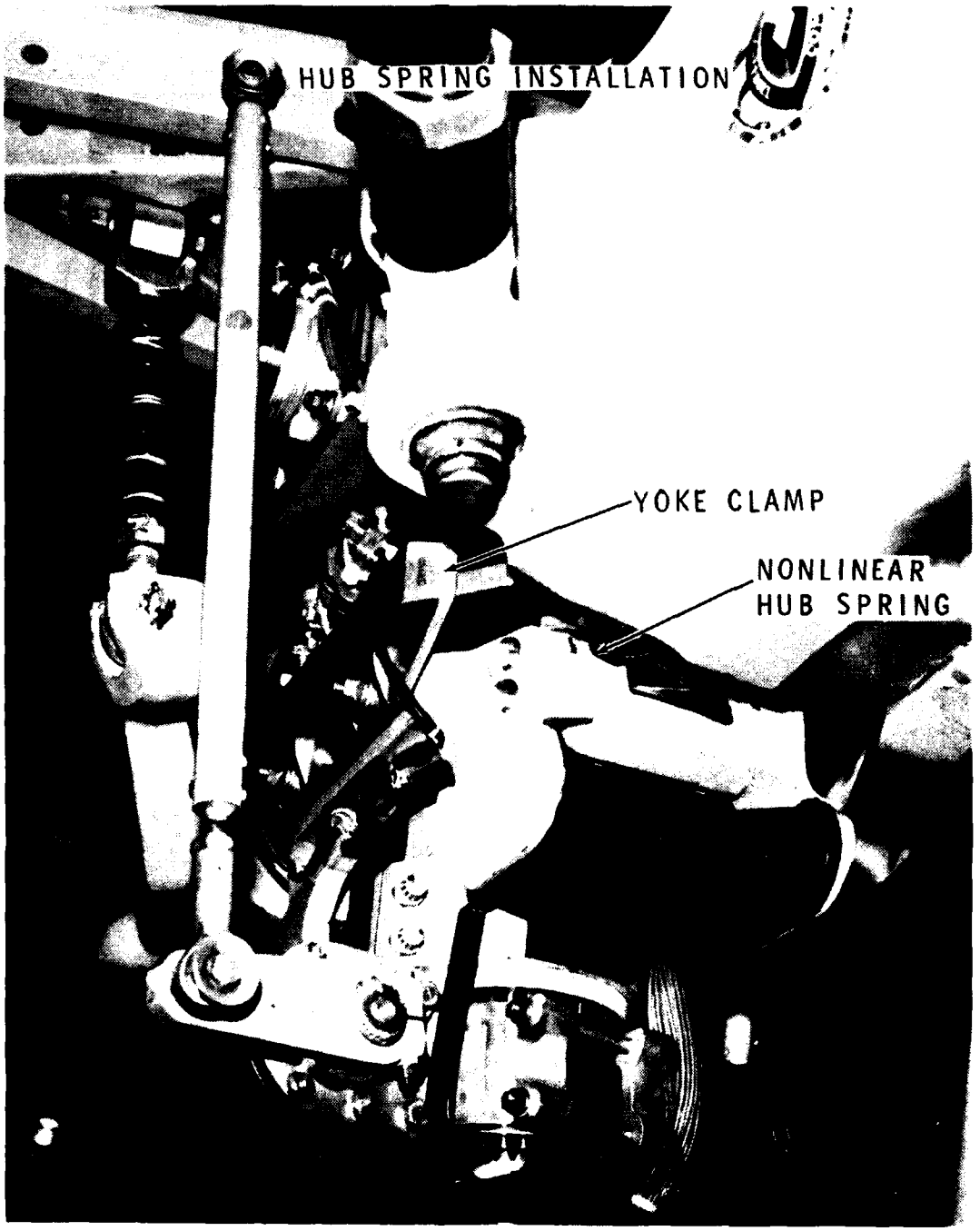

Figure 25. UH-1H nonlinear hub spring installation.

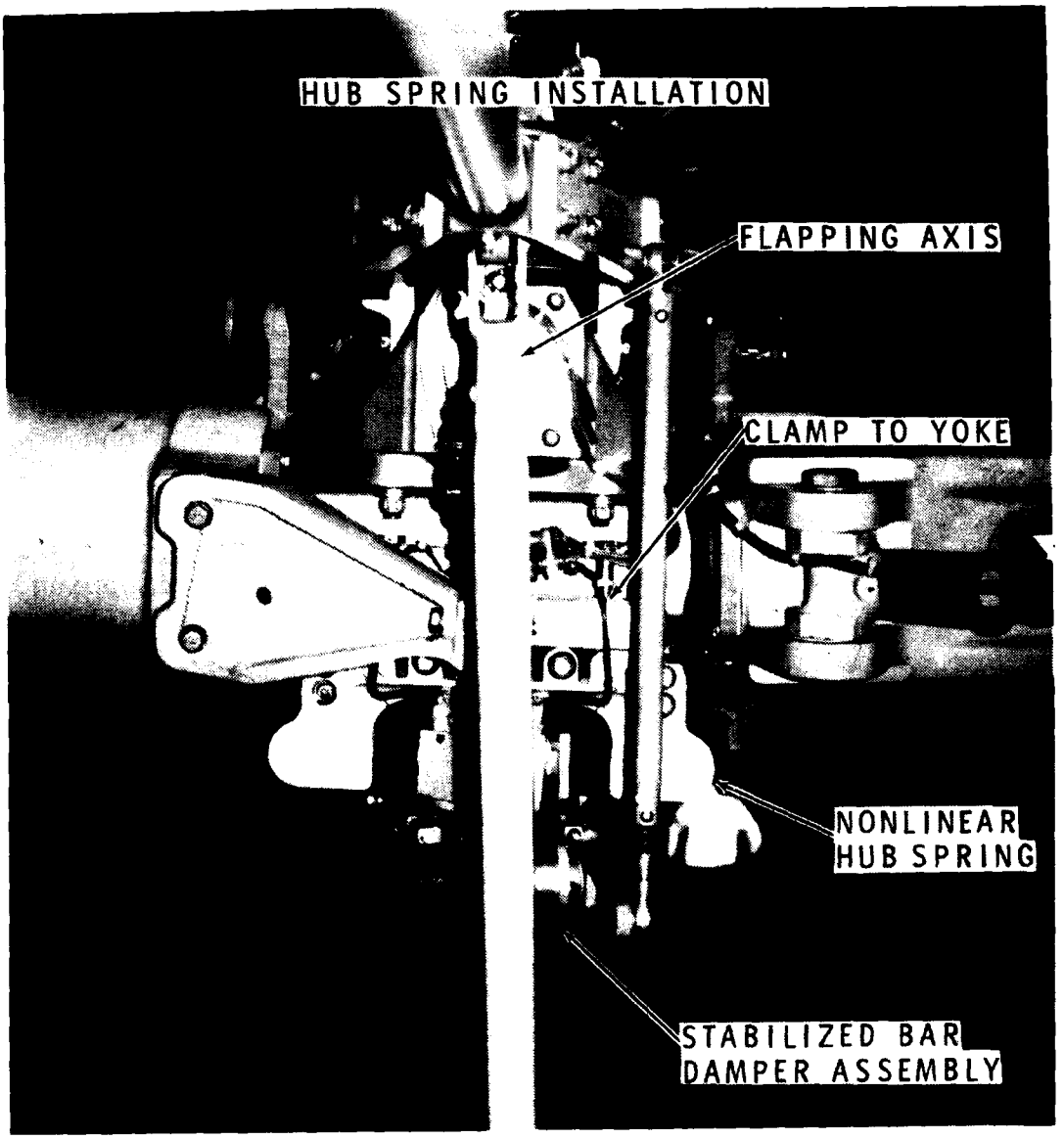

Figure 25. Concluded.

3.2 FAILURE MODES

The failure modes of the hub spring include the failure of the shear pads and/or failure of the snubbers. The failure of a shear pad or a snubber could result in two hazardous conditions. First, material from the failed item could fall from the hub and be struck by or lodged in rotating components. Second, the hub moment contribution of the failed item could be lost at a critical flight condition.

Foreign object damage by material from a failed item is thought to be a negligible hazard. This is a result of the size of the components and the failure modes necessary to fragment a shear pad or a snubber.

The second hazard would be the effect on the aircraft due to loss of hub moment as a result of a partial or a sudden, total failure of the hub spring. The loss of a single shear pad would result in a 25-percent reduction of the hub moment up to 4 degrees flapping and 8.25 percent at 11 degrees flapping. Because of the design there would be no vibrations introduced as a result of a shear pad failure. The complete failure (debonding) of a single snubber would have no effect at flapping angles below 4 degrees. Above this, a one-per-rev vibration of increasing (with flapping) severity would be experienced. The vibration would be the result of the unbalanced hub moment (maximum = 7370 ft-lb at 11 degrees) produced by the unfailed snubber.

Hybrid simulation of a complete hub spring failure indicates that no unusual or uncontrollable aircraft motions would follow the hub spring failure. In the unlikely event that there is either a partial or complete failure of the hub spring, the analysis shows that there would be little if any adverse effect to the aircraft or the mission.

4. DESIGN LOAD CRITERIA

In order to ensure that the helicopter can be able to withstand flapping stop impact, a conservative estimate of the loads generated during such an impact must be available. To provide a data base to compare estimation methods, a parametric analysis of stiffness parameters in the UH-1H rotor was conducted.

4.1 PARAMETRIC STUDY

Hybrid computer program ARHF01 has been used to study the effect of several variables on the value of mast loads experienced during flapping stop impact. A description of the computer analysis, and substantiating data, are provided in Section 2. The parameters to be varied were linear and nonlinear hub restraint, pylon stiffness, and mast stiffness. The simulations were conducted by placing the mast perpendicular to the ground with zero wind speed and trimming the rotor to 2500 pounds thrust or 9300 pounds thrust with the cyclic set to zero. The cyclic was then increased to introduce flapping and data recorded in the new steady-state condition. The mast shear and bending moment at the point at which the hub would contact the mast are plotted for a production UH-1H in Figure 26. (The production UH-1H rotor can undergo ±11.5 degrees of flapping before striking the flapping stop.)

4.1.1 Variation of Linear and Nonlinear Hub Restraint

The hub restraint as modeled in ARHF01 permits both linear and nonlinear components to be represented simultaneously. The equations for the moment about the teetering axis were given in Section 2.1, Equations (2) and (4).

For the production UH-1H, the parameters are $K_L = K_{NL} = 0$

K_{FS} = 130,000 foot-pounds/radian/rotor = 2269 foot-pounds/degree/rotor. K_{FS} is obtained from a NASTRAN analysis of the mast and pylon as described in Section 2.3. Note that since the hub spring characteristics are inputs to the ARHF01 program, changes in the hub spring will not require modification of K_{FS}.

The initial parameters for the proposed UH-1H hub restraint are:

K_L = 330 foot-pounds/degree/rotor

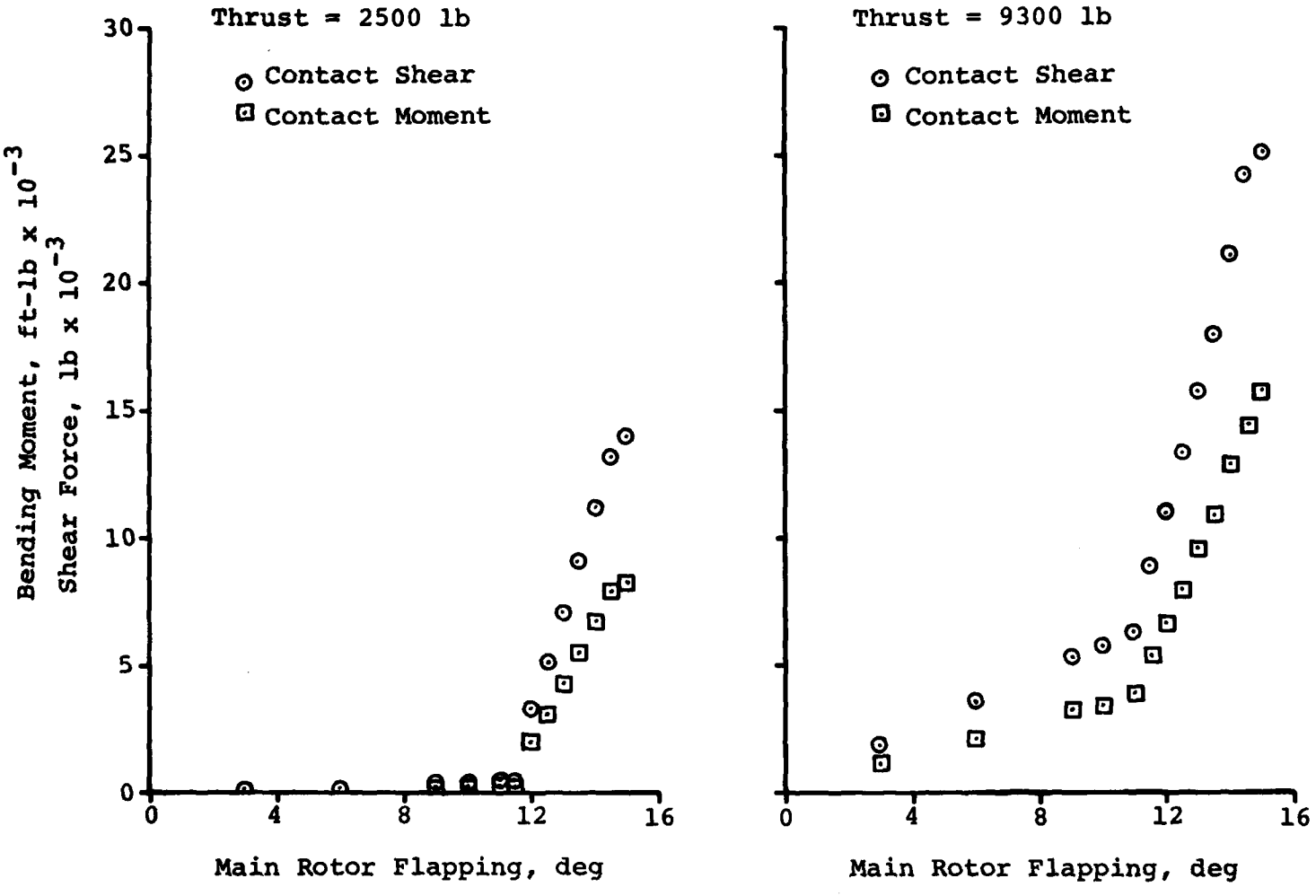

Figure 26. Loads at mast contact point for baseline UH-1H.

K_{NL} = 0.1 foot-pound/(degree)$^{4.71}$/rotor

r = 4.71

β_B = 4 degree

The shear and moment for this condition are shown in Figure 27.

Figures 28 and 29 give the mast loads for cases run with one-half the spring rates (K_L = 165, K_{NL} = 0.05) and twice the spring rates (K_L = 660, K_{NL} = 0.20), respectively.

The analysis shows that for the simulated tied-down configuration any hub restraint increases both the moment and the shear in the mast. In flight, the hub moment would reduce the flapping angle due to increased control power. The loads are introduced over a large surface area, though, which is an improvement over the essentially point-loading of hub-mast impact on the production UH-1H helicopter.

It must be noted that the mast loads for the nonlinear spring bear further investigation. The behavior of the spring will depend on the details of design in terms of how the compressive material is constrained under loads. This constraint will govern the compressive spring rate and thus the behavior of the spring at high flapping angles. The mast loads computed in this analysis are based on the assumption that the nonlinear spring force increases in the same manner (i.e., proportional to β^r) even after the conventional flapping stop angle is exceeded. A static test to the structural limit of mast, spring and hub components would be required to determine the actual spring characteristics at excessive flapping angles. The analysis of the high flapping loads by ARHF01 is thus restricted to the assumption of the high flapping spring characteristics.

4.1.2 Variation of Pylon Mount Spring Rate

Simulations were conducted for aircraft configurations which had half or double the pylon mount spring rate. For these cases, the NASTRAN model of the UH-1H was modified and new mode shapes were generated to represent the airframe. The pylon mount spring rate also determines the root boundary condition of the mast and, therefore, affects the flapping stop spring rate. Accordingly, new values of K_{FS} were computed for the modified pylon spring rate configurations, yielding

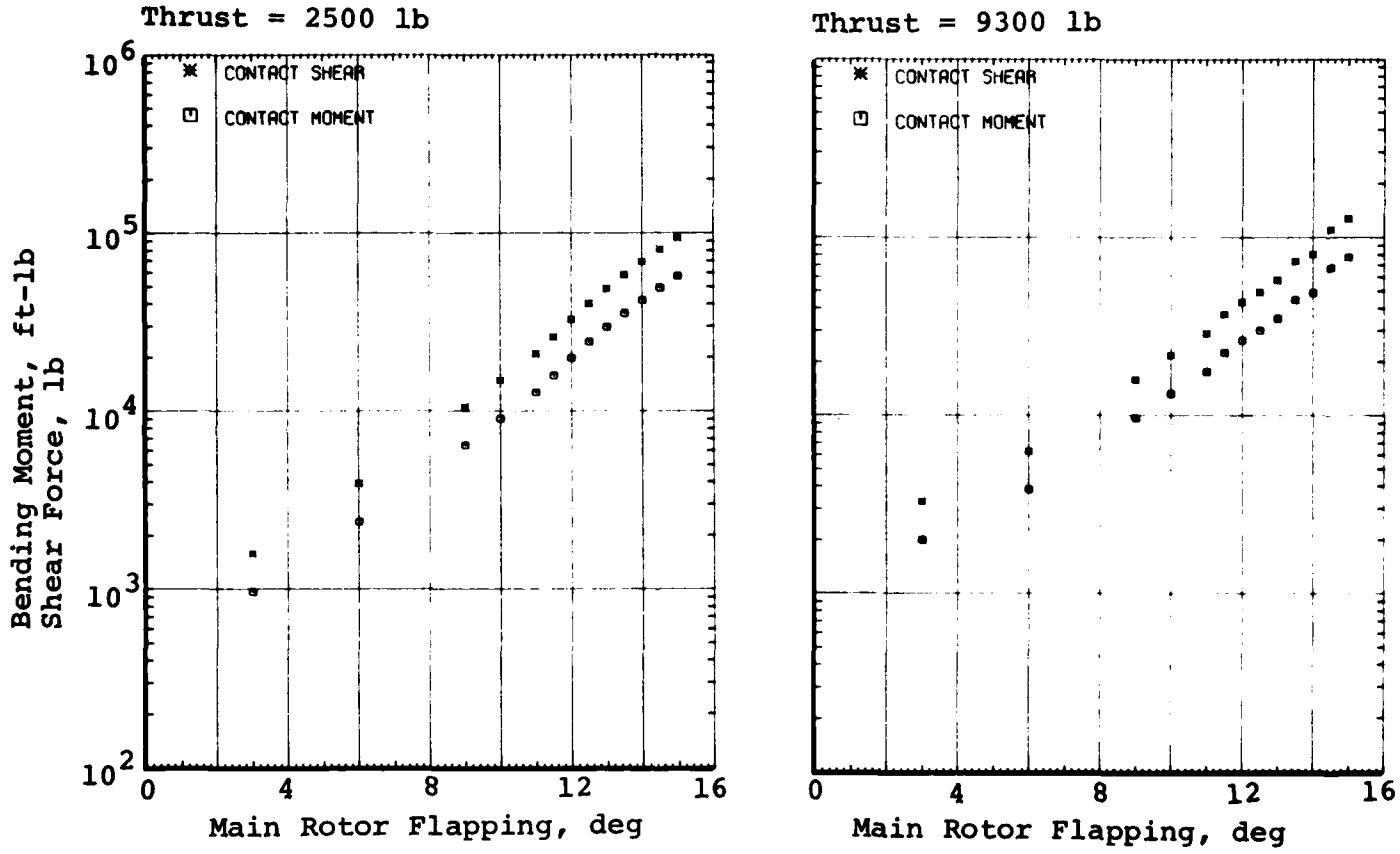

Figure 27. Loads at mast contact point for baseline UH-1H with proposed nonlinear hub spring.

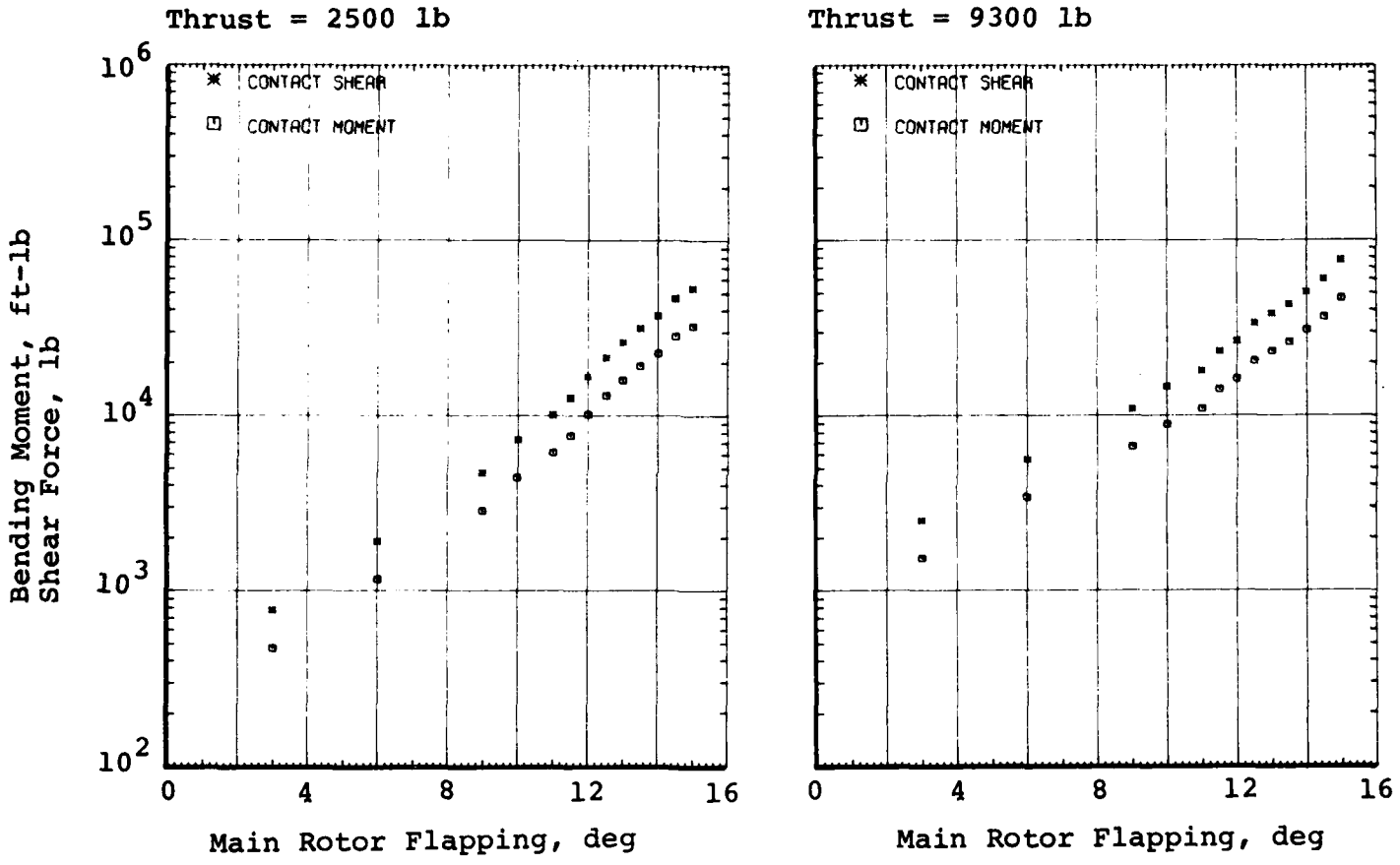

Figure 28. Loads at mast contact point for baseline UH-1H with nonlinear hub spring (half proposed spring rates).

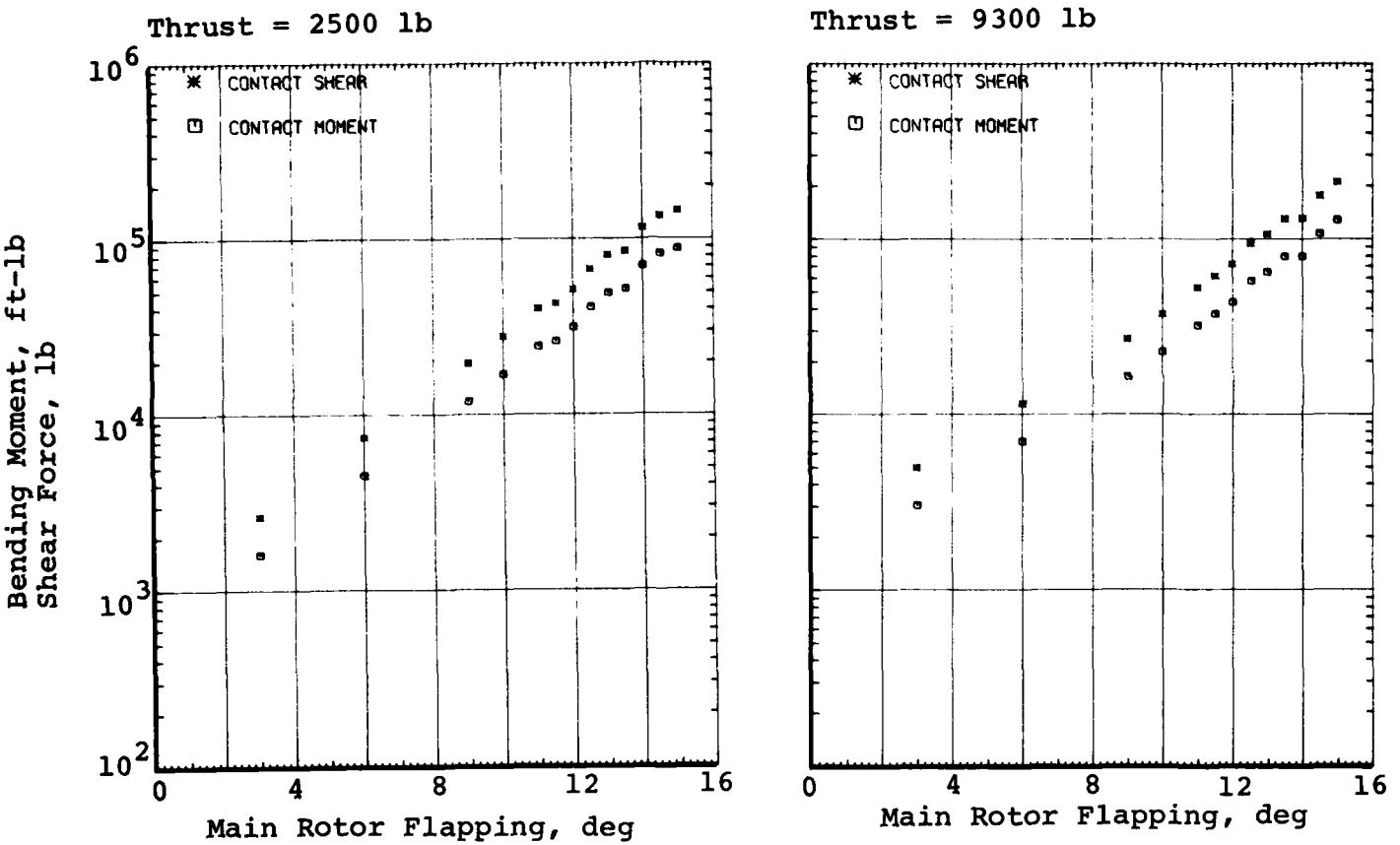

Figure 29. Loads at mast contact point for baseline UH-1H with nonlinear hub spring (double proposed spring rates).

Half Pylon Mount Spring Rate K_{FS} = 92,400 ft-lb/rad

Double Pylon Mount Spring Rate K_{FS} = 157,000 ft-lb/rad

The results of these runs are shown in Figures 30 and 31. Softening the pylon mounts by a factor of 2 reduces the mast loads markedly at low thrust, and a lesser reduction is observed at high thrust. This result is not surprising, as the moment due to flapping stop impact has been reduced due to the large reduction in K_{FS}. Doubling the pylon mount spring rate increases the mast loads a small amount due to the increase in K_{FS}.

4.1.3 Variation of Mast Stiffness

Calculations were made using aircraft configurations in which that portion of the mast above the transmission had half and double its normal stiffnesses. Again, the UH-1H NASTRAN model was modified and new aircraft mode shapes and flapping stop spring rates were computed. The resulting values of K_{FS} were:

Half Mast Stiffness K_{FS} = 83,750 ft-lb/rad

Double Mast Stiffness K_{FS} = 169,300 ft-lb/rad

The simulation results are given in Figures 32 and 33. As expected, softening the mast lowered the loads, while stiffening increased it.

4.1.4 Summary of Variation of Parameters

The only aircraft modifications that lowered the mast loads due to flapping stop impact were softening the pylon mounts or softening the mast. Both pylon mount stiffness and mast stiffness are determined by other criteria, though neither of these is a practical remedy. Installation of the linear and nonlinear flapping springs increases the mast loads but decreases the amount of flapping required for a given flight condition due to the significant increase in control power.

4.2 STOP CONTACT LOAD PREDICTION

The prediction of mast loads due to flapping stop contact by the ARHF01 program has been shown to be accurate for the

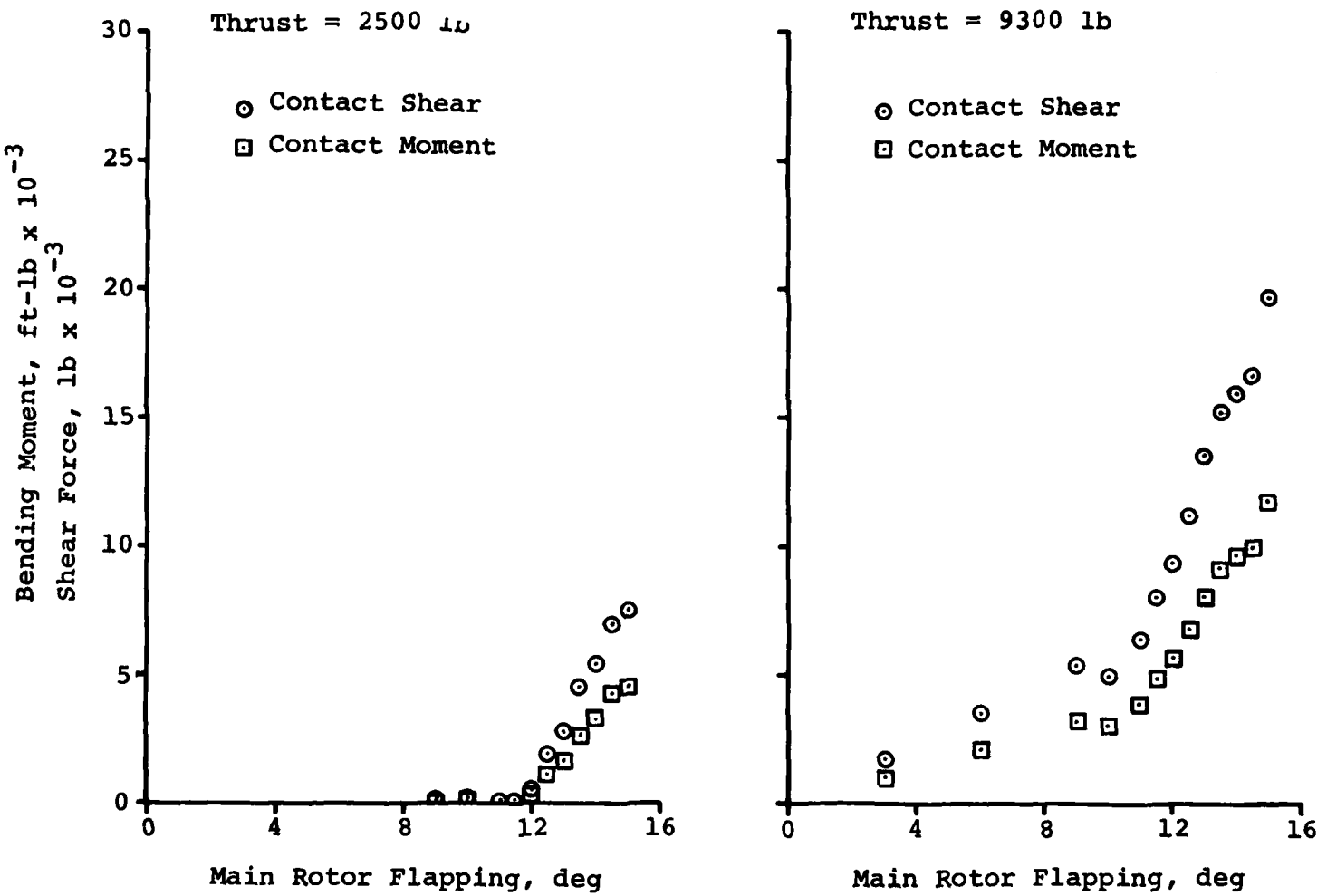

Figure 30. Loads at mast contact point for baseline UH-1H with half pylon mount stiffness.

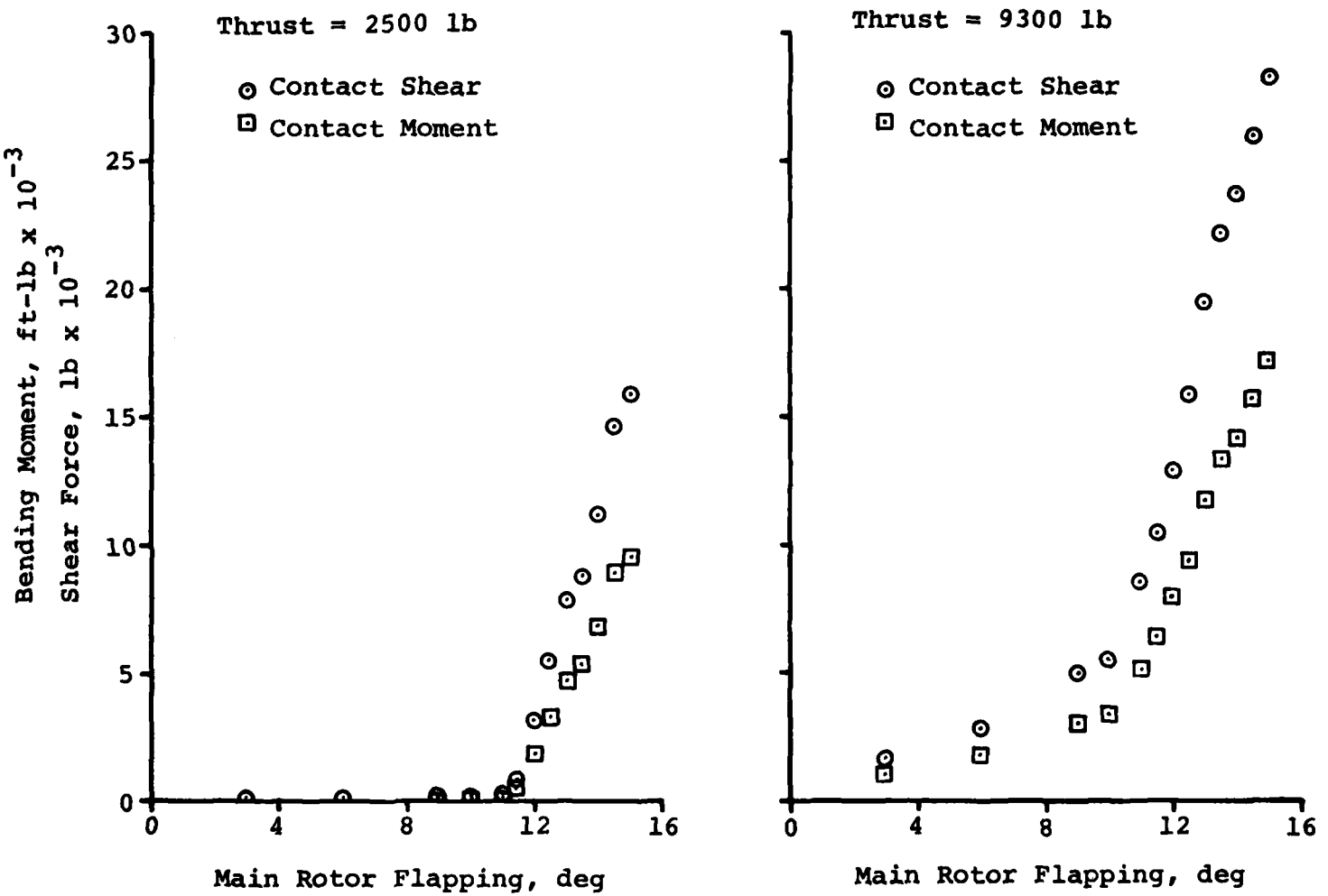

Figure 31. Loads at mast contact point for baseline UH-1H with double pylon mount stiffness.

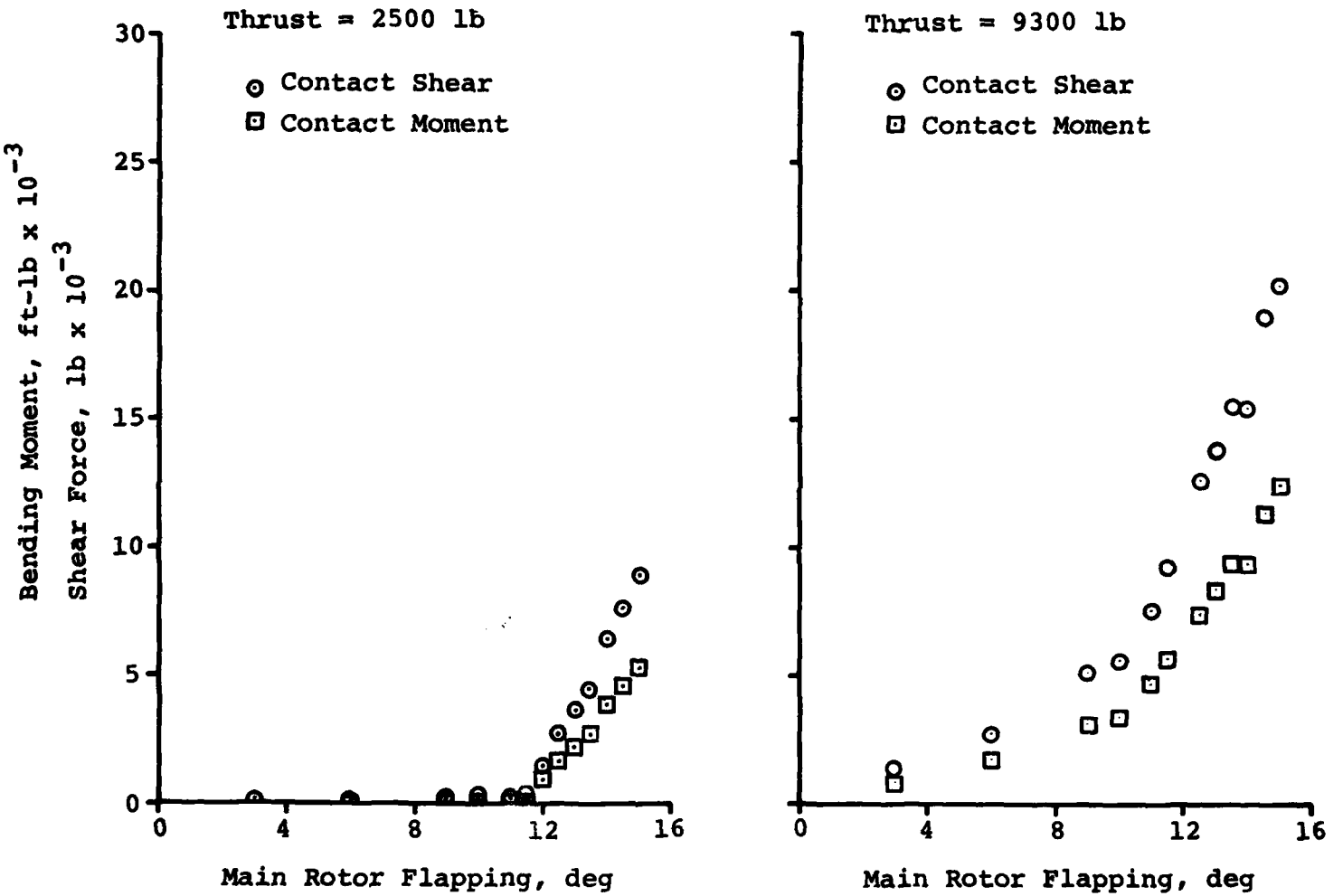

Figure 32. Loads at mast contact point for baseline UH-1H with half mast stiffness.

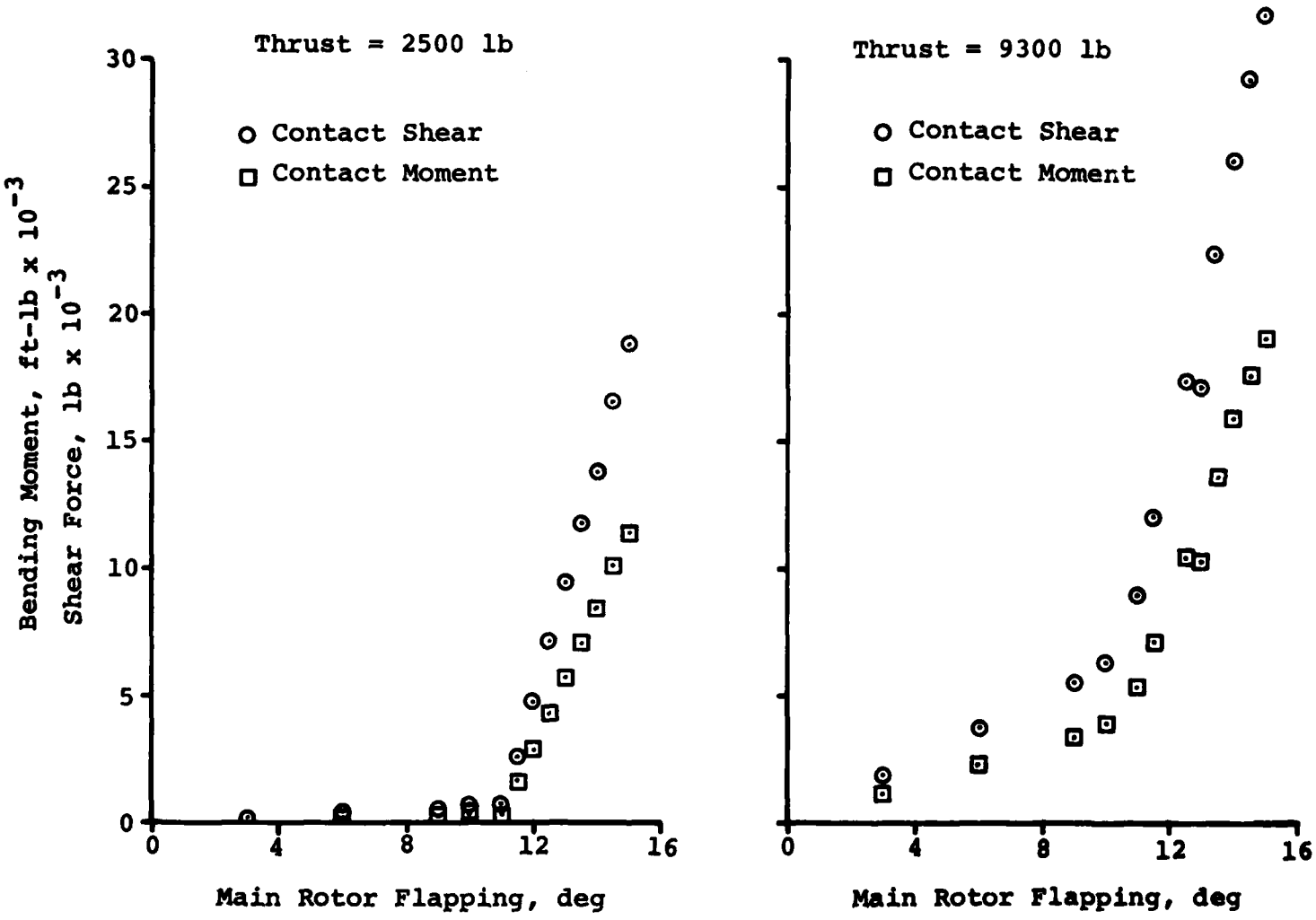

Figure 33. Loads at mast contact point for baseline UH-1H with double mast stiffness.

model rotor as discussed in Paragraph 2.2. For the full-scale UH-1H, however, the problem encountered in accounting for the inplane shear loads with the simple blade model used made correlation with test data more difficult. This is discussed in Paragraph 2.3.2.

The prediction of mast loads due to rotor flapping beyond the flapping stop has been discussed and presented graphically in Paragraph 2.2 for a model rotor and in Paragraph 2.3.2 for the full-scale UH-1H. While the model test agrees well with the prediction, no data are available for comparison with the full-scale prediction. However, both predictions follow the same trend of almost linear build-up in moment with commanded flapping. The proposed design criteria for flapping stop contact loads are based on a comparison with these predictions from the hybrid computer program ARHF01. The general trend of mast loads after flapping stop contact for the basic teetering rotor system (no hub restraint) is a linear variation at a constant slope as indicated in the sketch below.

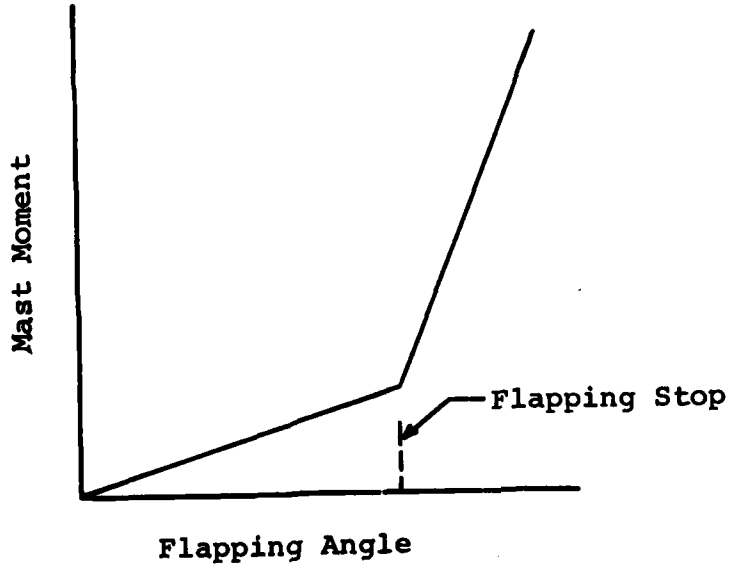

Prior to flapping stop contact, the moments are primarily governed by the level of rotor thrust and thrust vector inclination, while after stop contact, the flapping stop spring rate is the major source of moment. Table 5 gives the slope of moment versus flapping angle beyond the stop as measured from the ARHF01 simulation presented in Figures 30 through 33. These slopes may be considered as the effective flapping stop spring rate for the conditions listed.

The simple theoretical prediction of hub moment given in Table 5 uses an effective theoretical spring rate (K_{EFF_T}) given by

$$K_{EFF_T} = K_{FS} + K_T$$

The derivation of the flapping stop spring rate (K_{FS}) was presented in Section 2.2. The other term in the above equation is the effective spring rate due to rotor thrust (K_T). This term is derived using the moment on the mast at the flapping stop due to rotor thrust, and the flapping angle (β) that the rotor thrust is tilted. While this theoretical model does not include inplane inertial shears, it does provide a reasonable prediction of mast moment. As can be seen from Table 5, the simple prediction was within 25.2 percent of the simulation result in the worst case.

4.3 MAST LOAD CRITERIA

For teetering rotors, the ARHF01 simulation has predicted a linear variation of mast loads with commanded flapping beyond the flapping stop. A simple analysis based on the static calculation of a flapping stop spring rate using conventional structural analysis techniques is able to predict the character of these loads such that a safety factor may be applied to this simple method for design load calculations. With this prediction, the load due to flapping stop contact may be considered in the structural analysis of the rotor system.

Present design criteria consider the mast and hub loads for conditions where the flapping stop does not contact the mast. It is proposed that the following flapping stop shear load (and its associated reaction at the teetering pin) be applied, in addition to the loads considered by existing criteria, to ensure adequate load-carrying capability of the mast, hub, pylon, and fuselage in the event of excessive flapping.

This flapping stop shear load will be calculated as:

$$S \begin{cases} = 0 & \beta_x \leq \beta_s \\ = F_S \, K_{FS}(\beta_x - \beta_S) & \beta_x \quad \beta_x \end{cases}$$

where

S = flapping stop shear load

F_S = factor of safety

K_{FS} = flapping stop spring rate (lb/deg)

β_X = commanded flapping beyond the stop (deg)

β_S = flapping stop angle (deg)

The flapping stop spring rate is calculated statistically as the force at the flapping stop (balanced by a reaction at the teetering pin) which produces a degree of mast deflection at the flapping stop considering the entire mast, pylon suspension, and fuselage structure.

The commanded flapping angle, β_X, and the factor of safety, F_S, must be established by further tests and analysis to ensure that variations in pylon configuration, rotor thrust levels, and other design variables do not affect this formulation.

TABLE 5. EFFECTIVE FLAPPING STOP SPRING RATE

Variable Parameter	Stiffness	Thrust (lb)	ARHF01 Spring Rate (ft-lb/deg)	Simple Theory Spring Rate (ft-lb/deg)	Spring Rate* Ratio
Mast Stiffness	Baseline	2500	2269	2295	0.989
Mast Stiffness	1/2 Baseline	2500	1450	1488	0.974
Mast Stiffness	2 Baseline	2500	2850	2981	0.956
Pylon Spring Rate	Baseline	2500	2269	2295	0.989
Pylon Spring Rate	1/2 Baseline	2500	1560	1639	0.952
Pylon Spring Rate	2 Baseline	2500	2900	2766	1.048
Mast Stiffness	Baseline	9300	2900	2365	1.226
Mast Stiffness	1/2 Baseline	9300	1950	1558	1.252
Mast Stiffness	2 Baseline	9300	3450	3051	1.131
Pylon Spring Rate	Baseline	9300	2900	2365	1.226
Pylon Spring Rate	1/2 Baseline	9300	2050	1709	1.200
Pylon Spring Rate	2 Baseline	9300	3100	2836	1.093

$$*\text{Spring Rate Ratio} = \frac{\text{ARHF01 Spring Rate}}{\text{Simple Theory Spring Rate}}$$

5. ELASTIC ROTOR EFFECTS

The severity of the maneuvers required for high flapping is such that the aeroelastic effects may significantly affect the predicted values of hub flapping. In order to determine the influence of elastic blades on predicted hub flapping, main rotor blade mode shapes were included in the AH-1G Rotorcraft Flight Simulation Computer Program C81 (hybrid version) data deck. The mode type and its natural frequency are shown in Table 6.

TABLE 6. MODE SHAPES

	Mode Type	Natural Frequency (/Rev)
1	Rigid Body	0.999
2	Cyclic	1.678
3	Cyclic	2.522
4	Cyclic	2.903
5	Collective	1.043
6	Collective	2.438
7	Collective	3.044

The modified AH-1G data deck was used as input to the digital version of C81, which allows elastic blades; the predicted values of the hub flapping were compared to the hub flapping predicted by the hybrid version of C81, which allows only rigid blades. This comparison was made for steady flight conditions and transient flight conditions.

5.1 STEADY FLIGHT CONDITIONS

The steady flight conditions selected for comparison were level flight, airspeed sweeps. The airspeed was varied from 40 to 140 knots in increments of 20 knots. The gross weight and center-of-gravity combinations are shown in Table 7.

In general, the parameters exhibit good correlation. The differences in predicted main rotor flapping are less than 1.5 degrees in all cases.

TABLE 7. GROSS WEIGHT AND CENTER-OF-GRAVITY CONDITIONS

Condition	Gross Weight (lb)	Center-of-gravity (in.)
1	10,000	200.0
2	10,000	142.5
3	7,000	190.0
4	6,000	201.0

(Note: Main rotor hub centerline is located at sta 133 in.)

The values of main rotor flapping predicted by the hybrid version of C81, and the digital version using the quasistatic-time variant trim routines are shown in Figure 34.

5.2 TRANSIENT CONDITIONS

The transient maneuvers selected for comparison were a cyclic pullup to 1.85g and a cyclic pushover to 0.25g. Peak predicted flapping during both of these maneuvers was 6.5 degrees.

The hybrid version of C81 utilizes both stability augmentation and an autopilot as an aid to the user during steady state and transient flight conditions. These models are not available to the user of the digital version of C81, and the user must "fly" the model. Thus, the control motions for a simulated maneuver using the hybrid version of C81 will change dramatically when the same maneuver is simulated using the digital version of C81. The reverse is also true. Therefore, rather than duplicate control motions, an attempt was made to duplicate aircraft attitude rates of change.

Illustrated in Figure 35 is the comparison between the hybrid (rigid blades) and the digital (elastic blades) of the cyclic pull-up maneuver. Good correlation was obtained in the pitch axis, while only fair correlation was achieved in the roll axis. Both main rotor flapping and load factor do, however, show good correlation. In both cases, main rotor flapping peaks with maximum rate.

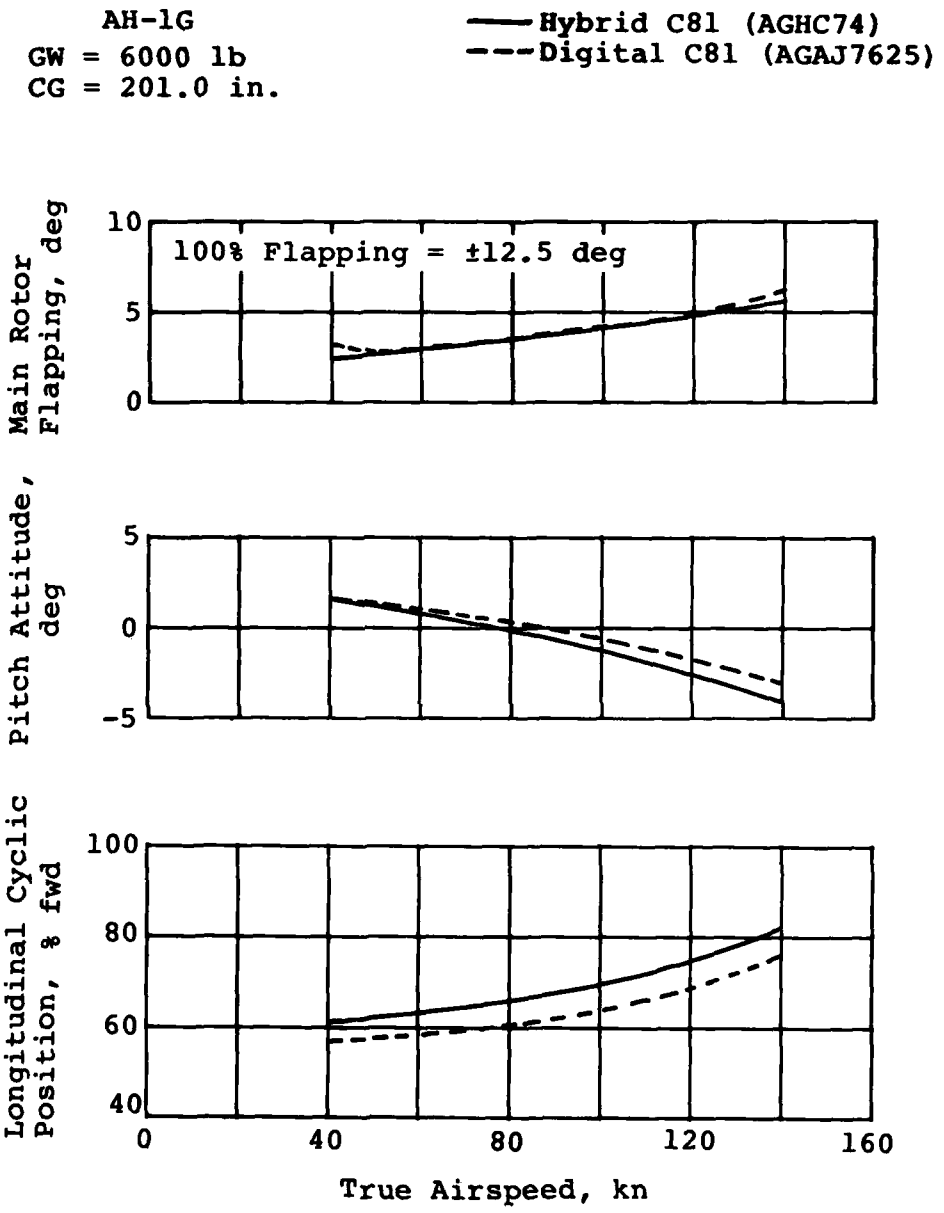

Figure 34. Effects of elastic main rotor blades on helicopter parameter predictions during simulated level flight.

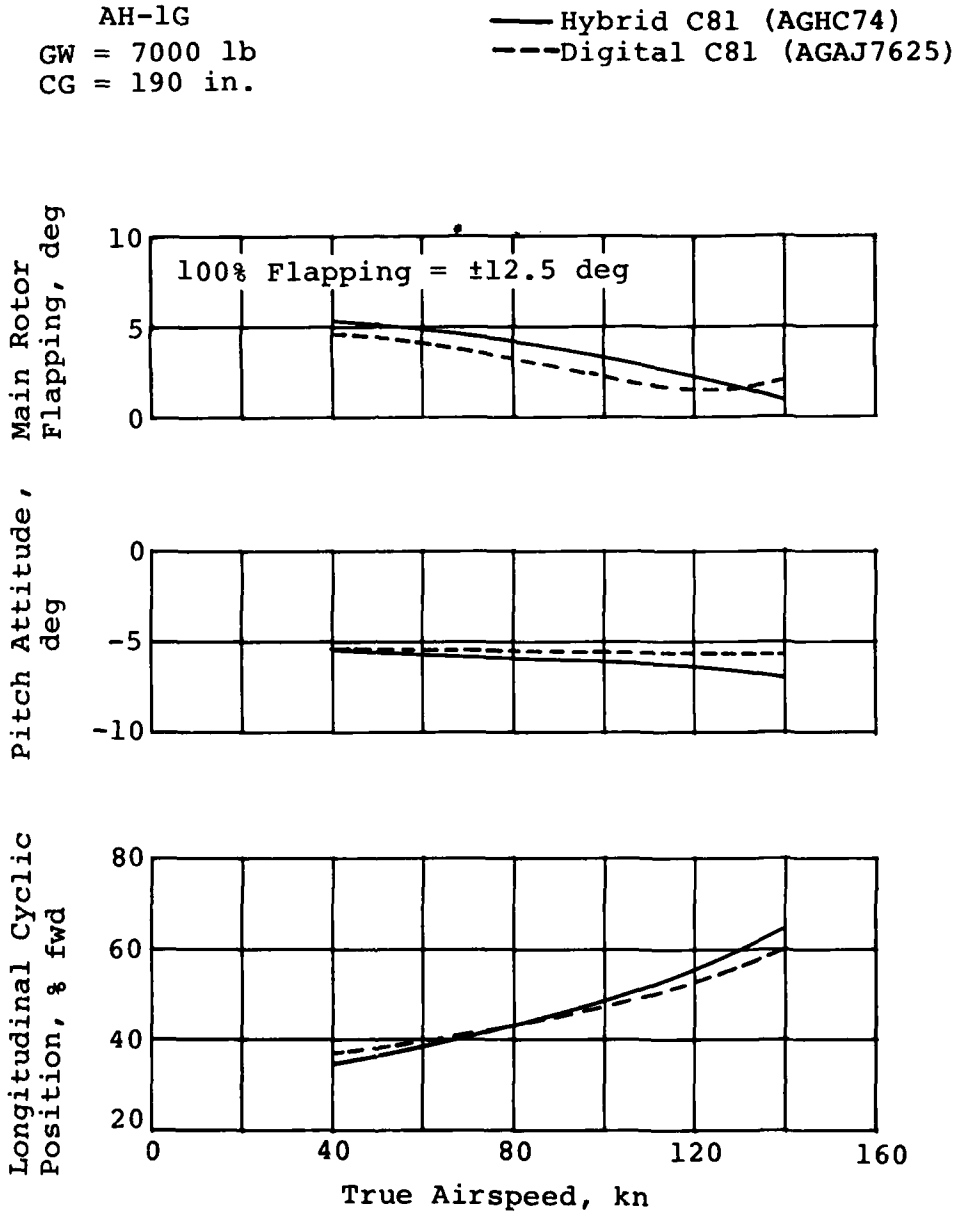

Figure 34. Continued.

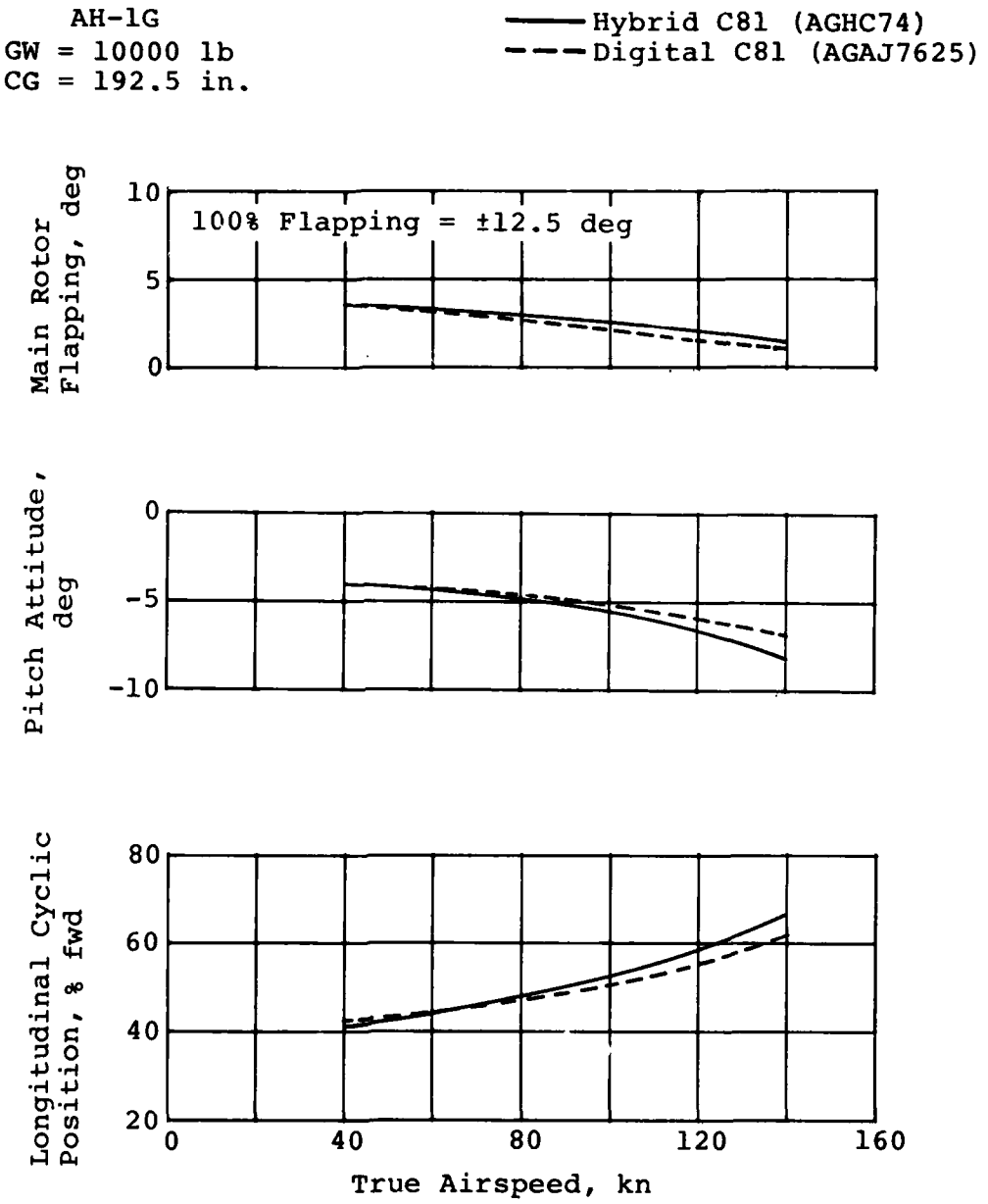

Figure 34. Continued.

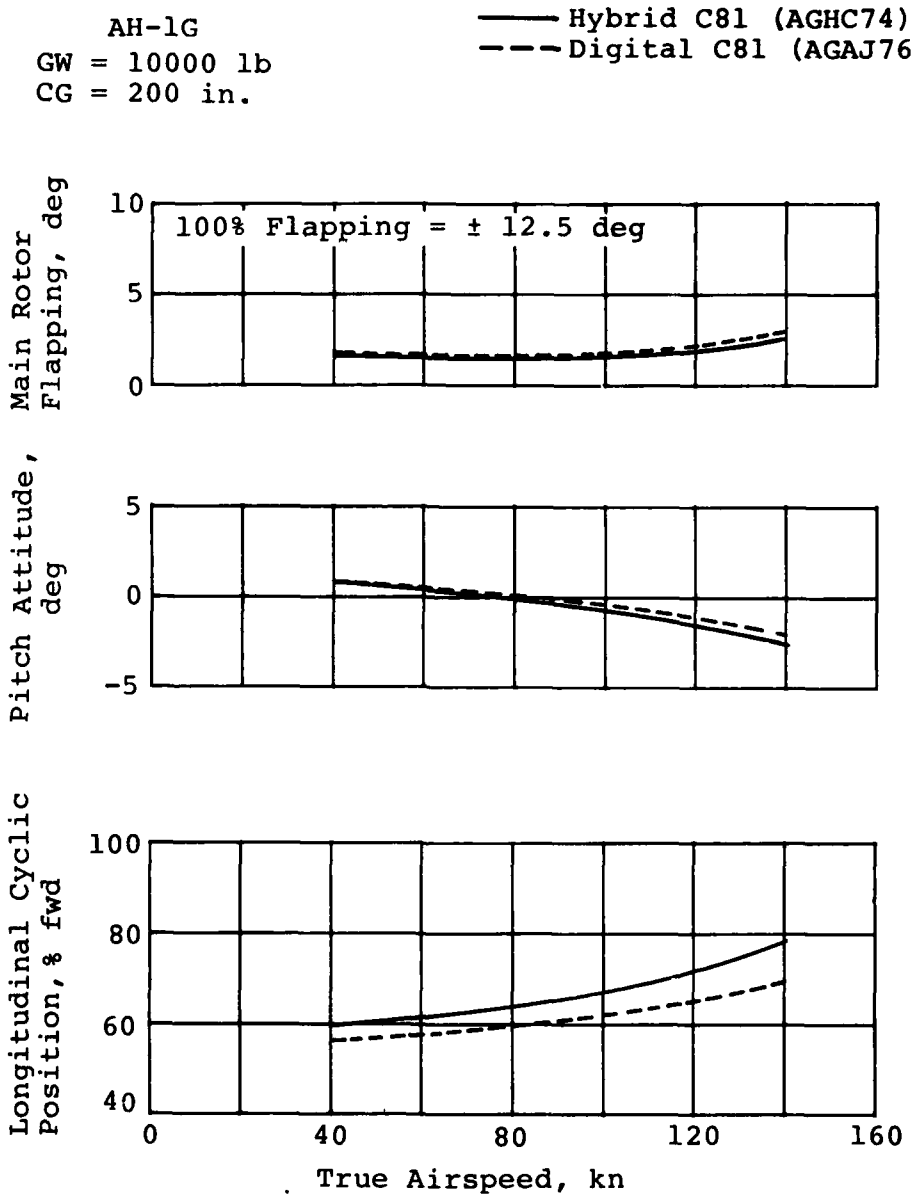

Figure 34. Concluded.

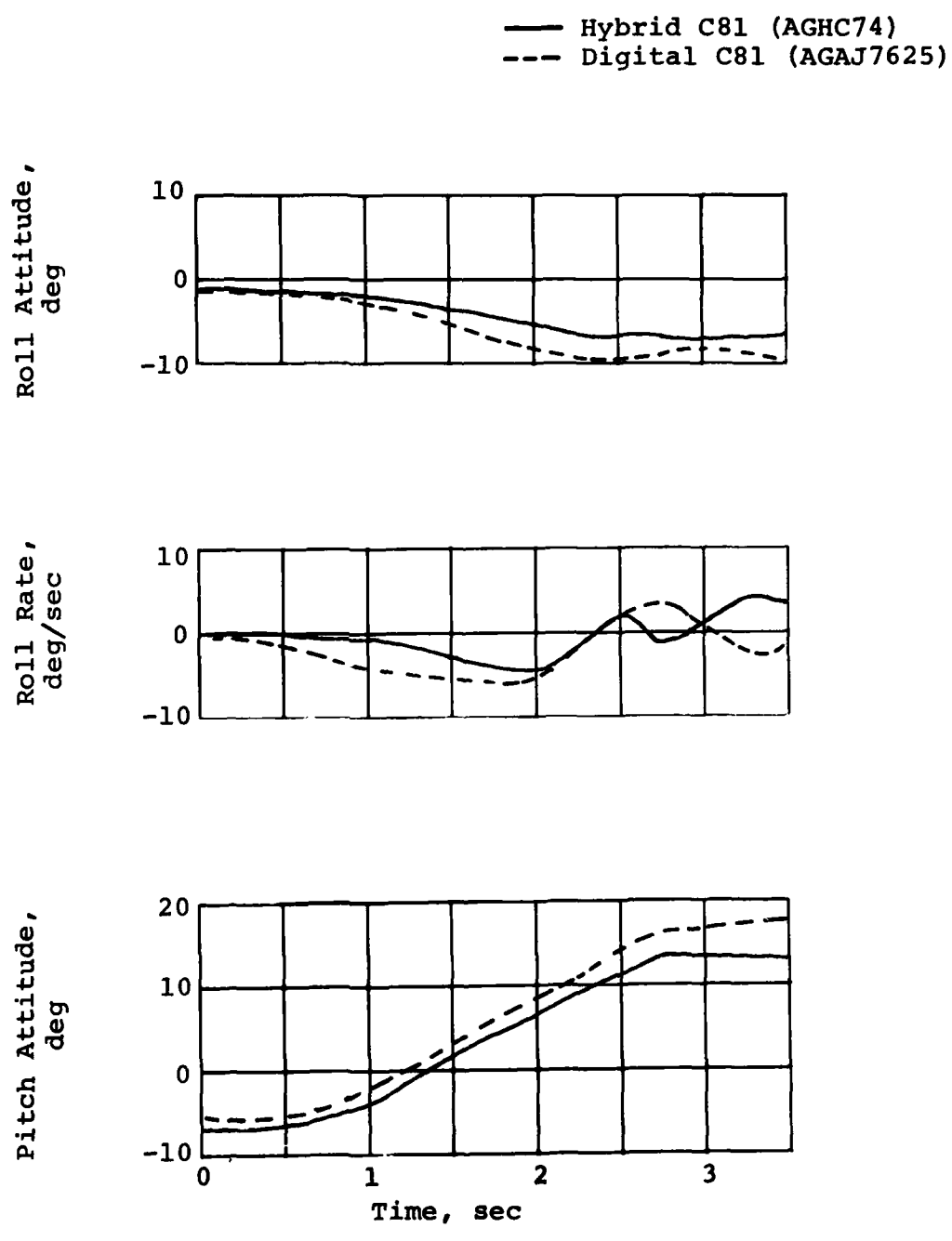

Figure 35. Effects of elastic main rotor blades on helicopter parameter predictions during a simulated pull-up.

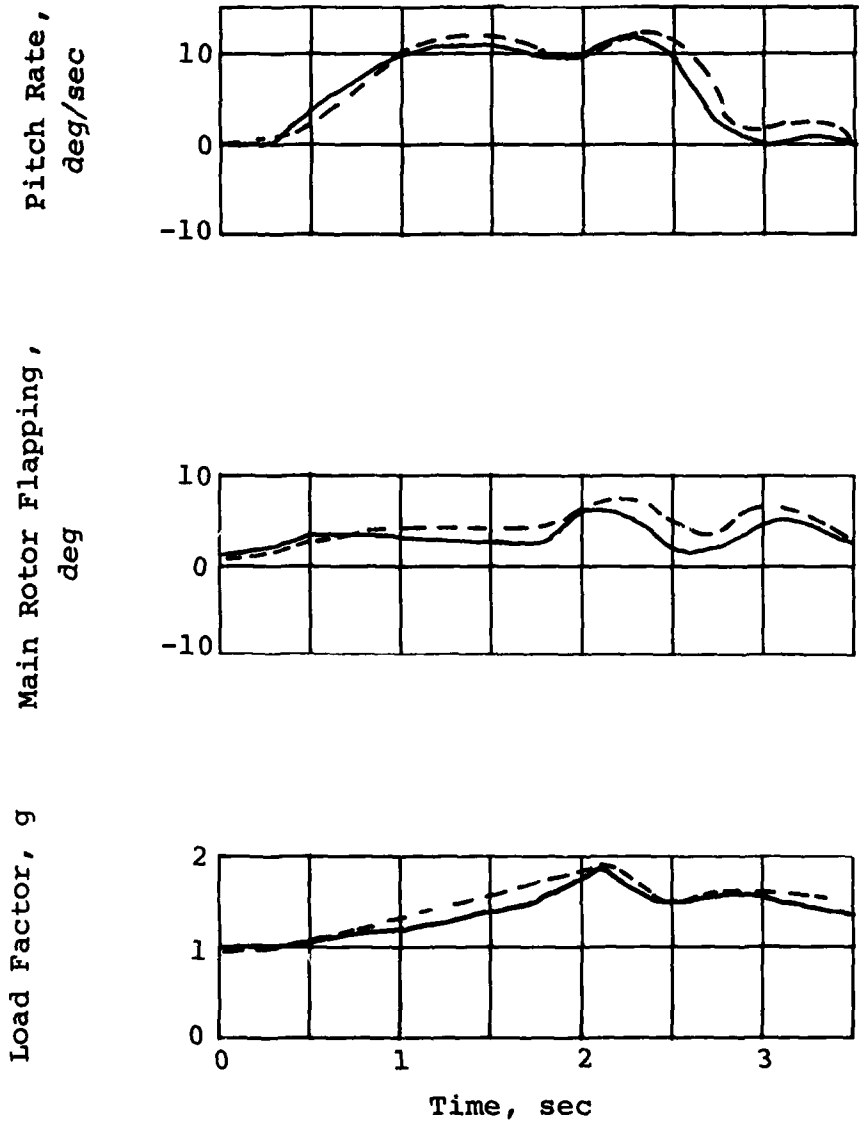

Figure 35. Concluded.

In the case of the pushover, shown in Figure 36, good correlation is obtained in both the pitch and roll axis until approximately 8 seconds into the maneuver. Main rotor flapping and load factor exhibit good correlation until approximately 6.5 seconds. Loss of main rotor flapping correlation and the large flapping amplitude predicted by digital C81 is not the result of the addition of elastic blades, but rather the increased sensitivity and lack of an autopilot in the digital model. These factors cause larger cyclic commands than were required for hybrid C81 to match fuselage motions. These larger cyclic commands can result in as much as 4 degrees more swashplate motion and, therefore, higher main rotor flapping. The poor correlation of main rotor flapping in the pushover maneuver is caused by the larger cyclic motions.

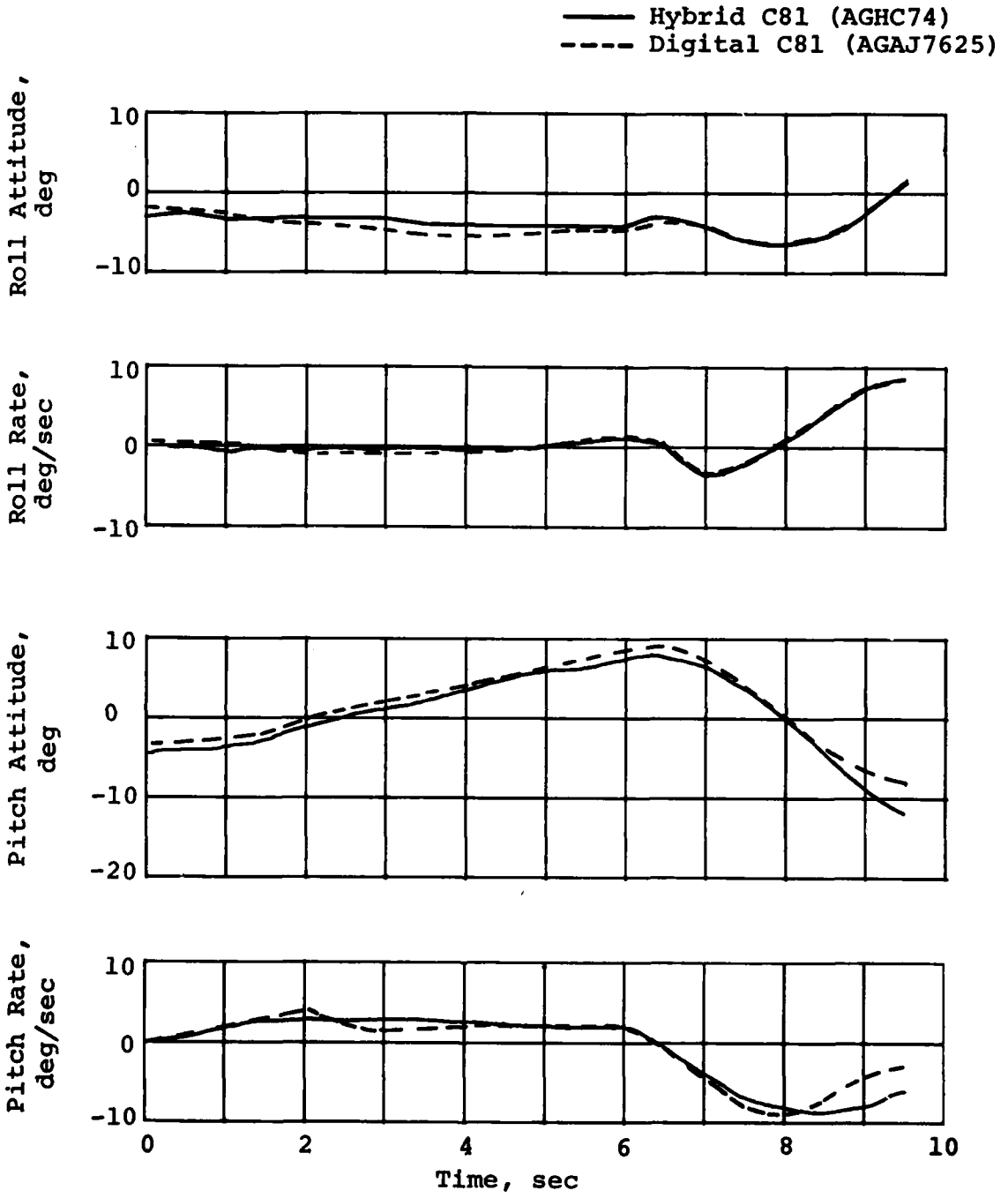

Figure 36. Effects of elastic main rotor blades on helicopter parameter predictions during a simulated pushover.

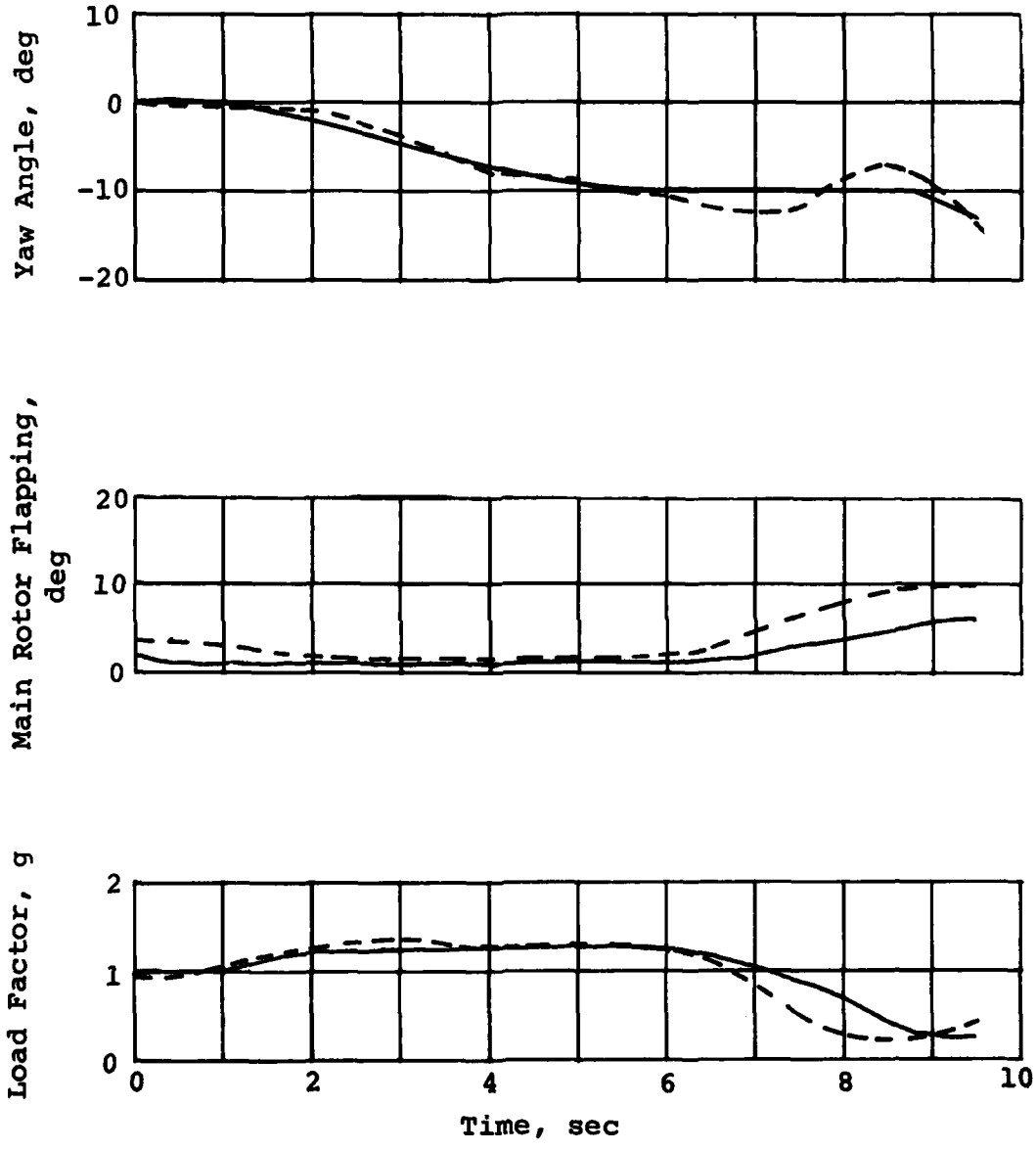

Figure 36. Concluded.

6. TACTICS EVALUATION

A review and evaluation of U.S. Army Aviation tactical literature and an observation flight at the Army's UH-1 nap-of-the-earth (NOE) course at Fort Rucker, Alabama, was made in order to evaluate the current U.S. Army helicopter tactics. The purpose of this evaluation was to assess the possibility of current tactics leading to high flapping situations. Any maneuvers so identified would be included in the flight test program.

6.1 EVALUATION OF TACTICAL LITERATURE

The U.S. Army Field Manuals (FMs) and Training Circulars (TCs) provided by the Army for analysis are listed in Table 8. The tactics and the associated maneuvers described in the literature were judged as potentially high flapping producers against the critical flight conditions identified in Reference 1 as distinct contributors to large flapping amplitudes. According to Reference 1, large flapping amplitudes could be expected when simulated helicopters were operated under any of the following conditions:

- at center-of-gravity extremes
- under low or negative g conditions
- with large, abrupt control inputs
- in conditions involving significant retreating blade stall

6.2 UH-1 NOE COURSE

An observation flight over the UH-1 NOE course at Fort Rucker, Alabama, was made with a Government/Industry team consisting of a Bell Helicopter experimental pilot and an engineer and the Army project engineer. The Army instructor pilot (IP) demonstrated the various techniques of low-level, contour and NOE flight over one of several NOE courses at Fort Rucker. The IP pointed out that these three flight categories differ in speed and altitude variations exercised by the pilot. The primary variable that governs which flight mode is to be employed is the type of enemy threat known or considered to be in the operating area. Low-level flight consists of constant airspeed and constant altitude, usually approximately 50 feet above the highest obstacle in the area. Contour flying demonstrates constant velocity with varying altitude to remain a

minimum safe height above major terrain features. Nap-of-the-earth flight requires the varying of both airspeed and altitude to maintain the least possible exposure.

TABLE 8. U.S. ARMY TACTICAL MANUALS

Number	Title	Date of Publication
FM 1-105	Aviator's Handbook	August 1974
FM 1-1	Terrain Flying	October 1975
TC 1-28	Rotary Wing Night Flight	February 1976
FM 1-51	Rotary Wing Flight	May 1974
TC 1-4	Helicopter Gunnery	September 1976
TC 17-17	Gunnery Training for Attack Helicopters	December 1975
FM 1-5	Instrument Flying and Navigation for Army Aviators	March 1976

Most of the demonstration flying was done at tree-top level in the 40- to 60-knot range, with some flight at several hundred feet and about 80 knots. Seldom did the aircraft venture below tree level except for a demonstration of the NOE "quickstop" and the masking/unmasking or bob-up maneuvers. The maneuvers determined to be most critical in requiring abrupt cyclic inputs and thus large flapping values, although none seemed to task the flapping limit of the vehicle, included evasive turn reversals and pull-up/push-over combinations. The turn or rcll reversals were characterized by a level flight zigzag maneuver. During the maneuver, the aircraft was sharply banked in one direction and then the other in order to return to the original course. Maneuvers that commenced from IGE hover were the NOE quickstop, the bob-up, and dashes; all of which were demonstrated. The IP indicated that large, abrupt cyclic inputs were uncommon. Such control inputs were encountered rarely and usually only when a student pilot responded incorrectly to a simulated or actual emergency condition. Following the demonstration flight, the Army/BHT

team met with several other UH-1 NOE IP's in order to determine if any other operational NOE maneuvers were susceptible to high flapping.

The BHT team interviewed the IP's at the Scout/ Attack School the following day. These conversations revealed that in addition to the NOE course, there was an agility course. This course is limited in its use to Scout and attack-type helicopters, and a more aggressive flight profile is flown in order to avoid simulated threats. Although no demonstration flights were given, the agility course should be evaluated in order to assess the possibility of NOE flight and NOE tactics, as associated with the Scout/attack environment, leading to high flapping situations.

6.3 TACTICS EVALUATION SUMMARY

Applying the criteria from Reference 1 for judging large flapping amplitudes, it was determined that flying at the forward center-of-gravity extremes, maneuvers requiring abrupt, large amplitude cyclic inputs such as evasive maneuvers, and the combination of these could result in large flapping amplitudes. In order to determine the order of magnitude of main rotor flapping during these NOE maneuvers, the sideward dash, the NOE quickstop, and the level flight roll reversal were added to the flight test program. As a result of the tactics evaluation, three NOE maneuvers were added to the flight test plan in order that main rotor flapping amplitudes could be determined. The level flight roll reversal and NOE quick-stop were determined to be of interest from the NOE demonstration flight, and the lateral, or sideward, dash was selected following evaluation of the tactical literature. The flapping amplitudes measured while performing these maneuvers are presented in section 7.2.2.

7. FLIGHT TEST PROGRAM

The helicopter used for this program was a U.S. Army Model UH-1H helicopter, pictured in Figure 37, equipped with a thick-wall mast (part number 204-011-450-7). The helicopter was instrumented as described in Reference 5. The contracted flight test program consisted of evaluating a baseline, or standard, helicopter against the same helicopter with a non-linear hub spring installed. The conditions that were to be flown are described in Reference 6. Cost and schedule constraints dictated that the hub spring be evaluated in less than ideal weather for handling qualities tests. In the following subsections, the objective and results of the flight test program are presented.

7.1 PROGRAM OBJECTIVE

The objective of this flight test program was to determine if a nonlinear hub spring would improve the mast bumping safety margin and, at the same time, not degrade the handling qualities, any component life, or the vibration levels of the UH-1H helicopter. Improved safety margin is demonstrated by reduced main rotor flapping in all flight conditions and increased control power at low-g flight conditions. In order to meet this objective, a flight test program that included steady flight conditions, handling qualities tests, nap-of-the-earth (NOE) maneuvers, low-g flight conditions, and steady high flapping flight conditions was defined and conducted.

7.2 EFFECT OF THE HUB SPRING ON MAST BUMPING SAFETY MARGIN

For the UH-1, an improved mast bumping safety margin can be shown if main rotor flapping is reduced for all flight conditions. This is achieved by increasing the flapping-stop-to-mast clearance. Additionally, positive control of the helicopter during low-g maneuvers would indicate an improved mast bumping safety margin, since mast bumping has been associated with loss of lateral control power at low g. In order to determine the effect of the hub spring on main rotor flapping and low-g control power, a series of tests representing

---

[5]Bonham, D. G., and Hollifield, P. J., UH-1 HUB SPRING INSTRUMENTATION TEST PLAN, BHT Report Number 699-099-095, Bell Helicopter Textron, Fort Worth, Texas, June 1978.

[6]Hollifield, P. J., UH-1 HUB SPRING TEST PLAN, Bell Helicopter Textron Report Number 699-099-099, Bell Helicopter Textron, Fort Worth, Texas, August 1978.

Figure 37. Bell Helicopter Textron UH-1H

steady, maneuvering, and steady high flapping flight conditions as well as flight at low-g were conducted. These conditions were first flown with the basic UH-1 helicopter and then repeated following installation of the hub spring. In order to minimize differences due to pilot technique, the same project pilot flew baseline and hub spring flights.

7.2.1 Main Rotor Flapping Comparisons During Steady Flight Conditions

As expected, the effect of the nonlinear hub spring was to decrease flapping in steady flight conditions. Flapping reductions are greatest when baseline flapping is greater than 4 degrees, due to the additional moment produced by the nonlinear compression spring.

7.2.1.1 Forward and Rearward Level Flight. Figure 38 compares main rotor flapping for worst-case conditions of baseline and hub-spring-installed flights. The greatest reduction is in rearward flight where baseline steady flapping is greatest. The flapping differential ranged from 1 to 3 degrees over the airspeed range tested. While overall flapping differentials were less in forward flight, the hub spring reduced steady flapping to levels below 4 degrees for the entire forward flight speed range.

Due to wind conditions at the time the hub spring tests were conducted, the hover point with hub spring installed is not available.

7.2.1.2 Sideward Flight. The comparison of main rotor flapping at the forward (worst-case) center-of-gravity loading is shown as Figure 39. Airspeeds from 30 knots left to 30 knots right sideward were tested. The increased flapping in right sideward flight is primarily due to the rotor inflow distribution at low advance ratios (Reference 7) causing down aft flapping which adds to the down aft flapping due to the forward center-of-gravity loading.

7.2.1.3 Autorotation and Maximum Continuous Power (MCP) Climb. The reduction in main rotor flapping during autorotation and MCP climb at both extremes of the center-of-gravity envelope is shown in Figures 40 and 41. Although the increase

---

[7]Harris, F. D., ARTICULATED ROTOR BLADE FLAPPING MOTION AT LOW ADVANCE RATIO, Journal of American Helicopter Society, January 1972.

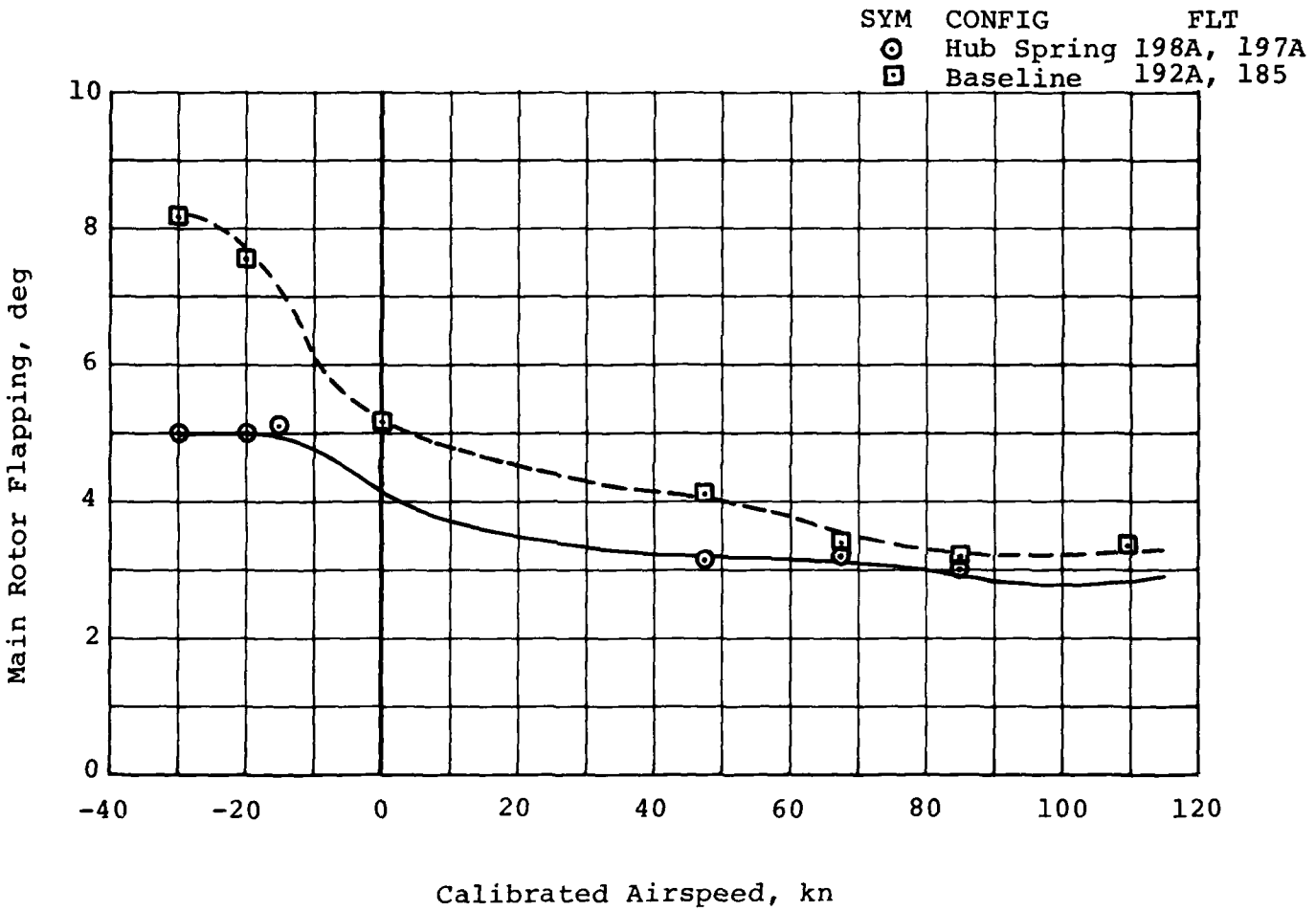

Figure 38. Effect of the hub spring on main rotor flapping in rearward and forward flight at the most critical loading condition.

AD-A098 794 BELL HELICOPTER TEXTRON FORT WORTH TX F/6 1/3
FLIGHT TEST EVALUATION OF A NONLINEAR HUB SPRING ON A UH-1H HEL--ETC(U)
APR 81 P J HOLLIFIELD, L W DOOLEY DAAJ02-77-C-0064
UNCLASSIFIED USAAVRADCOM-TR-80-D-27 NL

2 of 2
USAAVRADCOM

END
DATE FILMED
6-81
DTIC

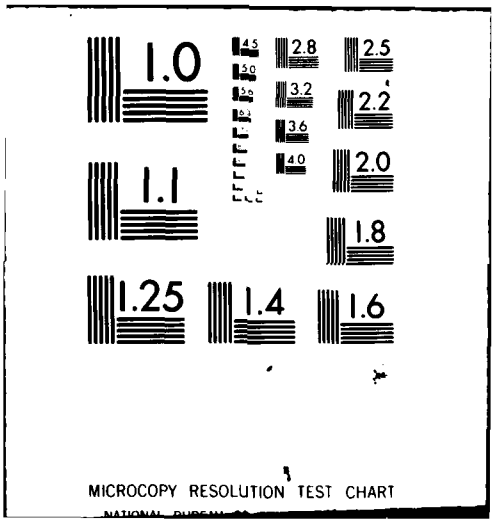
1.0
1.1
1.25
1.4
1.6
1.8
2.0
2.2
2.5
2.8
3.2
3.6
4.0
4.5
5.0
5.6
MICROCOPY RESOLUTION TEST CHART

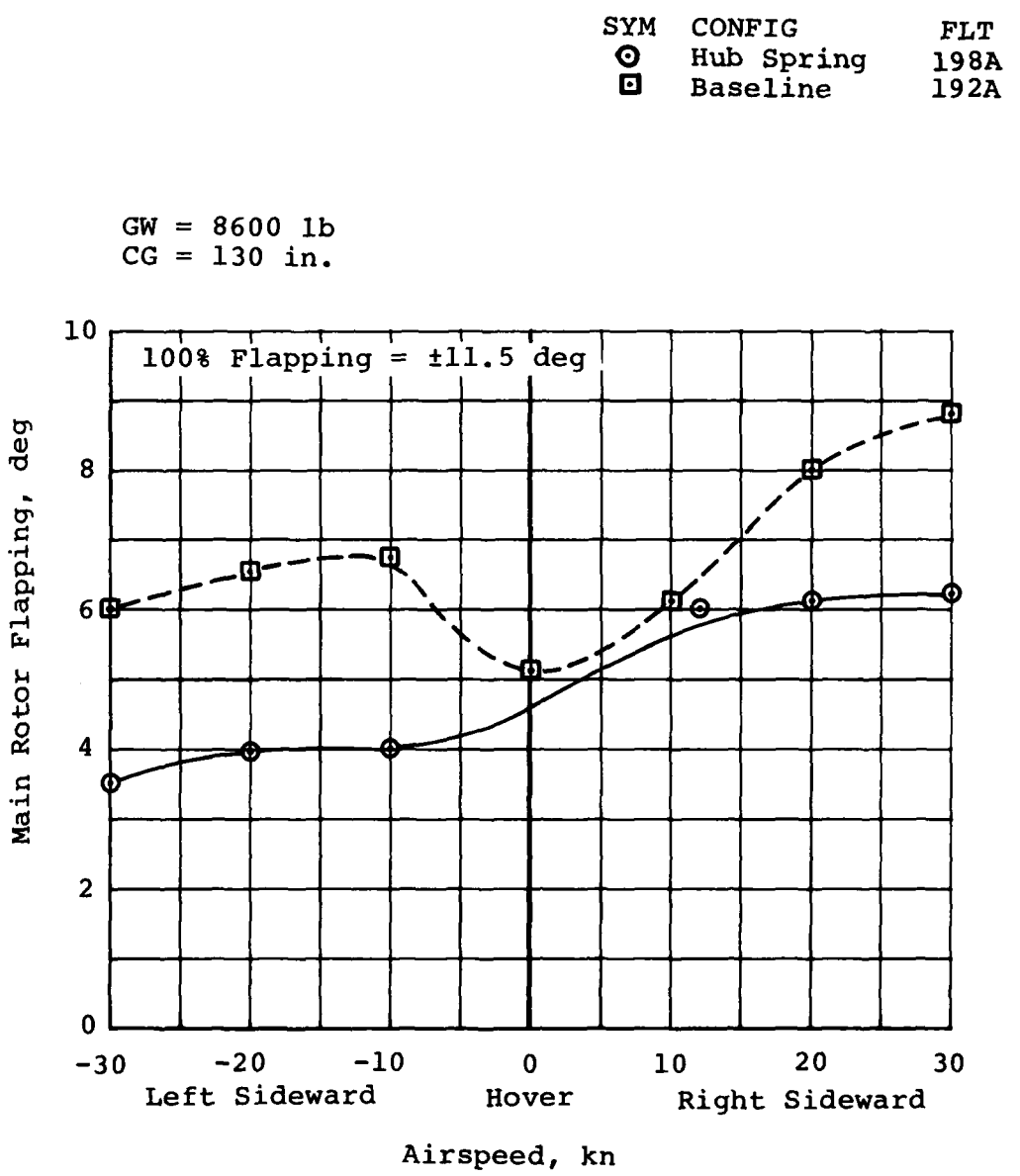

Figure 39. Effect of the hub spring on main rotor flapping in sideward flight.

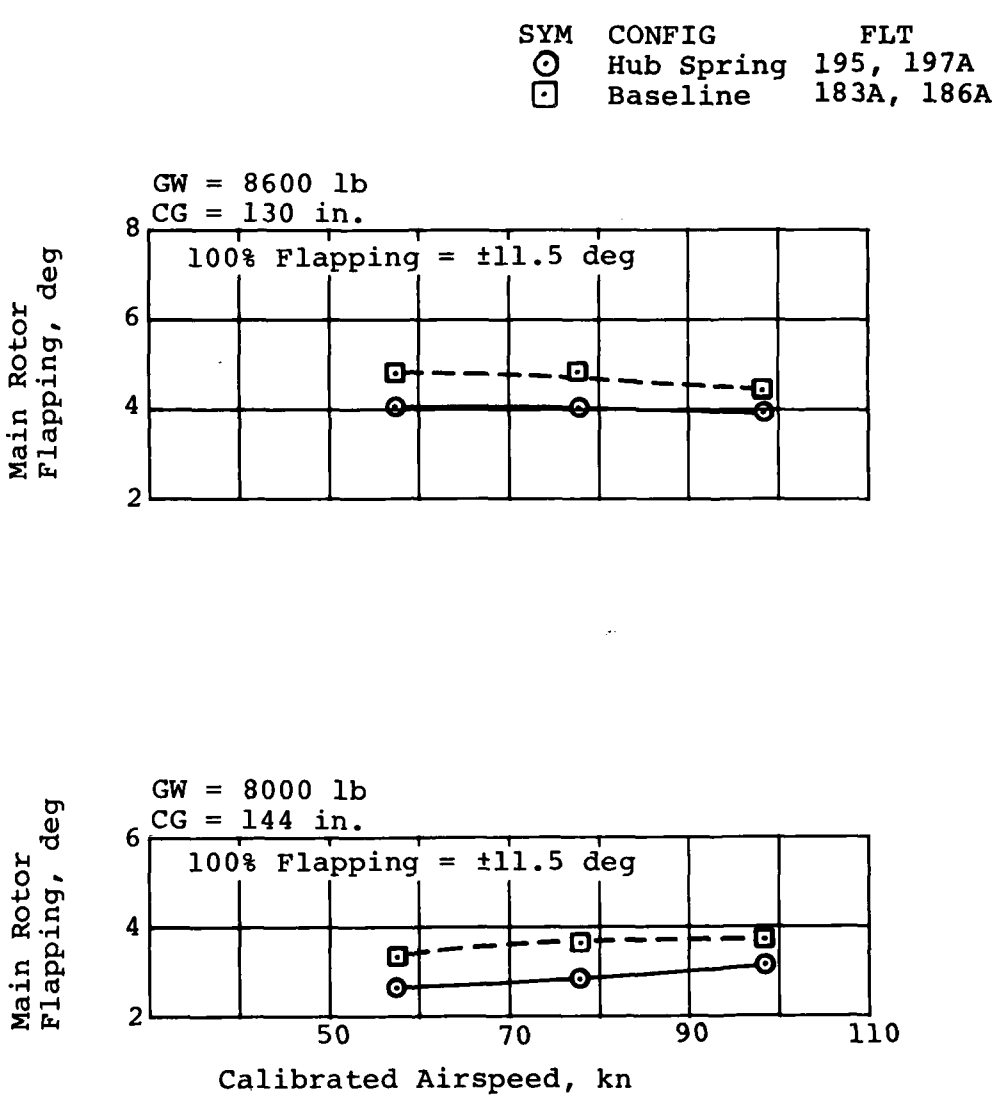

Figure 40. Effect of the hub spring on main rotor flapping during autorotation.

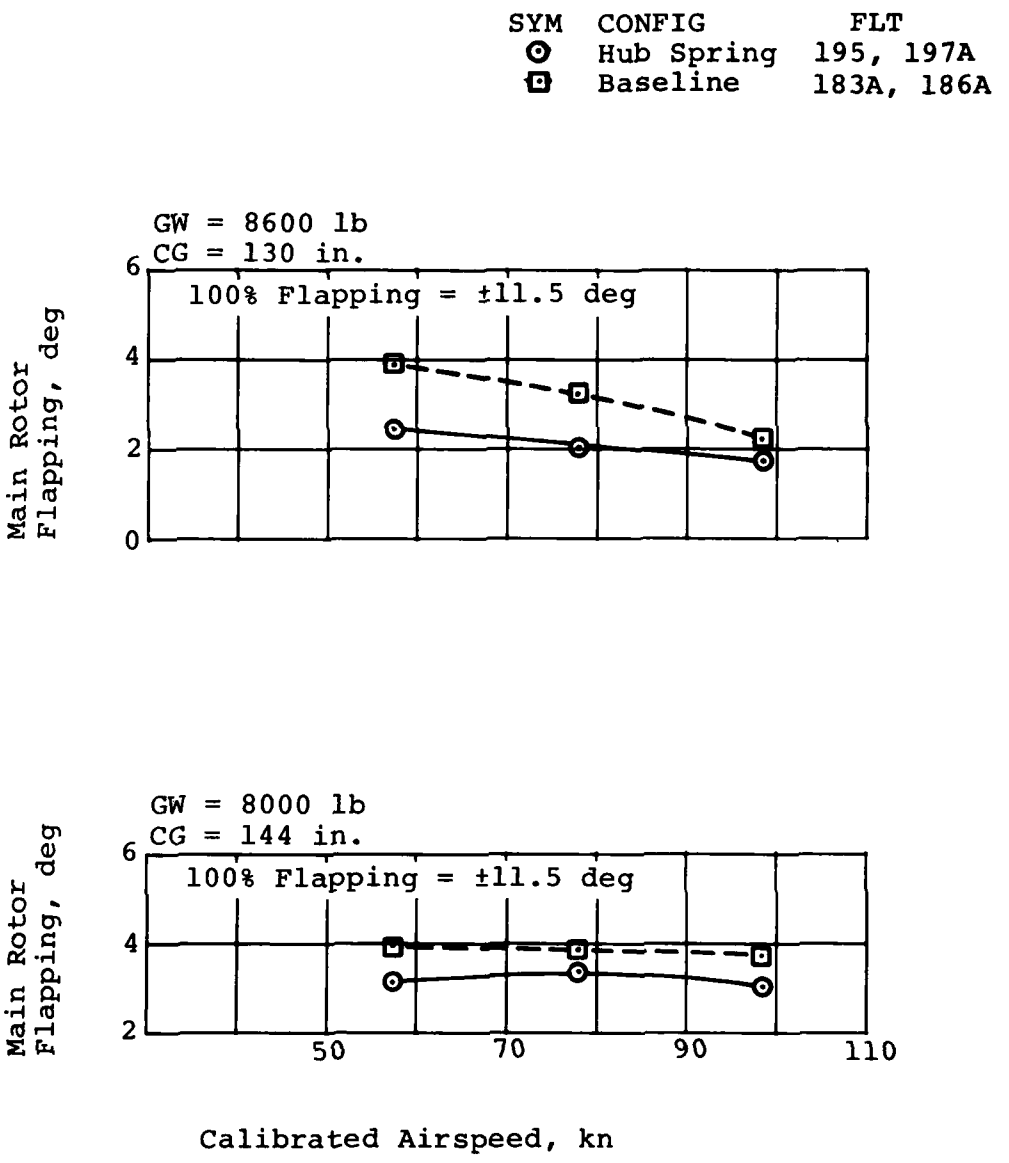

Figure 41. Effect of the hub spring on main rotor flapping during MCP climbs.

in mast bumping safety margin is not as great as in the previous conditions, main rotor flapping has been reduced by at least 1 degree in all cases. For these cases, the baseline flapping is less than 4 degrees, thus the nonlinear compression spring is not exercised.

7.2.1.4 Wind-up Turns. Main rotor flapping during coordinated wind-up turns to over 1.7g is shown in Figure 42. The test procedure used was to stabilize in level flight at the desired airspeed and, maintaining fixed collective, turn while descending in order to remain at the same airspeed. Steady-state data were recorded at several g-levels during the turn.

For wind-up turns at 72 knots ($0.6V_{NE}$), a near constant 1 degree of difference in main rotor flapping is held for all g-levels. At 115 knots (V_{NE}), an even greater flapping reduction is observed.

7.2.2 NOE Maneuver Flapping Comparison

The NOE maneuvers flown were the NOE quickstop, forward and lateral dashes, the pop-up and the bob-up, and the level flight roll reversal. Each of these maneuvers and the apparent effect of the hub spring are presented in the following subsections. Table 9 summarizes the results of the NOE maneuver comparisons. With the hub spring installed, the NOE maneuvers were characterized by either reduced flapping for the same level of maneuver performance, or increased maneuver performance with the same flapping.

7.2.2.1 NOE Quickstop. From 60 knots, the helicopter was decelerated to a hover by increasing collective pitch while simultaneously applying aft cyclic control in order to maintain the constant tail rotor altitude for obstacle clearance. With the hub spring installed, main rotor flapping increased slightly; however, the maximum pitch rate increased more than 50 percent over that of the baseline from 8.0 to 12.5 degrees/second indicating the capability to decelerate faster with the spring installed. As expected, the installation of the hub spring resulted in increased control power.

7.2.2.2 Forward Dash. For the forward dash, the helicopter accelerated from hover to 60 knots and then decelerated to a hover at the maximum rate. The dash, however, was not terminated by the NOE quickstop. In the case of the dash, main rotor flapping was decreased by 0.5 degree with the hub spring, while maximum pitch rate during the maneuver was approximately the same.

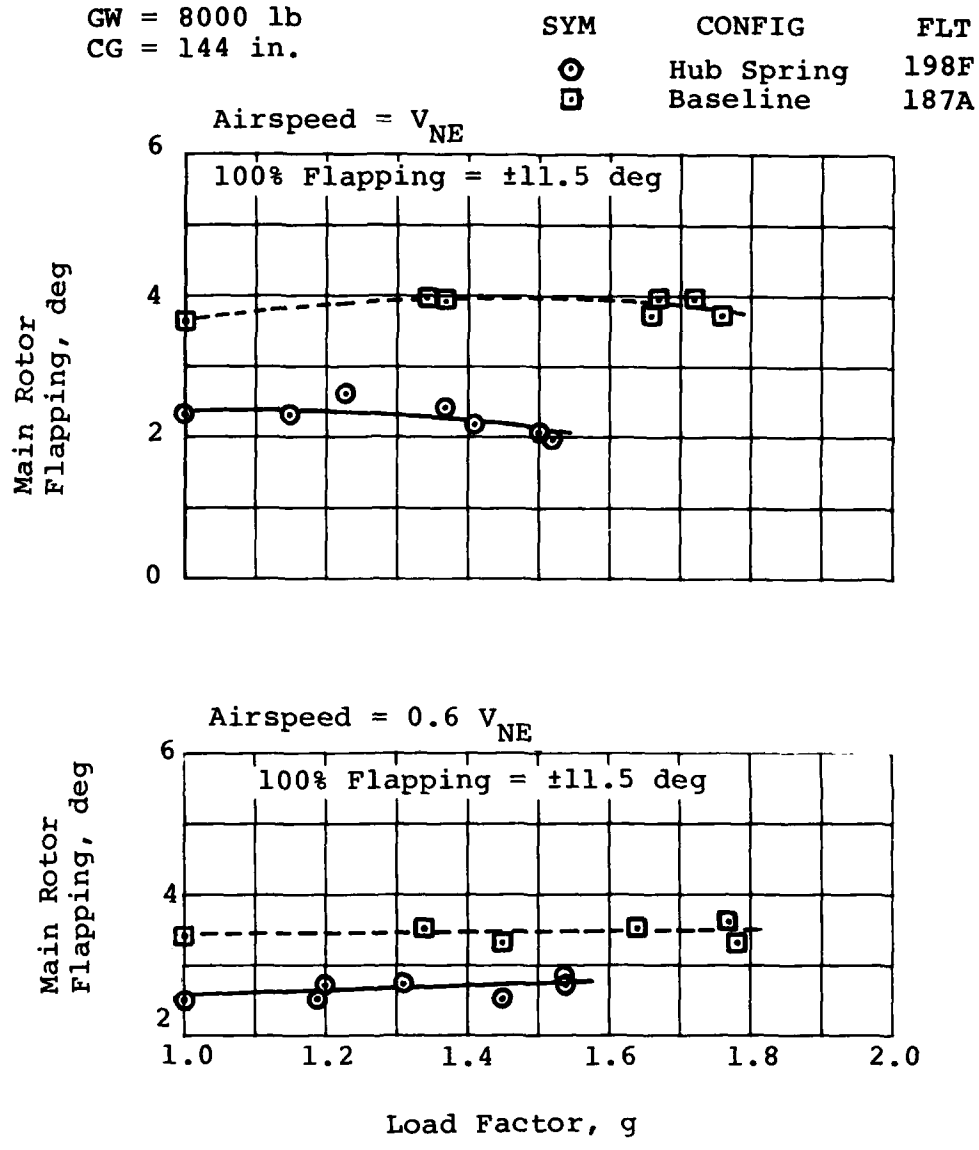

Figure 42. Effect of the hub spring on main rotor flapping during maneuvering stability testing.

TABLE 9. EFFECT OF THE HUB SPRING ON MAIN ROTOR FLAPPING AND AIRCRAFT RESPONSE DURING NAP-OF-THE-EARTH (NOE) MANEUVERS

NOE Maneuver	Baseline		Hub Spring	
	Maximum Flapping, deg	Maximum Rate, deg/sec	Maximum Flapping, deg	Maximum Rate, deg/sec
Bob-up	5.6	-	4.5	-
Pop-up	5.4	-	3.4	-
Forward Dash	5.3	9.9	5.0	10.0
Lateral Dash	11.0	20.0	7.75	22.0
Quickstop	5.6	8.0	5.7	12.5
Roll Reversal	5.2	38.8	5.4	49.2

7.2.2.3 Lateral Dash. The lateral dash was performed in the same manner as the forward dash; however, the direction of flight was sideward and the maximum airspeed was 30 knots. Of all the NOE maneuvers, the right sideward dash, at the heavy/forward center-of-gravity loading configuration, resulted in the highest main rotor flapping. Figure 43 presents a time history of the lateral dash as flown by the standard UH-1H helicopter and with the hub spring installed. At the time of the hub spring flight, surface winds were approximately 10 knots so that the maneuver was started and terminated at approximately 10 knots right sideward flight. Figure 43 shows that main rotor flapping was at the target limit (10 degrees) for an extended period in the baseline configuration. Peak main rotor flapping was reduced 2 degrees.

7.2.2.4 Level Flight Roll Reversal. As stated previously (Section 6), this was the only maneuver added to the test program as a result of the tactics evaluation. As flown during this program, the roll reversal was an evasive, zigzag maneuver entered at a 60-knot, trimmed, level flight condition. The helicopter was flown rapidly into a 45-degree banked turn, followed immediately by a banked turn of 45 degrees in the opposite direction, and then returned to level flight. Figure 44 presents a time history of a roll reversal as flown with the standard helicopter and by the hub spring-equipped helicopter.

Although there was a slight increase in maximum main rotor flapping with the hub spring installed, the maximum roll rate increased 25 percent from 38.8 to 49.0 degrees/second, a characteristic that was seen in other maneuvers. That is, if main rotor flapping increased during a maneuver flown with the hub-spring installed, there would be an attendant increase in fuselage angular rate of change.

7.2.2.5 Pop-up and Bob-up. In the case of the vertical bob-up, the helicopter started from an IGE hover, climbed vertically into an OGE hover, and returned to IGE hover. For the pop-up, the helicopter was accelerated into translational lift while climbing. Installation of the hub spring reduced maximum main rotor flapping 2 degrees during vertical bob-up and 1.1 degrees during the pop-up (see Table 9).

7.2.3 Steady High Flapping Conditions

In order to evaluate the hub spring during conditions of sustained high flapping, the test helicopter was loaded to the maximum allowable weight (8600 pounds) at the most extreme forward center of gravity (FS 130 inches). Data were then collected during 30-knot rearward and right sideward flight,

GW = 8600 lb
CG = 130 in.

Flight 188A

Configuration
Baseline

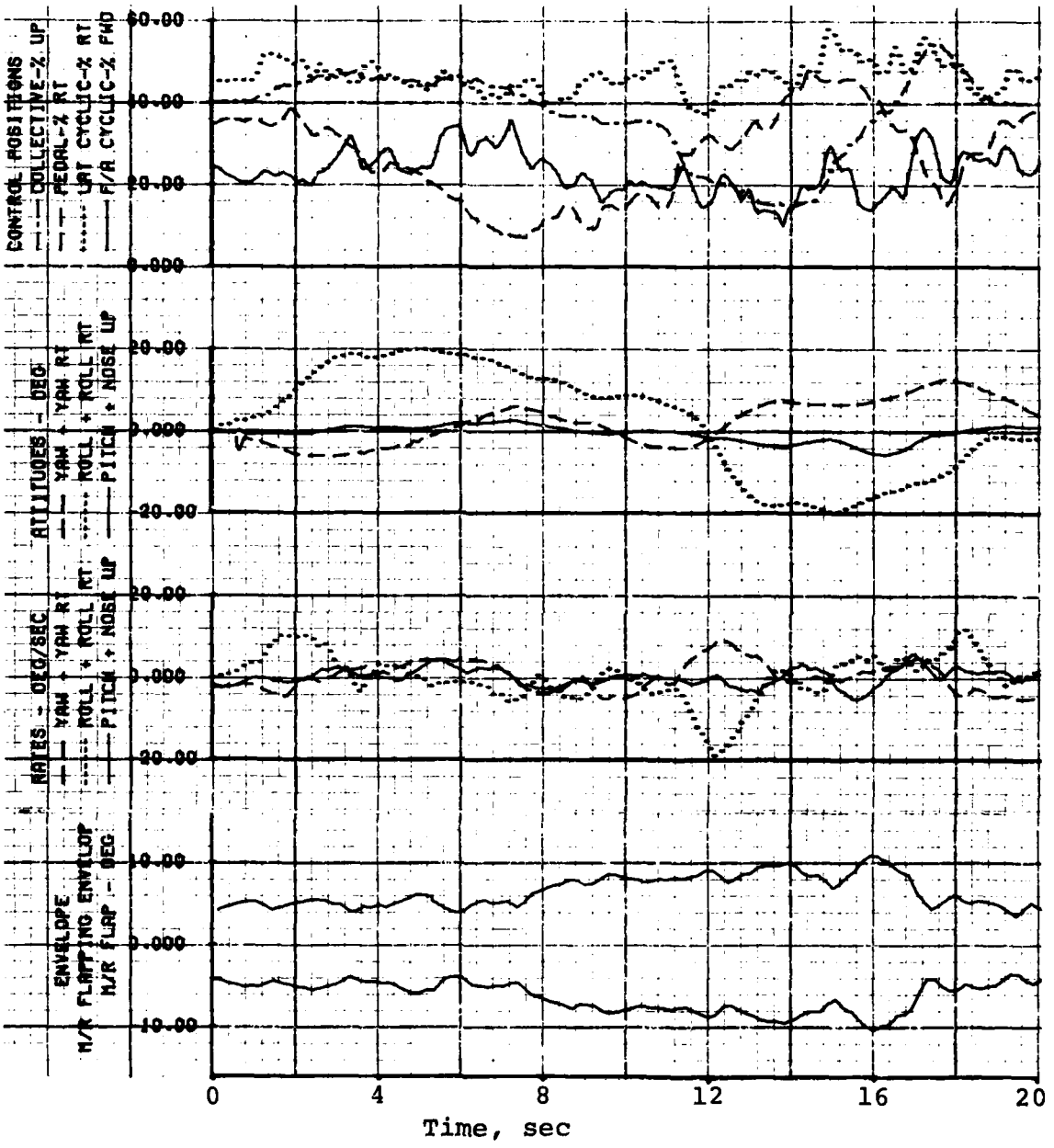

Figure 43. Effect of the hub spring on main rotor flapping and helicopter response during a right sideward dash.

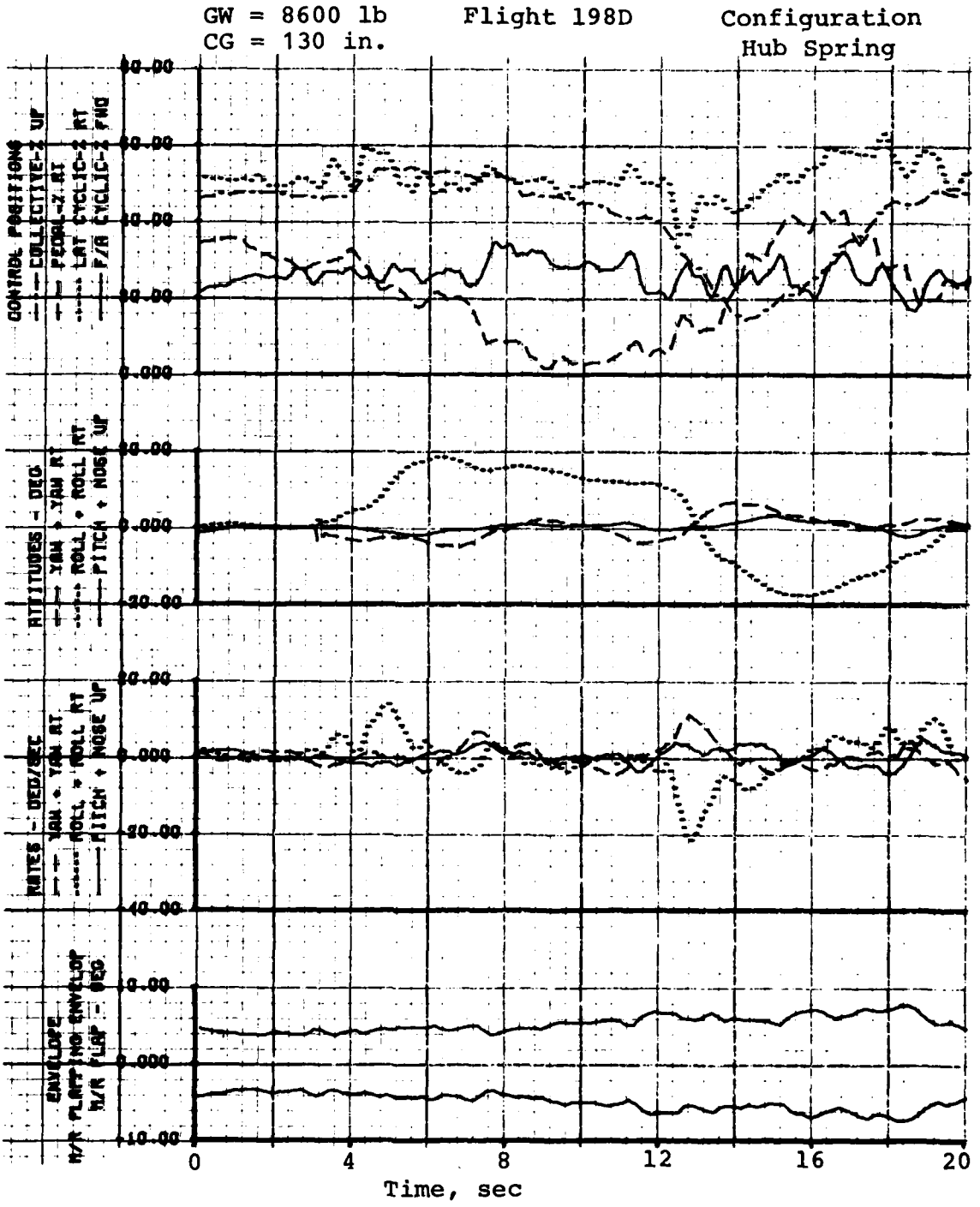

Figure 43. Concluded.

GW = 8600 lb
CG = 130 in.

Flight 183B

Configuration
Baseline

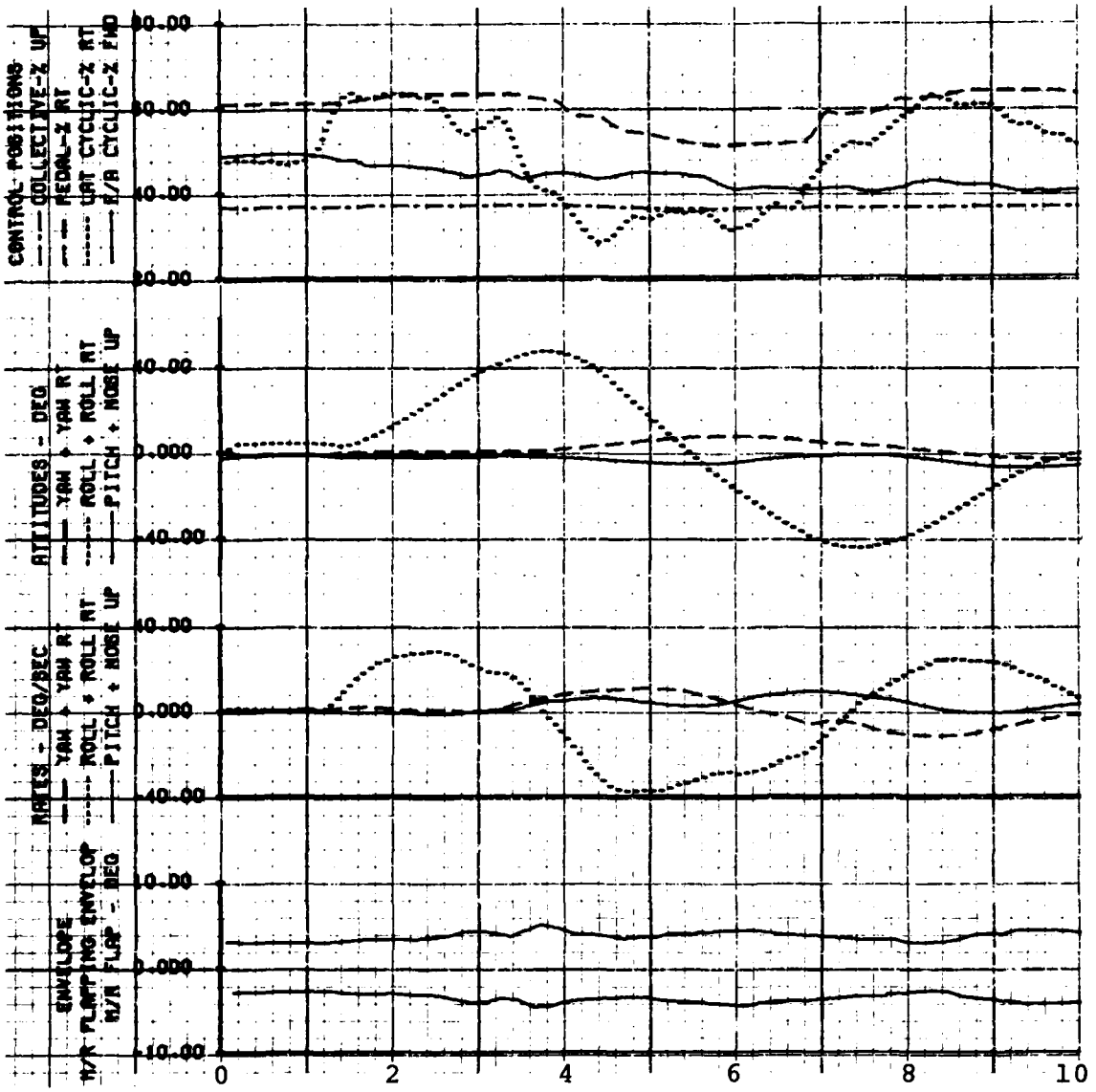

Figure 44. Effect of the hub spring on main rotor flapping and helicopter response during a level flight roll reversal entered at 80 knots.

GW = 8600 lb
CG = 130 in.

Flight 198D

Configuration
Hub Spring

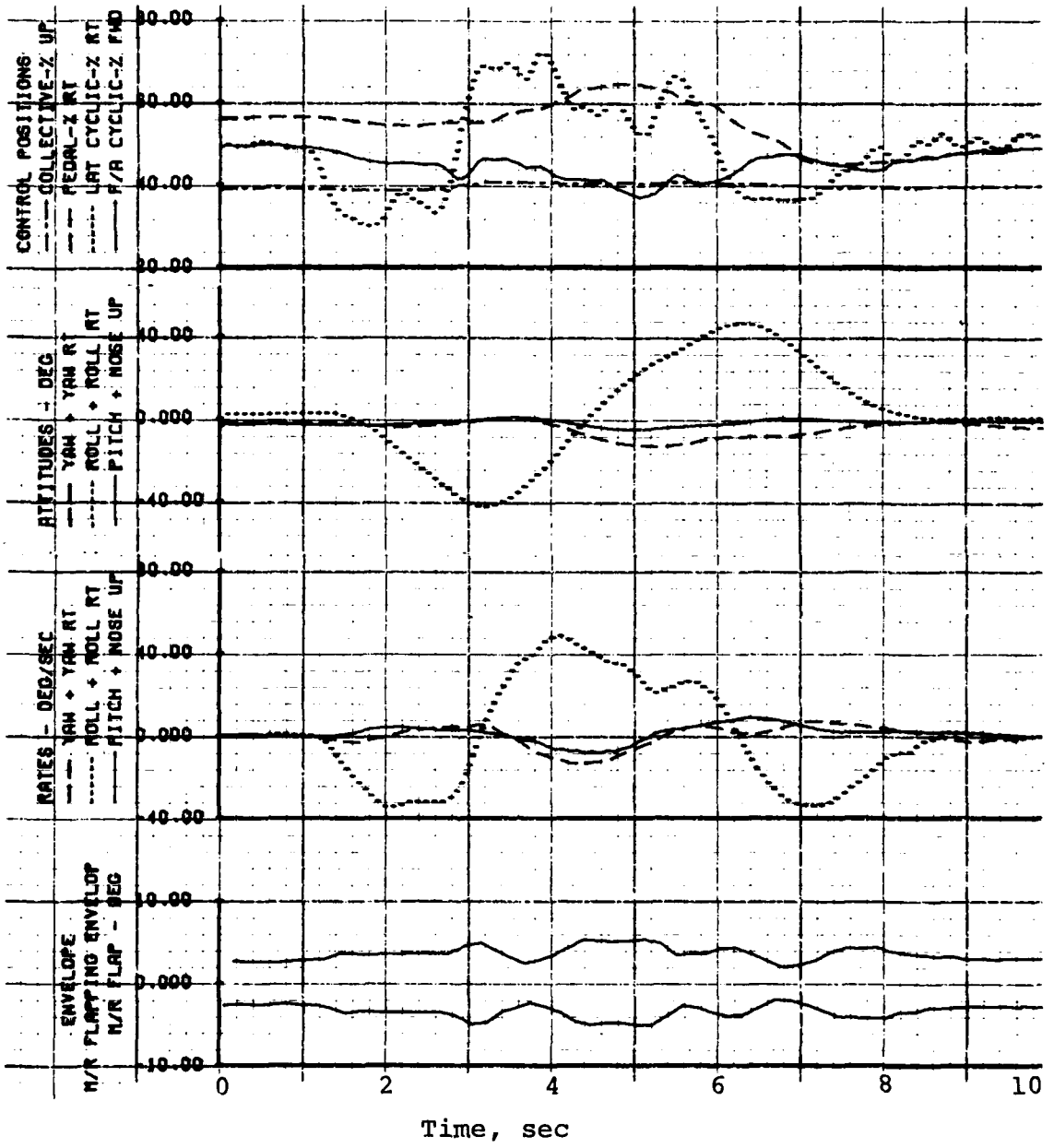

Figure 44. Concluded.

which are conditions of known high flapping (Reference 1). As necessary, the center of gravity would be moved forward in order to obtain desired main rotor flapping values of approximately 9 degrees. In the baseline configuration, tests were discontinued at FS 129.5 due to lack of sufficient aft cyclic control margin for gust correlation and the 9-degree main rotor flapping target being met. With the hub spring installed, testing continued to FS 128.88 and discontinued due to high loads in the hub spring hardware. At this extreme center of gravity, sufficient control margin remained for gust correction, and main rotor flapping was 2.8 degrees less than that measured during baseline flights at a more aft center of gravity. Table 10 shows the results of these flights.

7.2.4 Low-g Flight Control Power

A low-g flight investigation was conducted in order to determine the effect of the hub spring on control power at low g. The low-g condition was achieved at the termination of a roller coaster maneuver, which was entered at an airspeed of 70 knots. The helicopter was placed in a dive until the airspeed built to 100 knots, a climb was initiated and continued until the airspeed decreased to 80 knots; at this time, a pushover to the desired g-level was executed (Figure 45). Load factor during the pushover maneuvers was incrementally decreased toward a target value of 0.2g.

During the period of low g, left lateral steps up to 0.75 inch were made in order to determine low-g control power. This maneuver as done with the baseline configuration and with the hub spring installed is shown in Figure 46. Figure 47 shows that the hub spring increased the low-g control power for all g-levels tested. This figure also shows that at 0.2g, 42 percent of the 1g lateral control power is available with the hub spring configuration; however, via extrapolation only 16 percent of the 1g lateral control power is present at a 0.2g for the standard UH-1H helicopter. The pilot was never able to actually reach 0.2 g in the baseline configuration. The maximum main rotor flapping measured during all low-g, and low-g with control power steps, was only 4.5 degrees.

7.2.5 Summary of Improved Mast Bumping Safety Margin Tests

As shown, the mast bumping safety margin of the UH-1 helicopter has been improved by installation of the hub spring. Main rotor flapping was reduced in all conditions tested and lateral control power was increased. Although a numerical value cannot be assigned to quantify the improvement of safety margin, reduced flapping and increased control power verify that an increased flapping stop-to-mast clearance has been achieved.

TABLE 10. STEADY HIGH FLAPPING CONDITIONS

Flight Condition	Center-of-Gravity Location (in.)	Maximum Flapping*	
		Hubspring	Baseline
30-knot rearward	130.0	5.5°	8.2°
	129.5	5.8°	9.3°
	128.88	6.5°	-
30-knot right sideward	130.0	6.2°	8.8°
	129.5	6.7°	-
	128.88	7.2°	-

*Maximum flapping target value was 9 deg. (80% of total flapping limit).

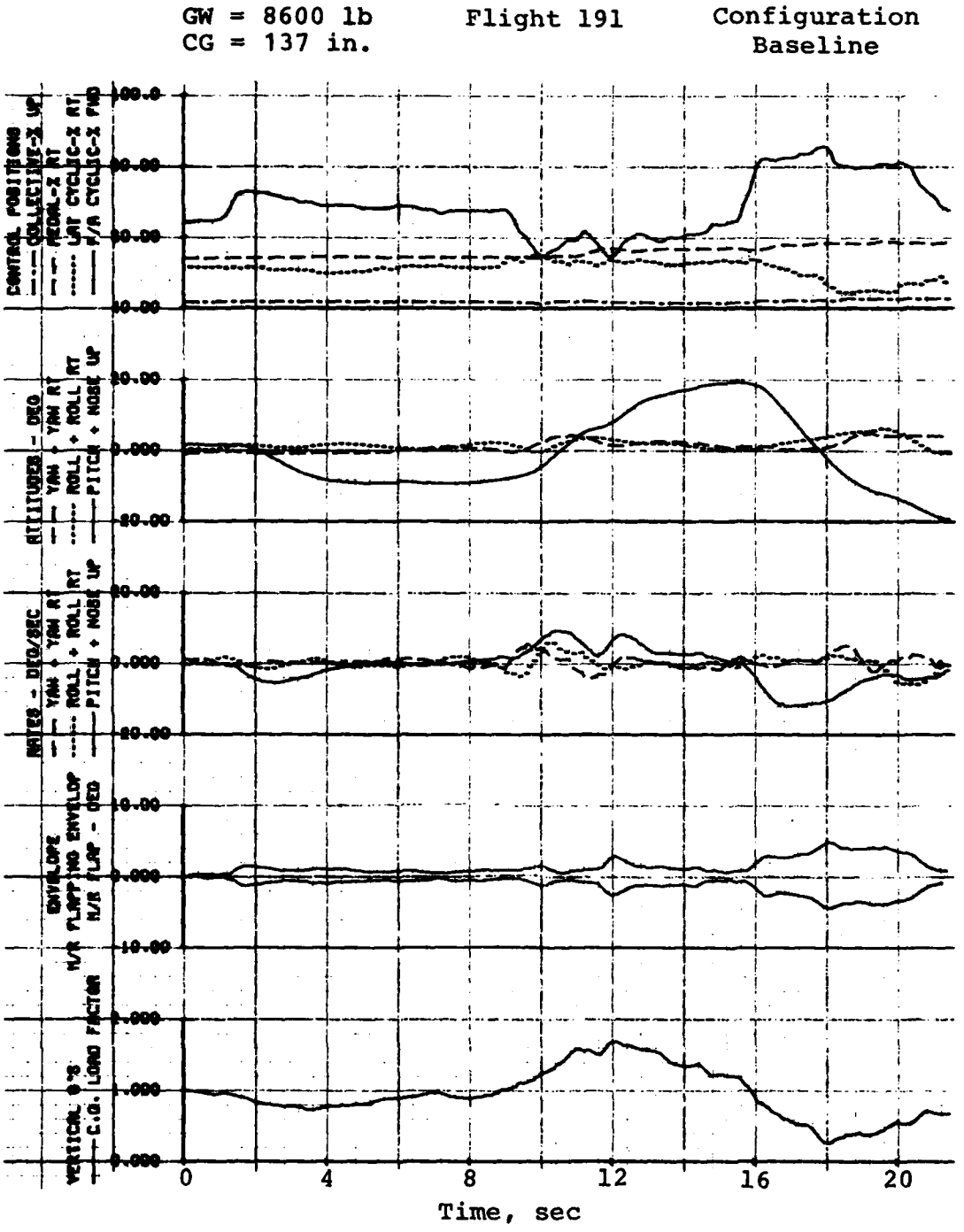

Figure 45. Effects of the hub spring on main rotor flapping and helicopter response during a roller coaster maneuver to low-g.

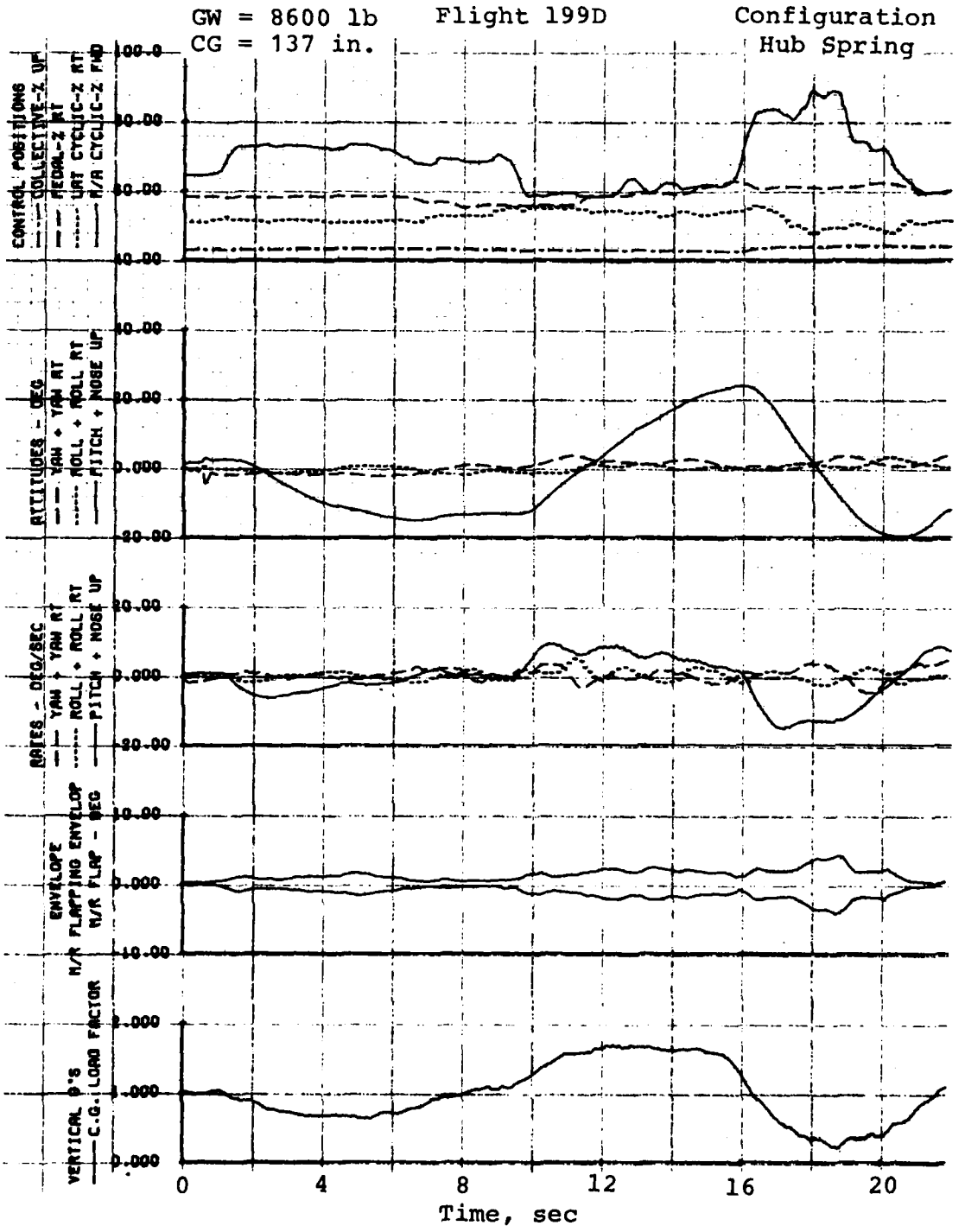

Figure 45. Concluded.

Flight 191

GW = 8600 lb
CG = 137 in.

Configuration
Baseline

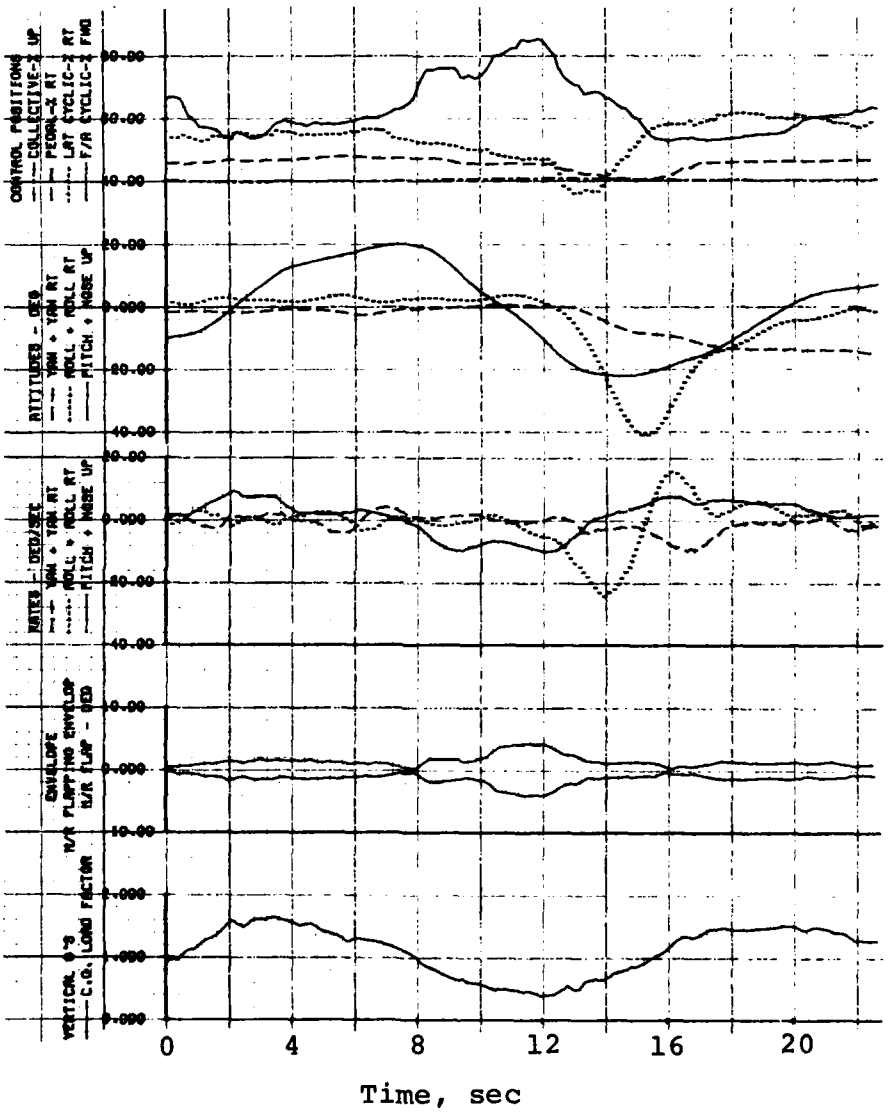

Figure 46. Effect of the hub spring on main rotor flapping and helicopter response following a left control step at low-g.

GW = 8600 lb
CG = 137 in.

Flight 199D

Configuration
Hub Spring

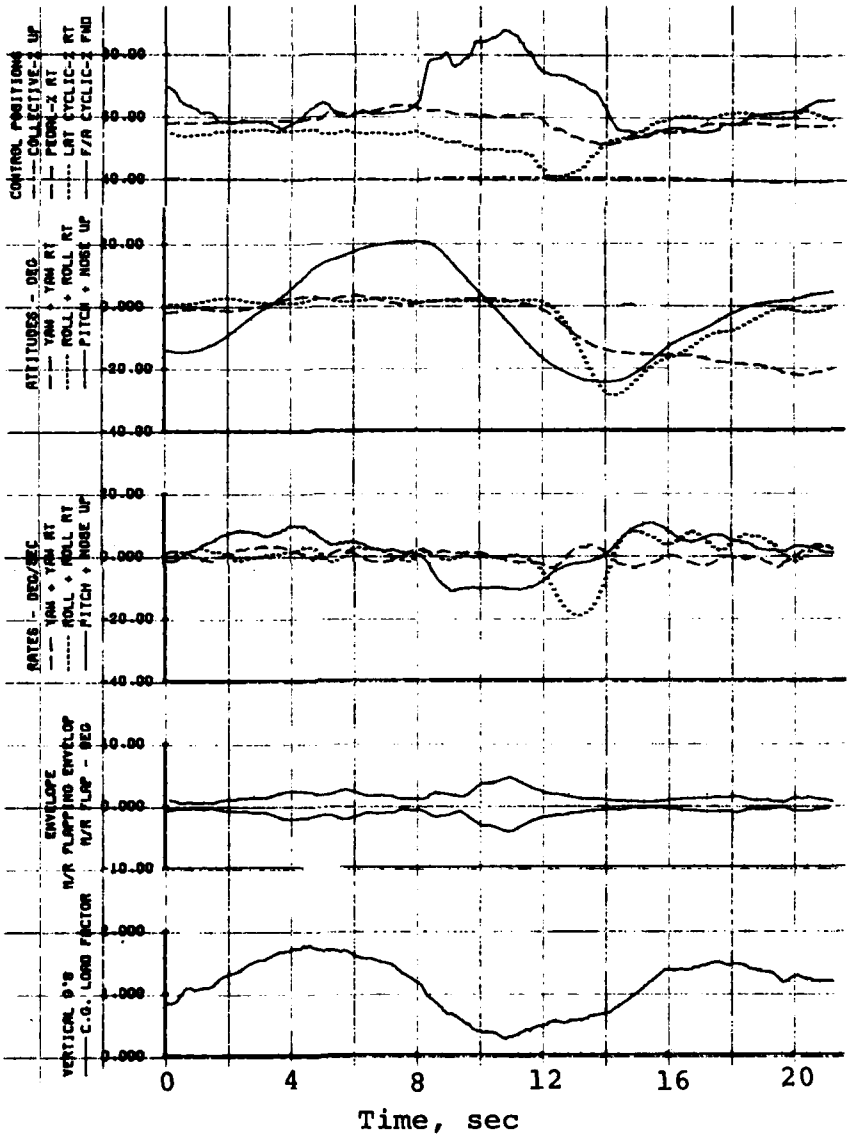

Figure 46. Concluded.

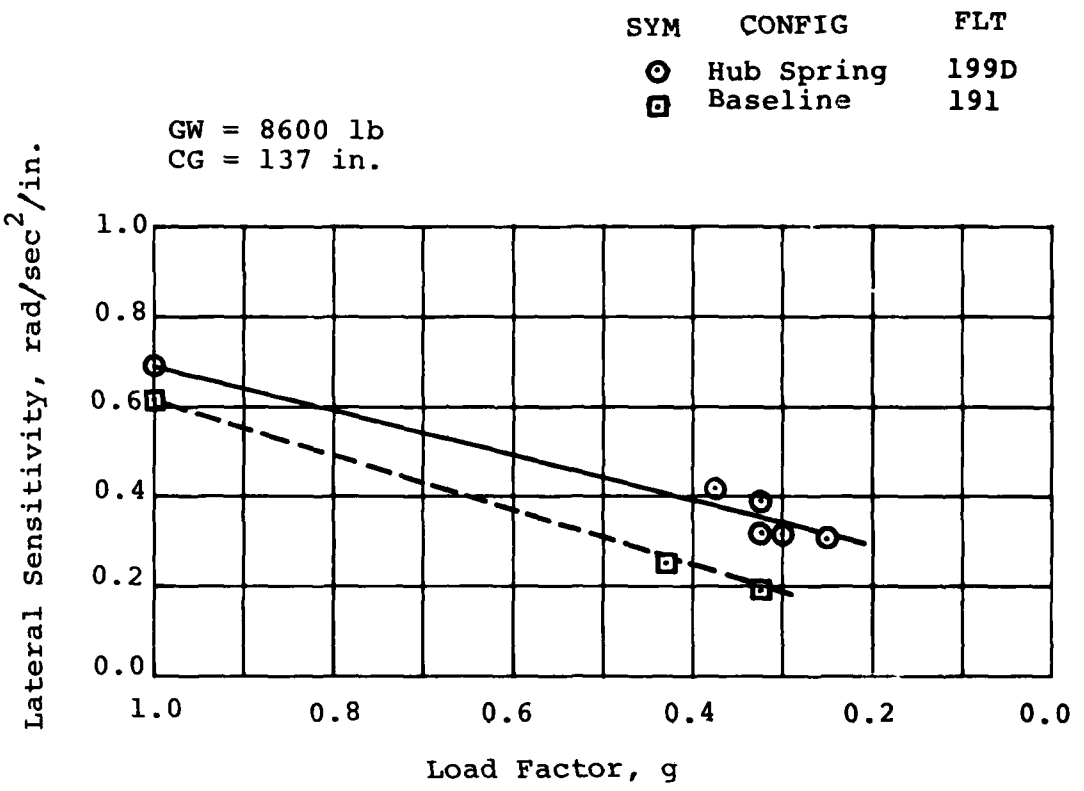

Figure 47. Effect of the hub spring on lateral sensitivity at g-levels less than 1.0.

7.3 EFFECT OF HUB SPRING ON HANDLING QUALITIES CHARACTERISTICS

In order to determine the effect of the hub spring on the handling qualities characteristics of the model UH-1H, a series of test points were flown in the baseline configuration and repeated with hub spring installed. The following subsections present effects on control margin, static stability, maneuvering stability, dynamic stability, and controllability. The baseline flights were conducted with atmospheric conditions consistent with those acceptable during handling qualities testing; however, the hub spring flights were conducted at levels of atmospheric turbulence greater than those normally considered acceptable for reliable handling qualities testing.

7.3.1 Control Margins during Steady Flight

Figure 48 shows longitudinal control positions during level flight from hover to 30 knots rearward and from 45 knots forward to V_{NE} at critical loading conditions. The critical weight/cg loading condition for rearward flight is heavy/forward and for forward flight it is light/aft. At the heavy forward center-of-gravity extreme, an increase of 5 percent longitudinal control margin at -30 knots is provided by hub spring installation. Control positions during sideward flight are shown in Figure 49.

7.3.2 Static Longitudinal Stability

The apparent static longitudinal stability as indicated by the positive gradient of the longitudinal control position with respect to airspeed about a trim condition of 0.08 V_{NE} is presented as Figure 50. As shown, the collective fixed static longitudinal stability at aft center of gravity of the UH-1H test vehicle increased from a 0.07 percent per knot baseline to 0.12 percent per knot with hub spring, as shown in Figure 50. There was no significant change in the static longitudinal stability at the forward center-of-gravity loading condition.

7.3.3 Maneuvering Stability

In order to determine the effect of the hub spring on maneuvering stability, flight tests were conducted to determine the longitudinal control position displacement required to develop a steady-state acceleration during steady turning flight. Longitudinal cyclic position during wind-up turns to 1.7g were recorded at 72 and 115 knots and presented in Figure 51. As shown, the hub spring does not significantly change the maneuvering stability of the UH-1H helicopter.

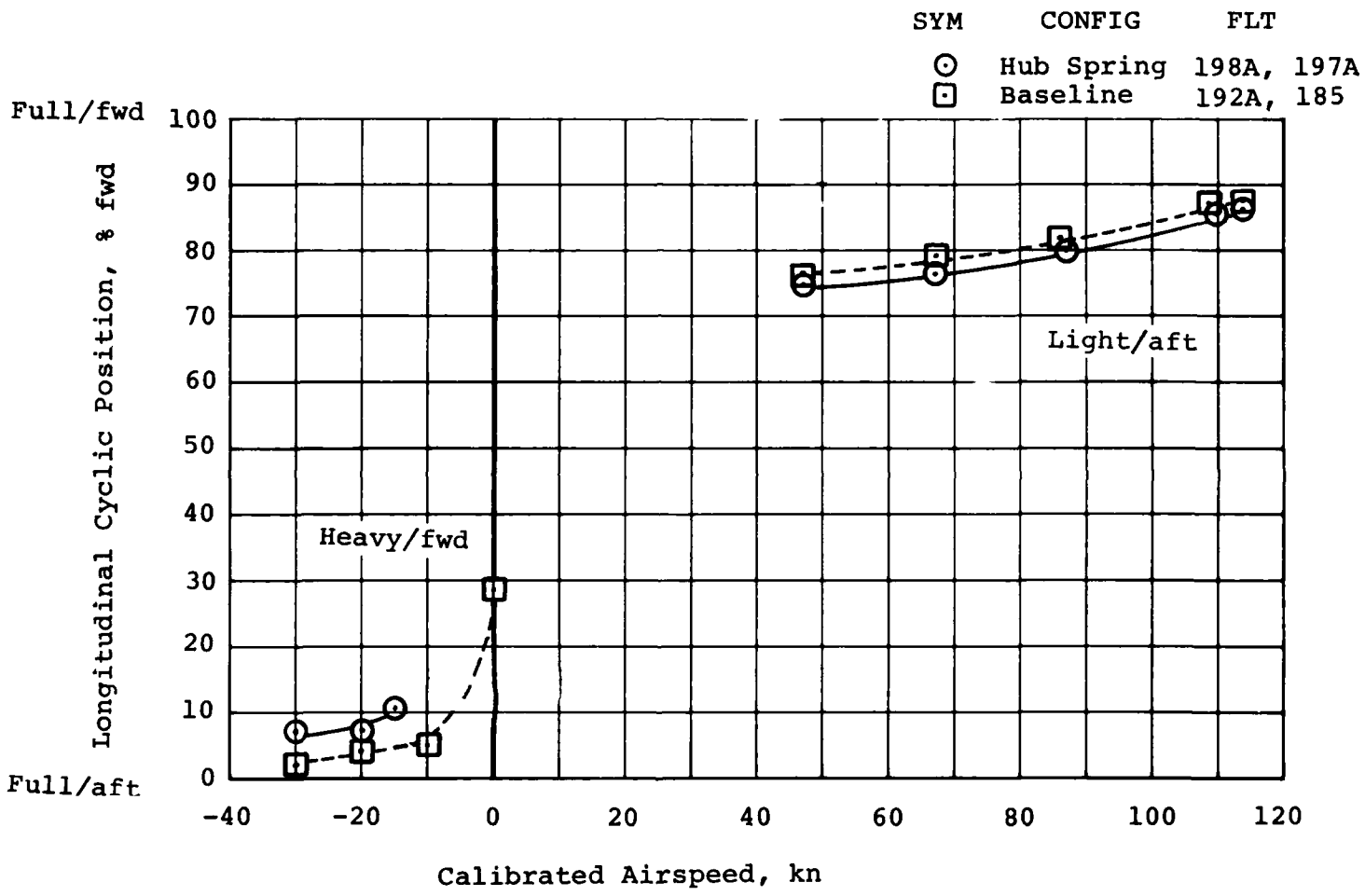

Figure 48. Effect of the hub spring on longitudinal control positions during level rearward and forward flight at the most critical loading condition.

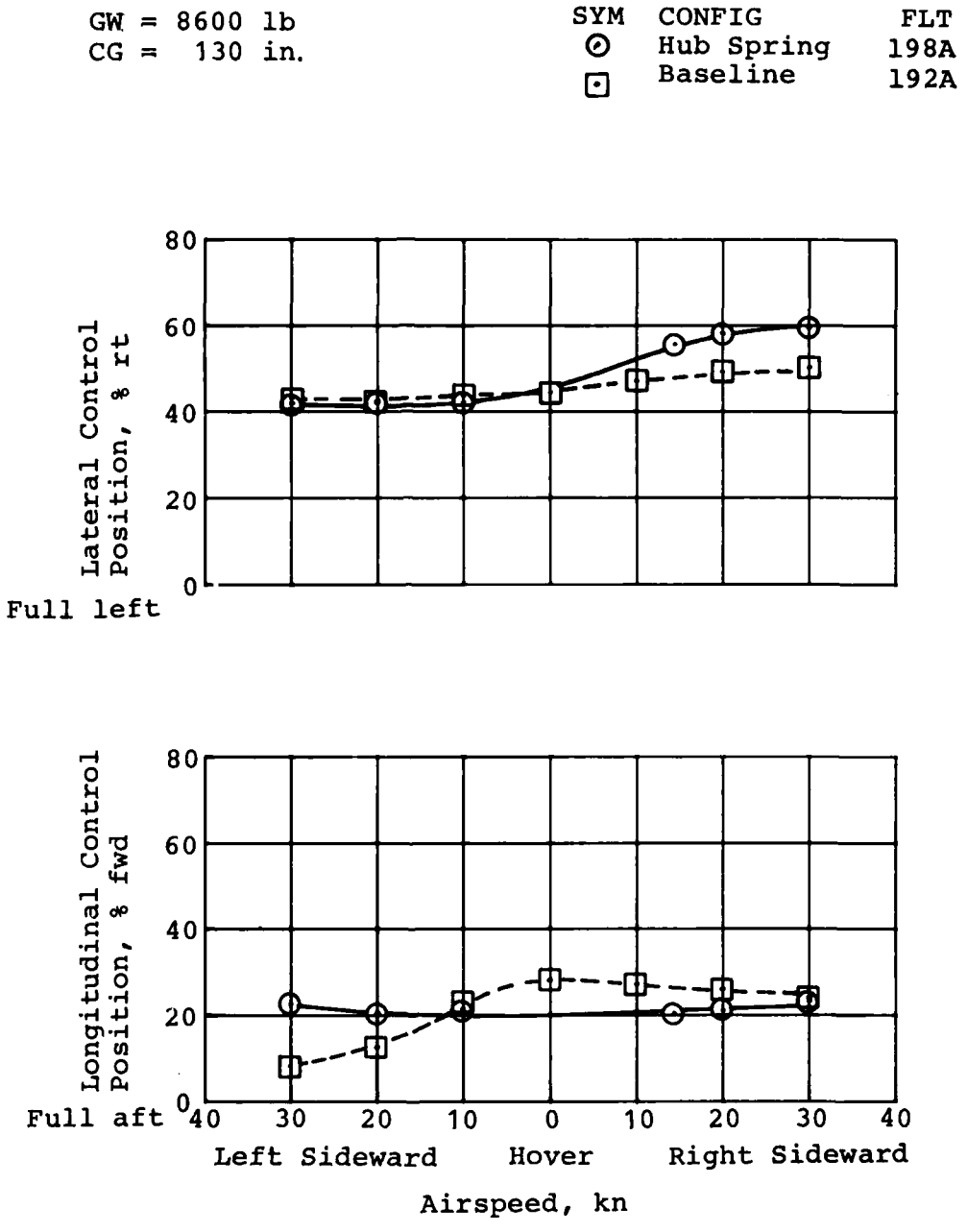

Figure 49. Effect of the hub spring on control positions during level sideward flight.

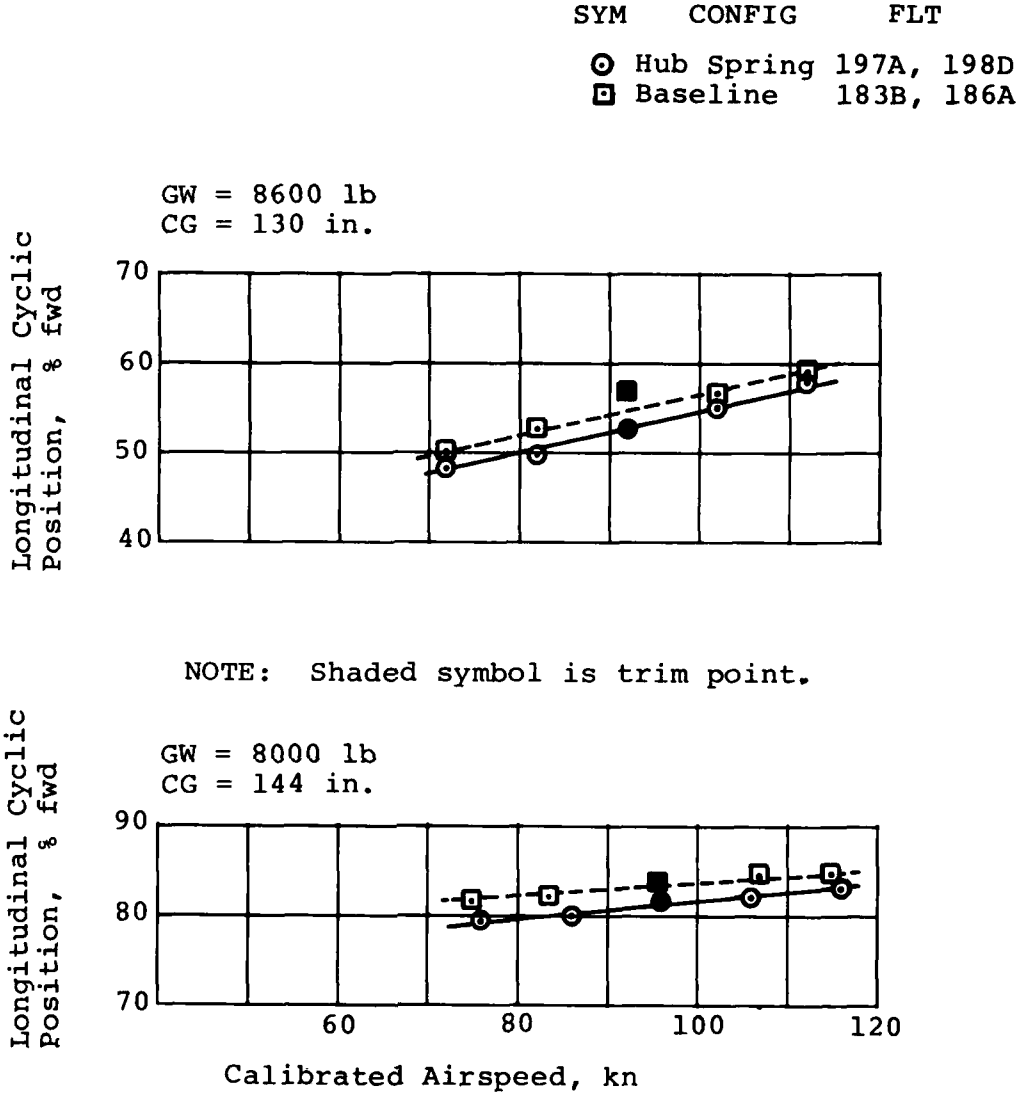

Figure 50. Effect of the hub spring on static longitudinal stability in level flight.

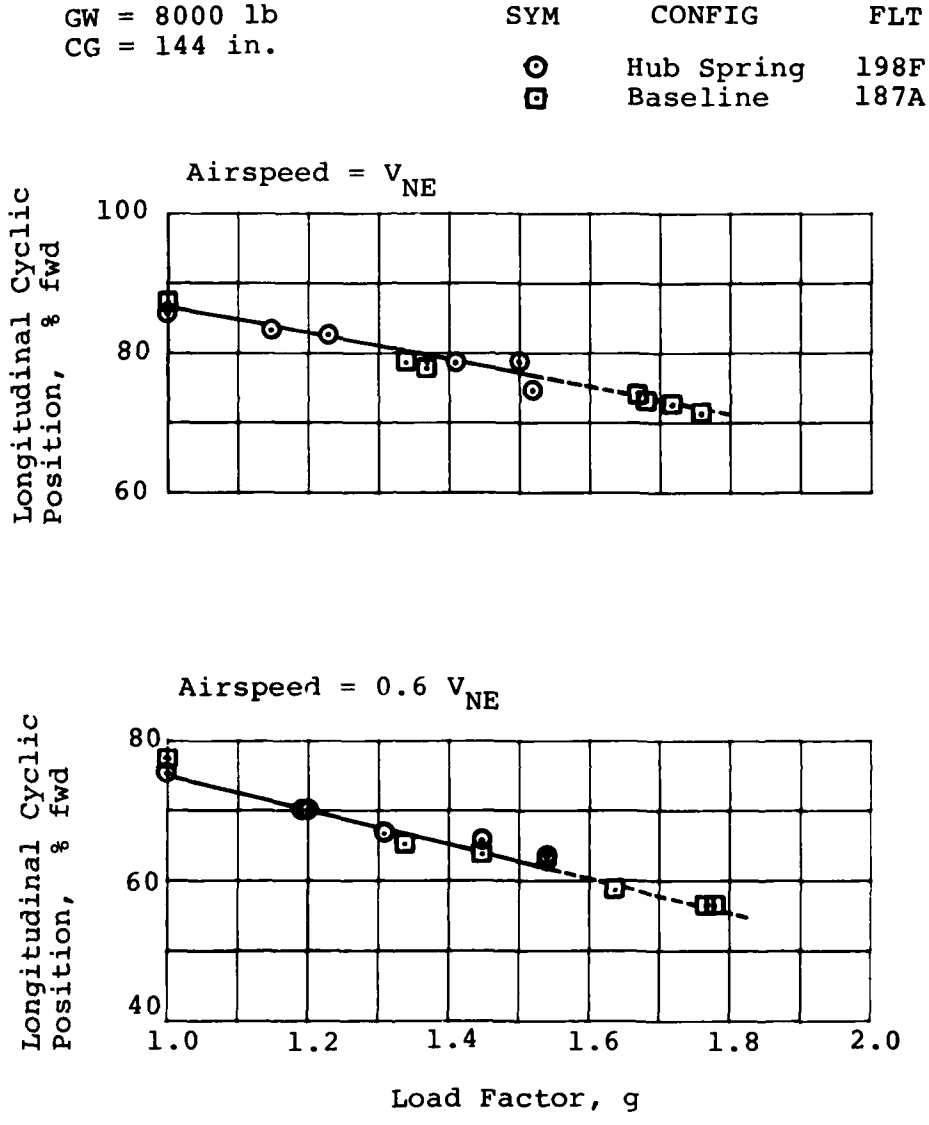

Figure 51. Effect of the hub spring on maneuvering stability at $0.6V_{NE}$ and V_{NE}.

With hub spring installed, wind-up turns to load factors greater than 1.7g's at a main rotor speed of 314 rpm were conducted. During these tests, there was increased vertical vibration and detectable cyclic feedback. Although no conclusive explanation for the increased vertical vibration was found, retreating blade stall was suspected at the 2g load factor condition reached during hub spring tests which resulted in cyclic feedback. During baseline flights, load factors of only 1.6g were reached and no increased vertical vibration or cyclic feedback was noted.

7.3.4 Controllability

In order to determine the effect of the hub spring on controllability characteristics, aircraft motions following rapid control displacement were recorded and analyzed. Although controllability is usually conducted in still air, tests with the hub spring were conducted during a period when surface winds were approximately 10 knots.

Controllability testing was conducted at a hover and in level flight at 70 knots with the test aircraft at both the heavy/forward and the light/aft gross weight and center-of-gravity loading configurations. Figures 52 through 54 are time histories of aircraft motions following a cyclic control step and are considered to be typical of these tests. Figure 55 presents a summary of the hovering control characteristics as measured during these tests. Control sensitivity, the maximum vehicle angular acceleration per inch of control input, was increased by the hub spring by approximately 15 percent in both the pitch and the roll axis. Angular velocity damping also appears to be increased as a result of the hub spring. Control response, the maximum vehicle angular rate per inch of control input, in the pitch axis was increased 36 percent, from 6.7 to 9.1 deg/sec by installation of the hub spring. This increase in control response is not reflected in the roll axis. This is due, in part, to greater rate damping being provided by the stabilizer bar, which is indicated by the maximum roll rate of the basic aircraft being 40 percent greater than the maximum pitch rate.

7.3.5 Dynamic Stability

Acceptable handling qualities require that forces are set up to damp oscillations resulting from disturbances from trim conditions and that the vehicle tends to return to the trim condition. In order to evaluate the effect of the hub spring on this dynamic stability requirement, external disturbances were simulated by applying a rapid pulse control input about a single axis. The aircraft controls are then held at the trim

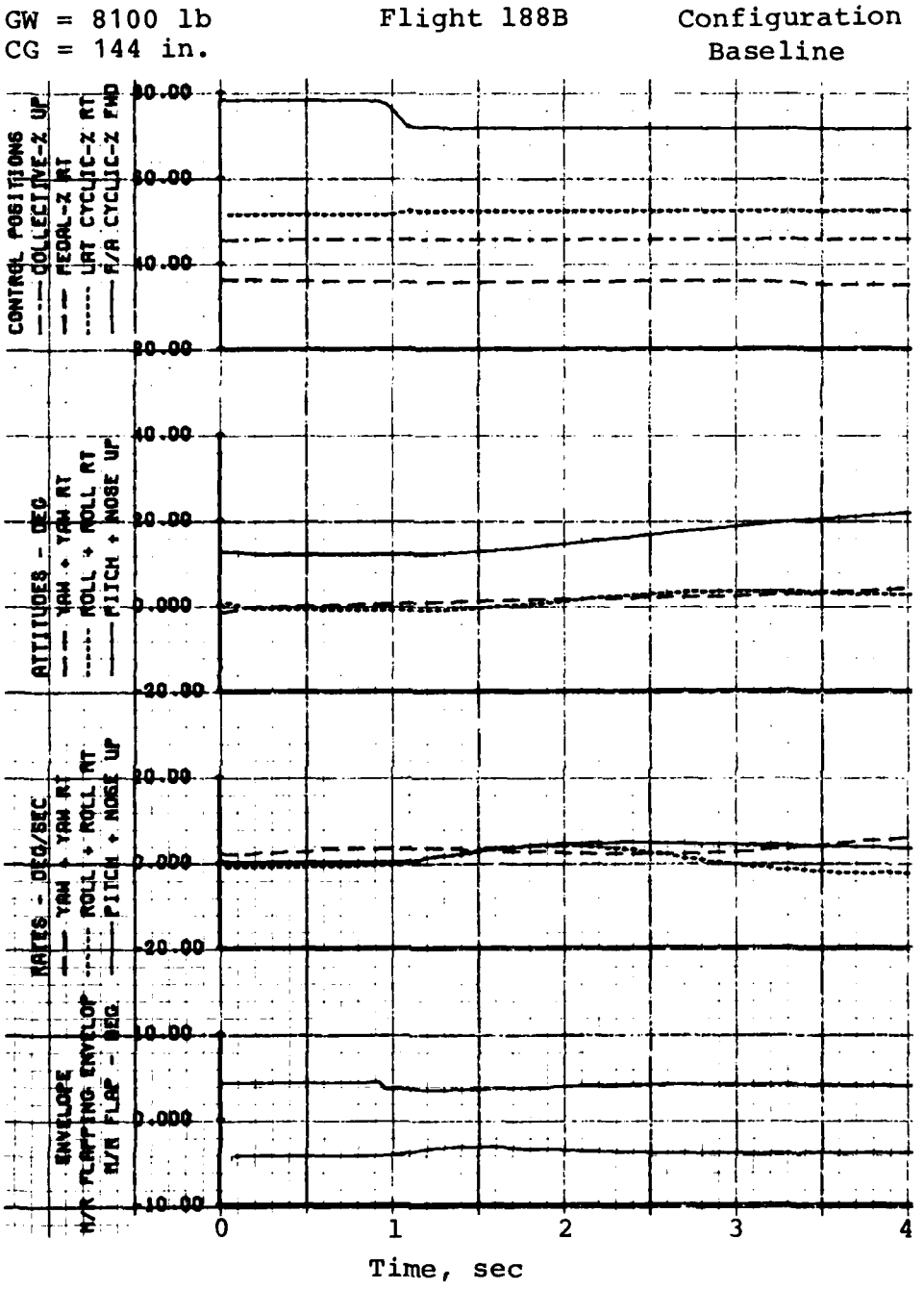

Figure 52. Effects of the hub spring on main rotor flapping and helicopter response to an aft cyclic control step at OGE hover.

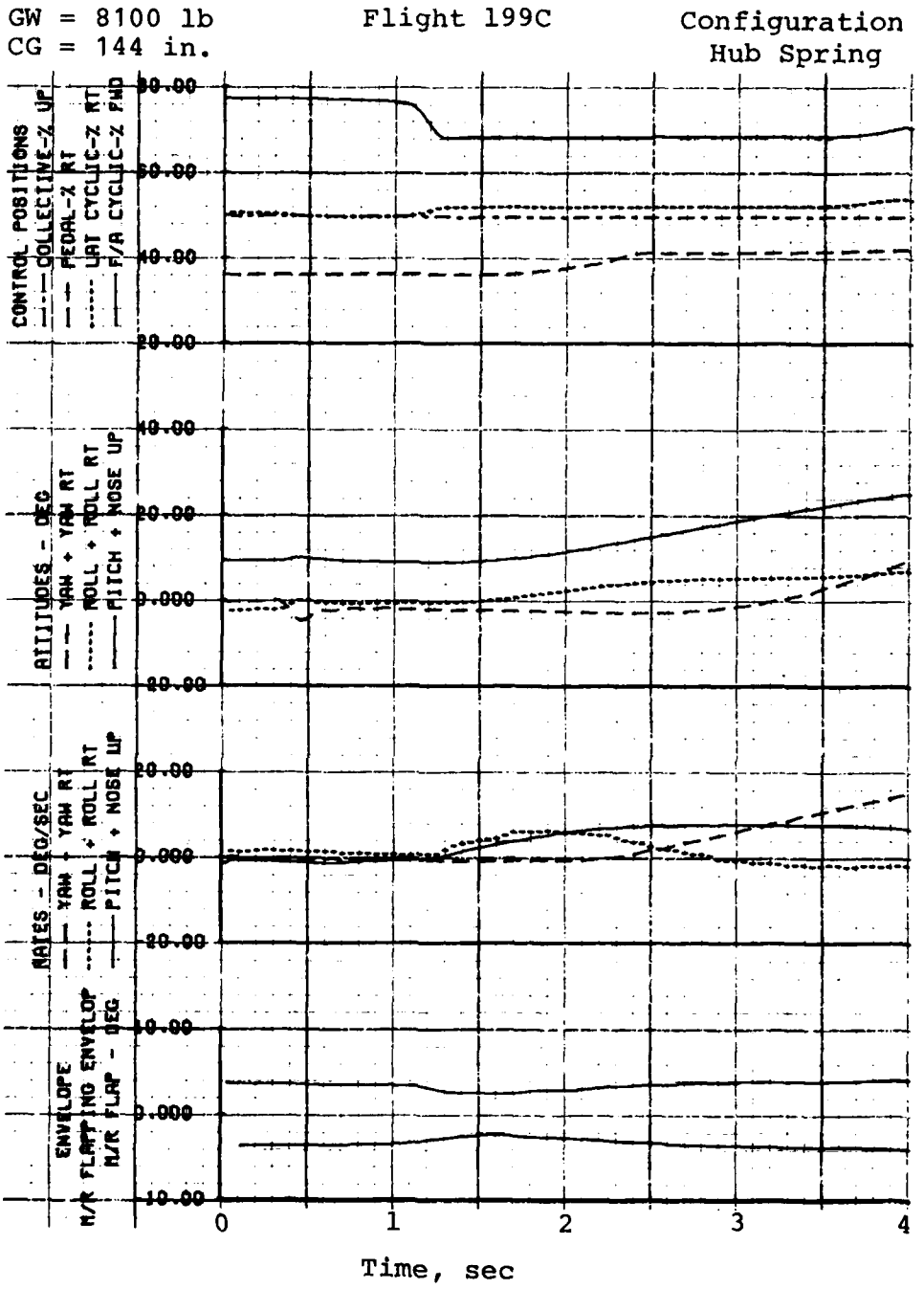

Figure 52. Concluded.

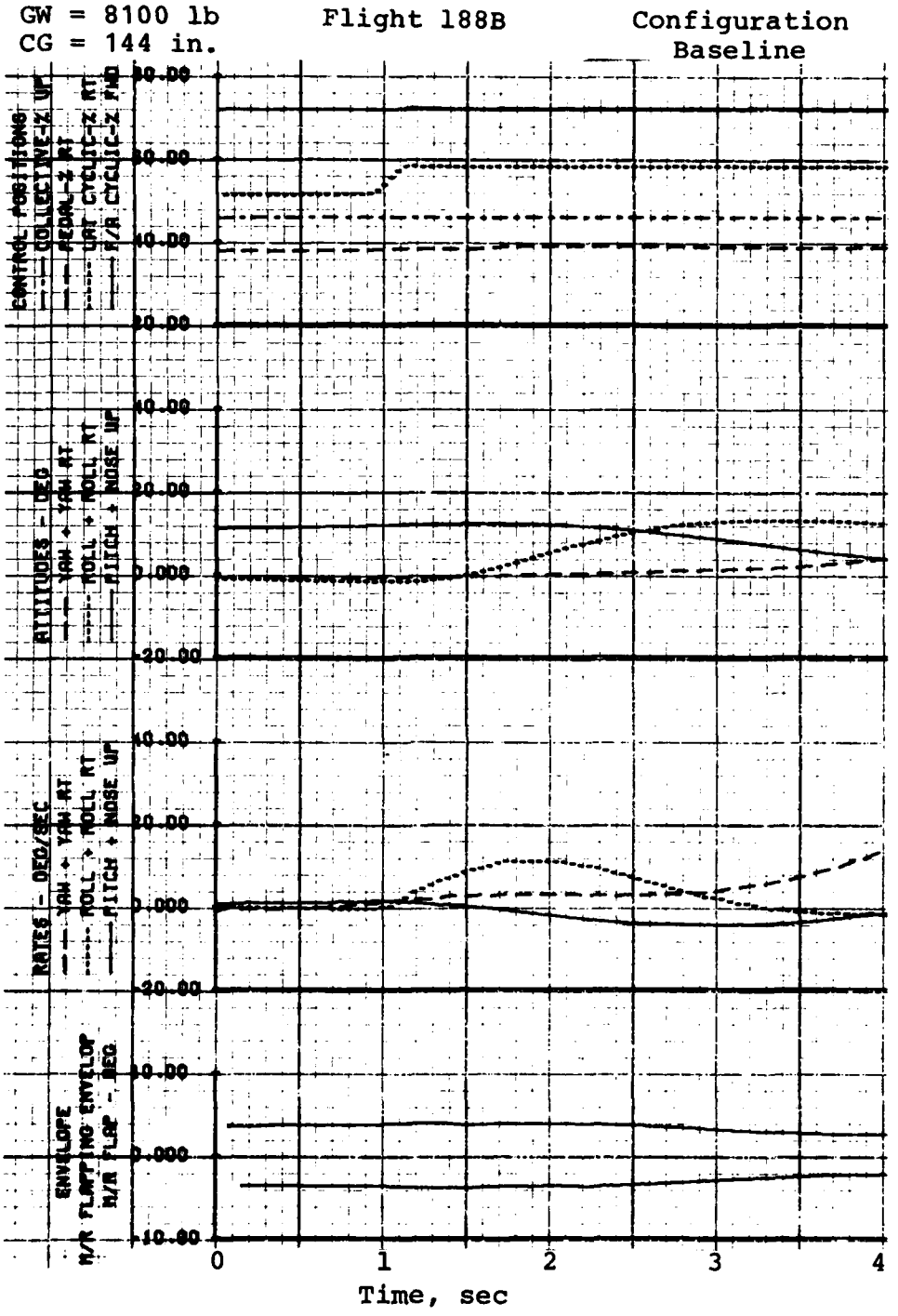

Figure 53. Effects of the hub spring on main rotor flapping and helicopter response to a right lateral cyclic control step at OGE hover.

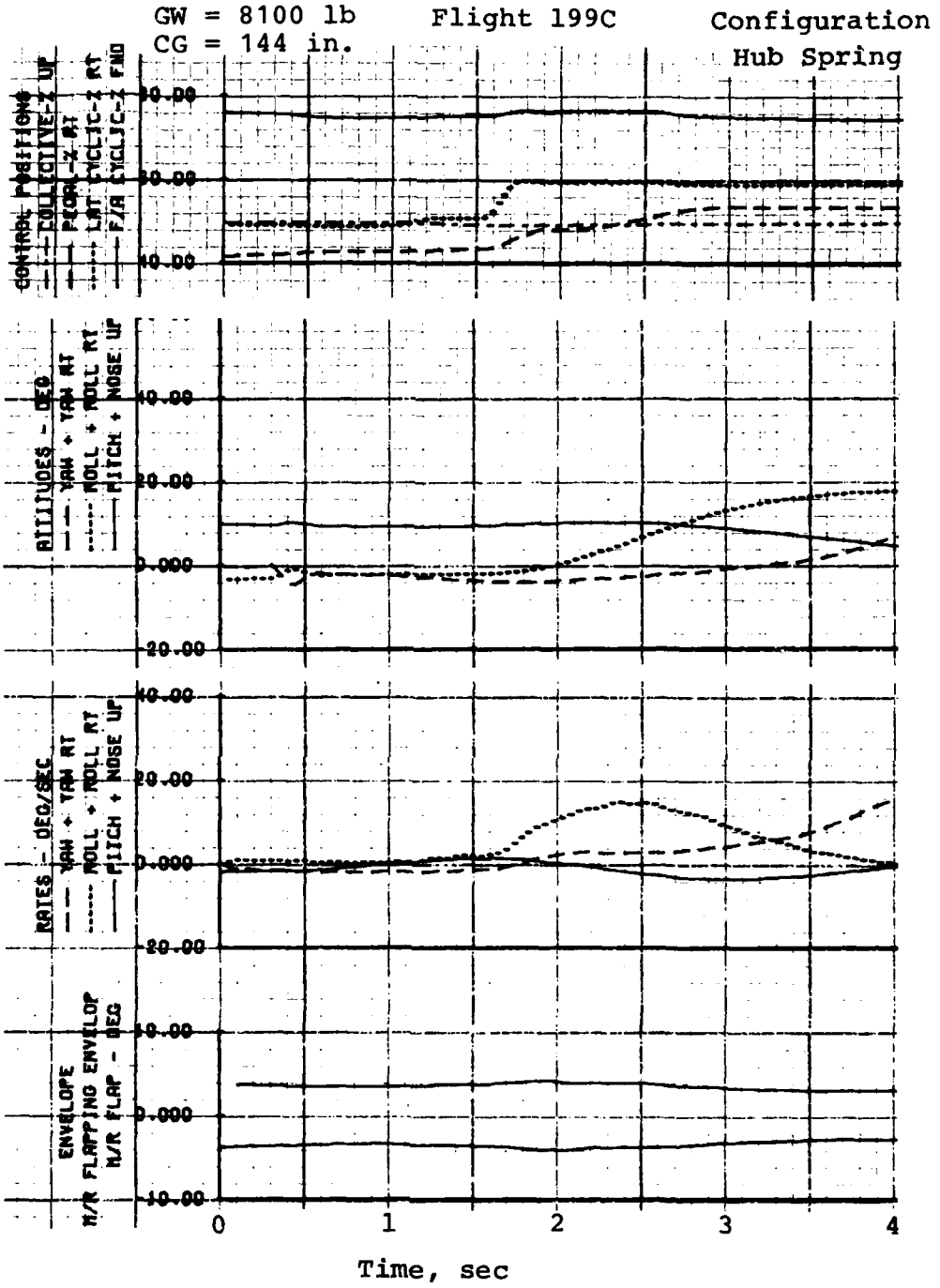

Figure 53. Concluded.

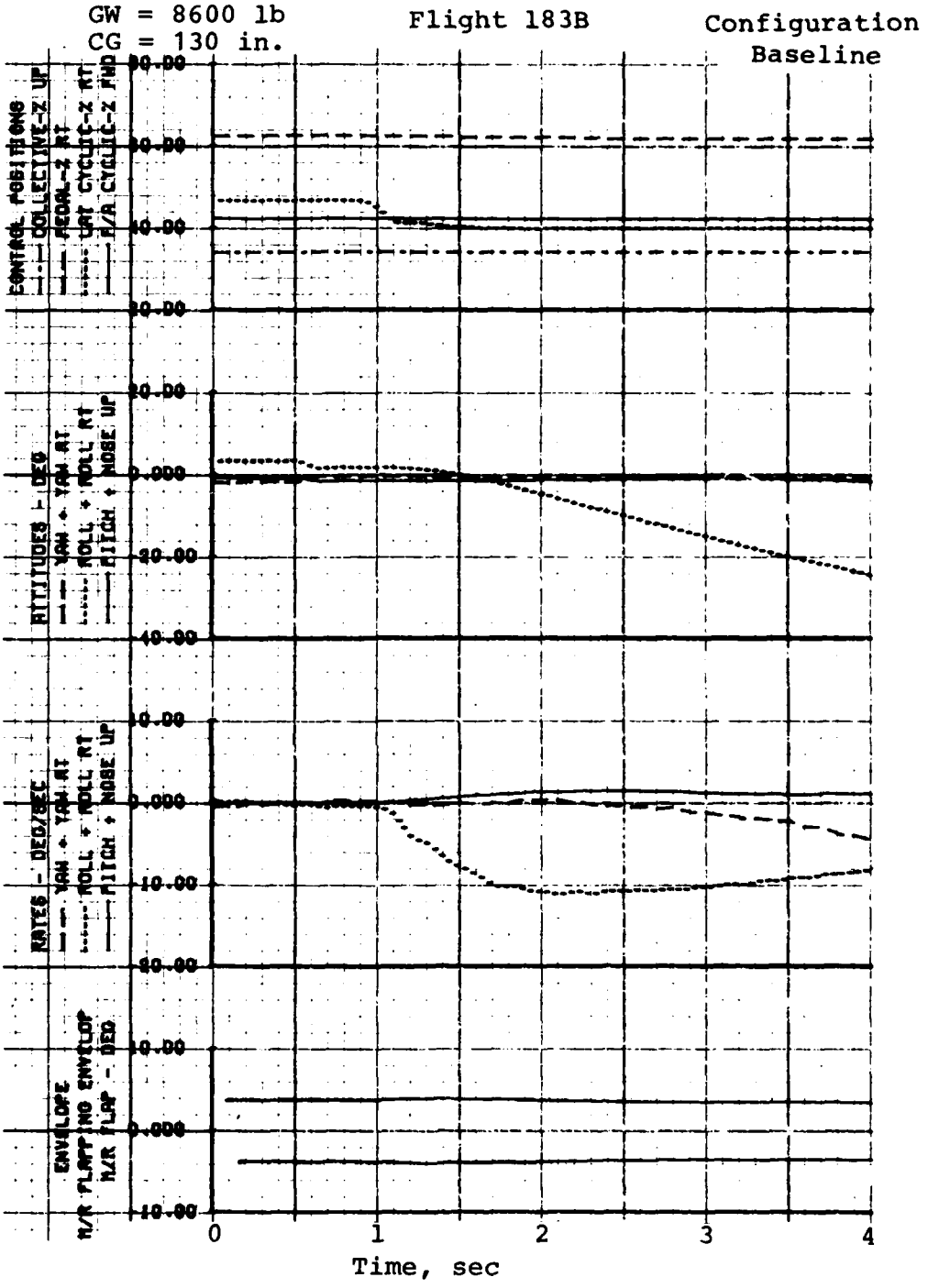

Figure 54. Effects of the hub spring on main rotor flapping and helicopter response to a left lateral cyclic control step at 0.6 V_{NE}.

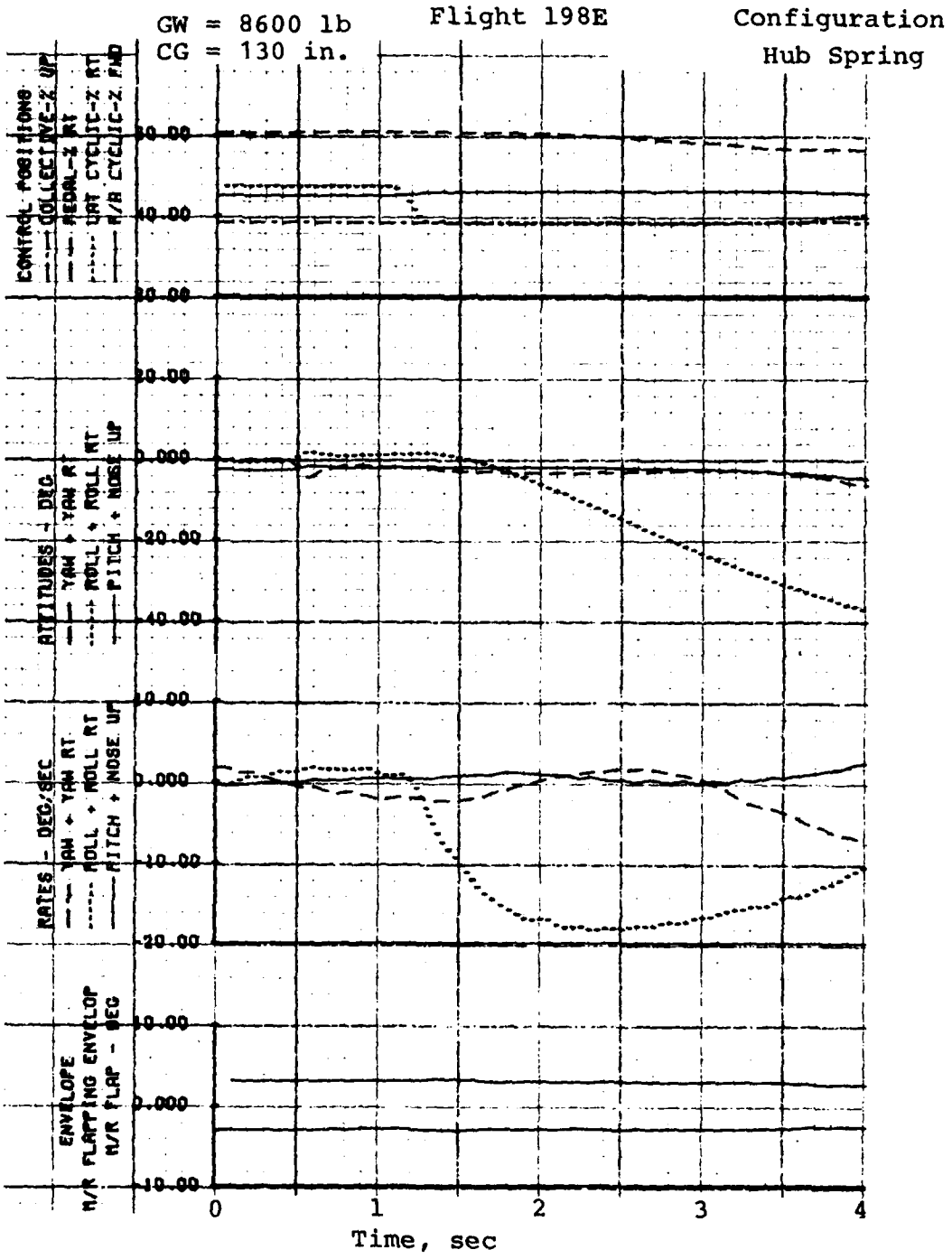

Figure 54. Concluded.

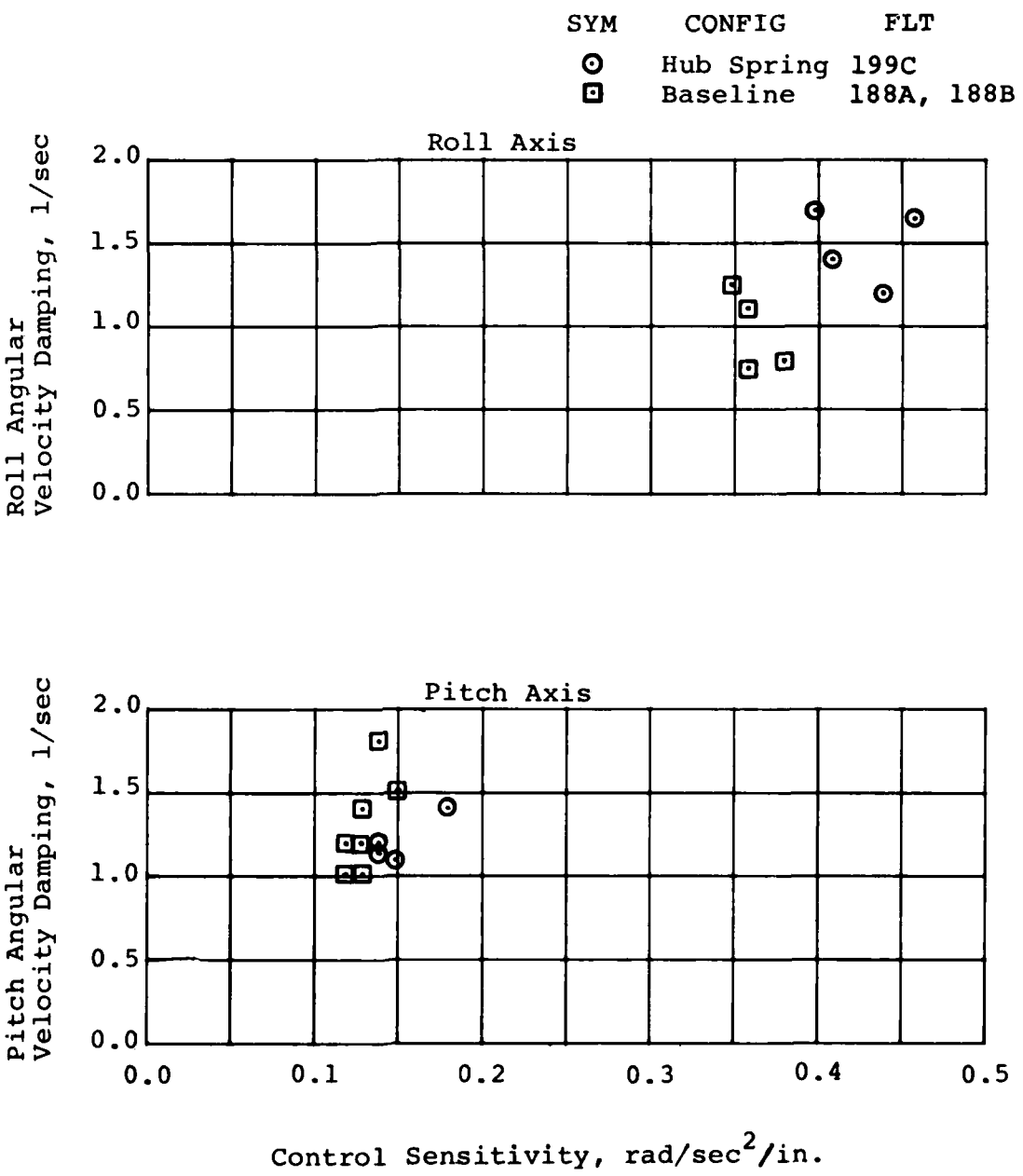

Figure 55. Effect of hub spring on control sensitivity and damping.

condition and aircraft motions recorded. The dynamic stability tests were conducted at the light/aft loading configuration at airspeeds of 70 and 110 knots. As stated before, atmospheric turbulence levels during hub spring testing were above normally accepted values.

In comparing the time histories of the lateral control pulses presented in Figure 56, it can be seen that the lightly damped, small amplitude, roll oscillation found in the baseline configuration is apparently eliminated by the hub spring. Additionally, coupled oscillations in the pitch and yaw axis are not present in the hub spring configuration.

If the time histories of the longitudinal control pulses (Figure 57) are compared, little difference in damping in the pitch axis is noted. As in the case of the lateral control pulse, however, cross-coupled roll oscillations are apparently eliminated by the hub spring.

7.3.6 General Handling Qualities Summary

The principal objective of the nonlinear hub spring was to minimize or eliminate mast failure due to severe flapping stop contact, not to improve rotorcraft handling qualities. However, test results indicate a general improvement of the handling qualities of the UH-1H helicopter following installation of a hub spring.

The following improvements were noted:

- Increased control margins in forward and rearward flight.
- Improved static longitudinal stability at light gross weight and aft center of gravity.
- Eliminated persistent roll oscillations following cyclic control pulses.
- Increased control sensitivity and angular rate damping.

Although the presence of the hub spring was not readily apparent to the pilot in all flight conditions, the data show improvement in most areas tested.

Another improvement is the absence of large main rotor flapping excursion during start-up in high winds. Although this condition was not tested, it was apparent that main rotor problems associated with starting in high winds were improved by the installation of the hub spring.

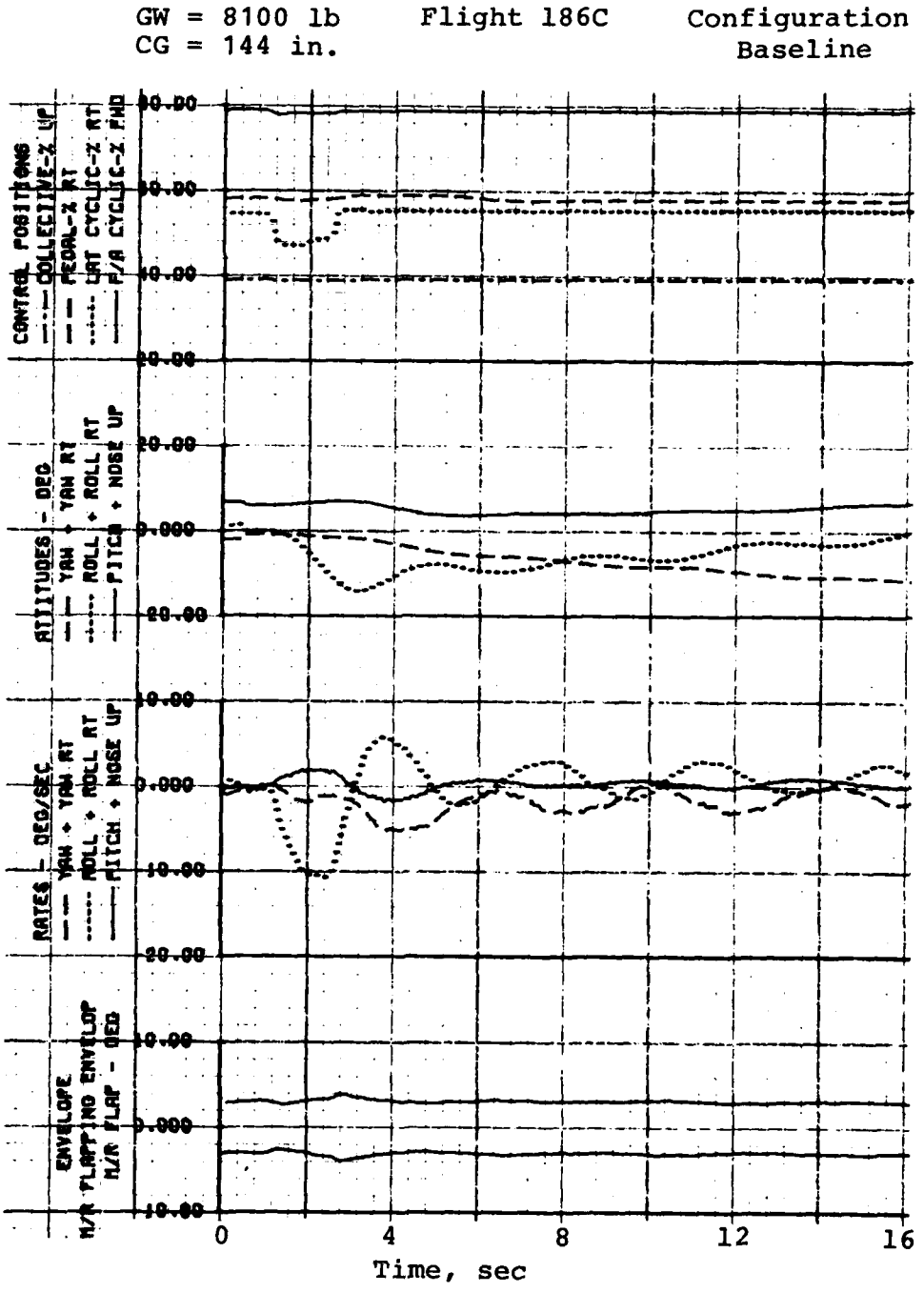

Figure 56. Effects of the hub spring on main rotor flapping and helicopter response to a left lateral cyclic control pulse at 0.6 V_{NE}.

GW = 8100 lb
CG = 144 in.

Flight199B

Configuration
Hub Spring

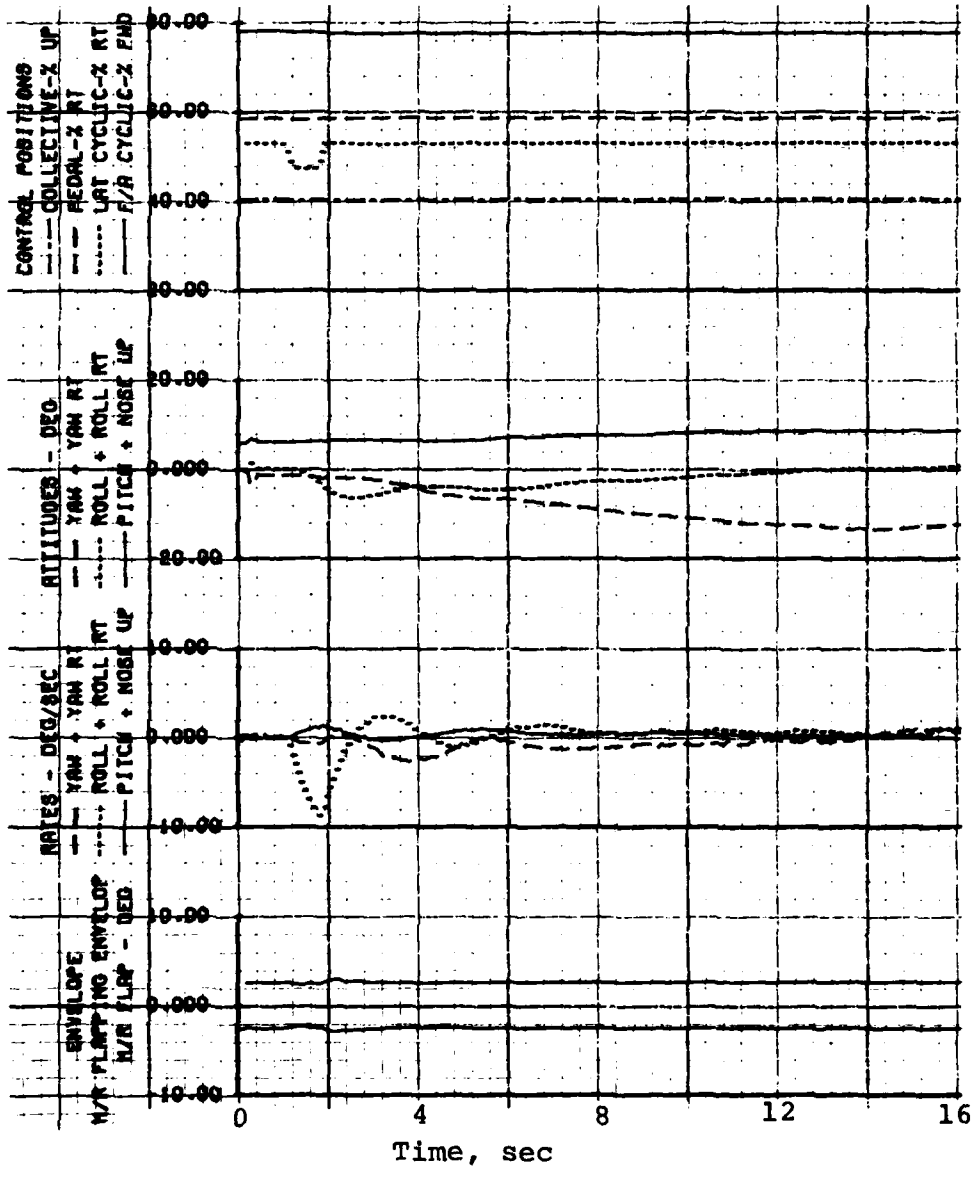

Figure 56. Concluded.

GW = 8100 lb Flight 186C Configuration
CG = 144 in. Baseline

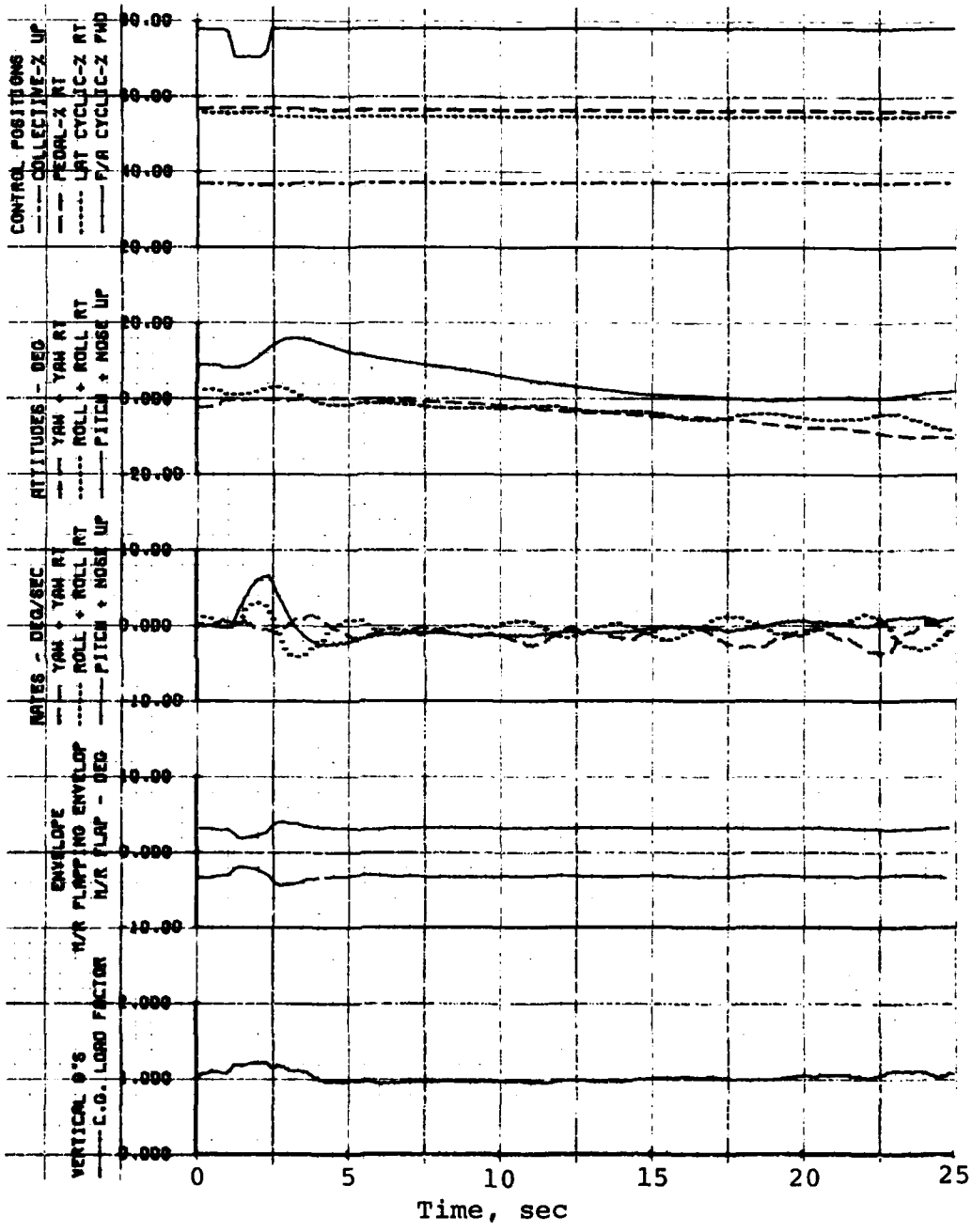

Figure 57. Effects of the hub spring on main rotor flapping and helicopter response to an aft cyclic control pulse at 0.6 V_{NE}.

GW = 8100 lb
CG = 144 in.

Flight 199B

Configuration
Hub Spring

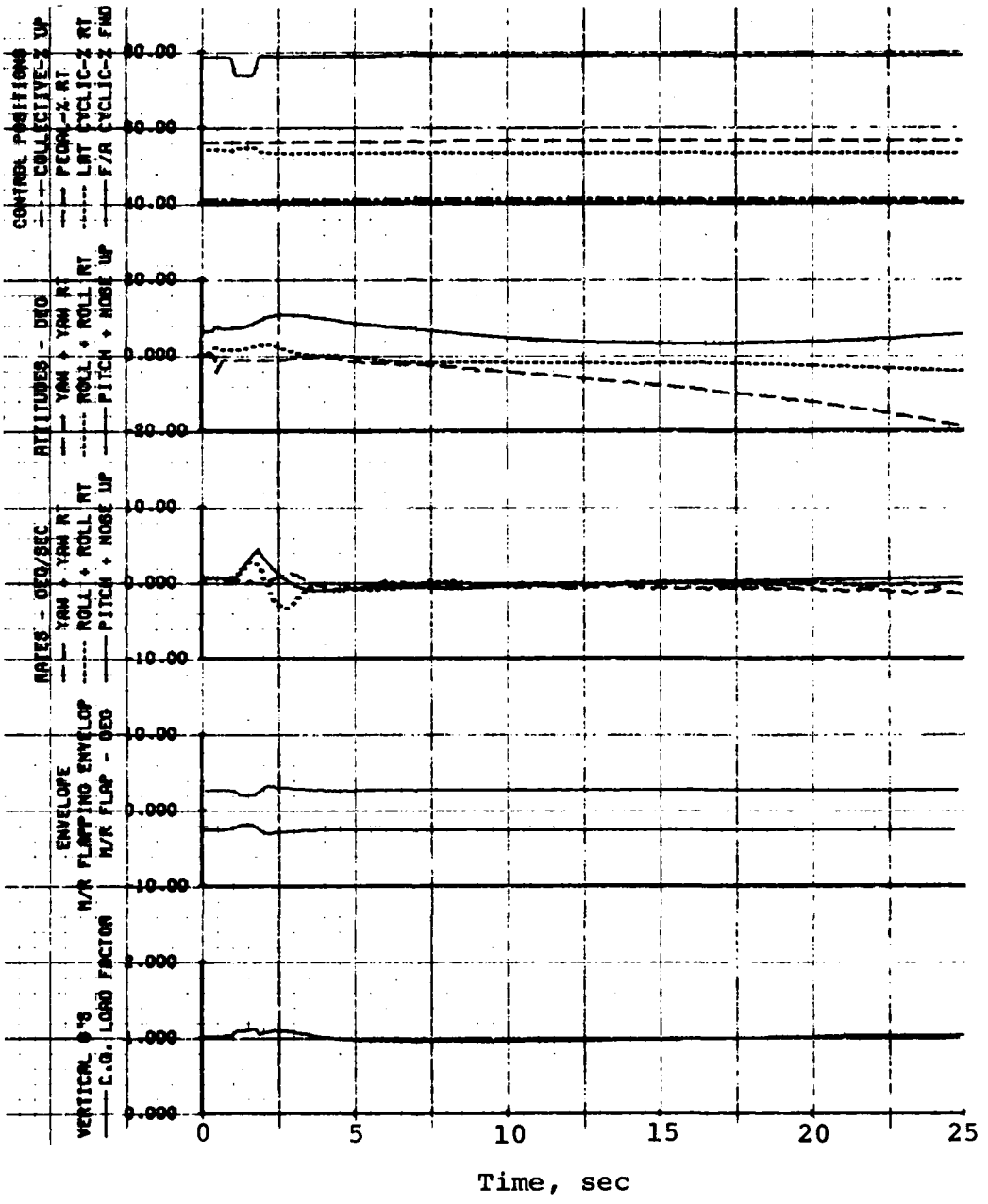

Figure 57. Concluded.

7.4 EFFECT OF HUB SPRING ON VIBRATION CHARACTERISTICS

In order to determine the effect of the nonlinear hub spring on vibration characteristics of the UH-1H helicopter, accelerometers were located in the nose, at the crew stations, at the aircraft center of gravity, and at the top of the vertical fin. Since the main area of concern is the vibration acceleration at the crew and passenger stations, only the vibration acceleration data at the frequency of 10.8 cps (2-per-rev) during steady level flight are presented. Passenger station vibrations were measured in three axes (vertical, lateral, and longitudinal) by accelerometers at the center-of-gravity and crew station by measuring (with accelerometers under the crew seats) copilot (left-side) vertical vibrations and pilot (right side) vertical and lateral vibrations. There should be little, if any, difference in longitudinal vibrations between the center of gravity and the crew stations.

7.4.1 Center-of-Gravity Vibration Characteristics

The vibration accelerations at the 2-per-rev frequency for three axes (vertical, lateral, and longitudinal) at the center of gravity are shown in Figure 58. This figure presents the data for both loading configurations investigated. With one exception, the data indicates that the vibration accelerations are increased by installation of the hub spring at both loading configurations. The increased vibration accelerations are, however, within the acceptable limit of 0.15g up to cruise airspeed, and 0.20g between cruise airspeed and limit airspeed as specified by MIL-STD-850l.

7.4.2 Crew Station Vibration Characteristics

Vibration accelerations measured at the pilot's station (vertical and lateral) and the copilot's station (vertical) are shown at 2-per-rev frequency in Figure 59. In the case of the light/aft loading configuration, the vibration accelerations were decreased at the crew stations. In the heavy/forward configuration, however, the vibration accelerations increased following installation of the hub spring. In addition to the data presented in Figures 58 and 59, the program test pilot stated that he felt that there was increased 2-per-rev vibration in all flight conditions (Appendix B).

7.4.3 Summary of Vibration Characteristics

The variations of the data presented in Figures 58 and 59 can be attributed to normal data scatter; therefore, from the data presented, no definite conclusion concerning the effect of the hub spring on vibration levels can be made.

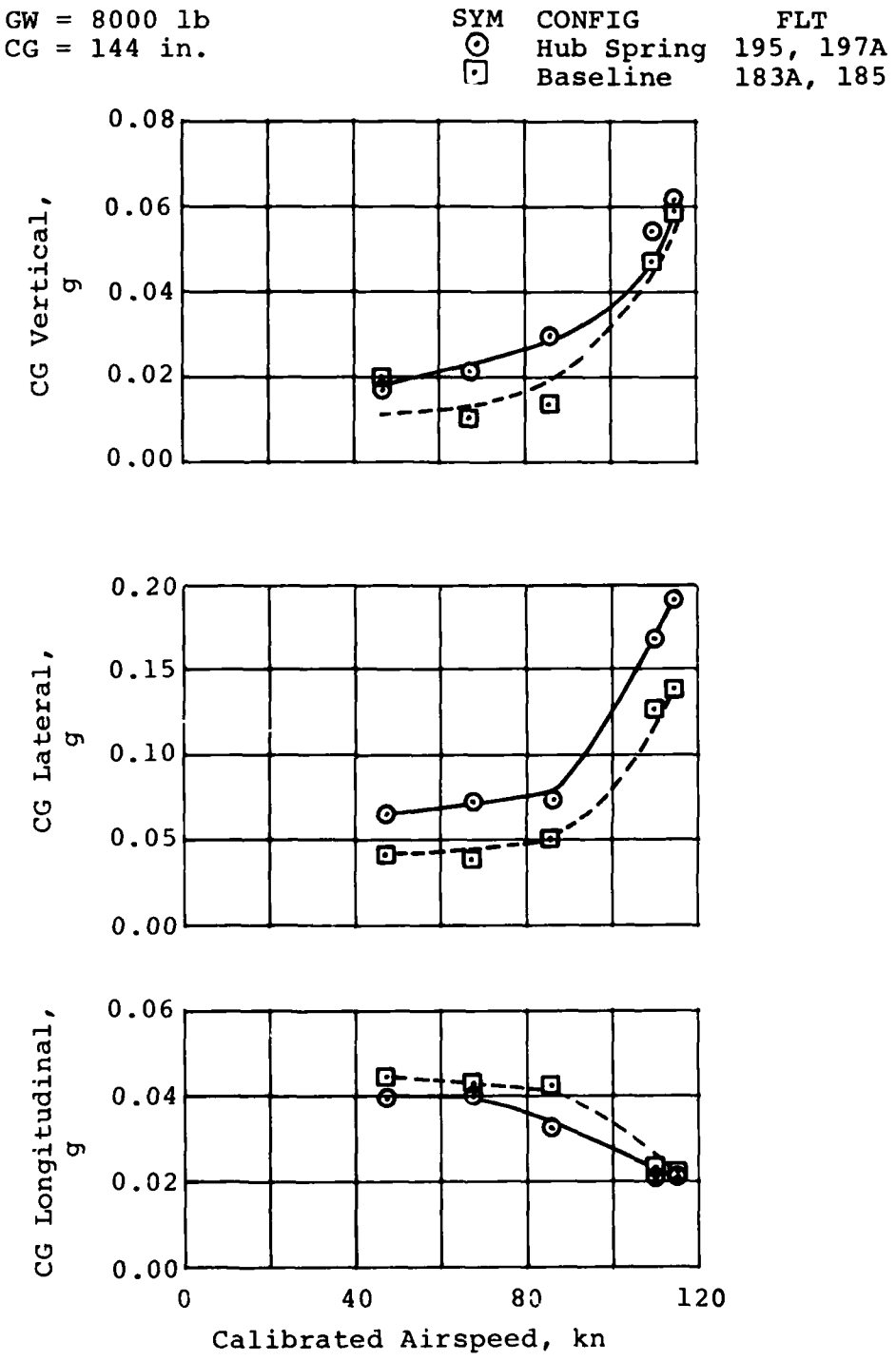

Figure 58. Effect of the hub spring on center-of-gravity 2-per-rev vibration acceleration in level flight.

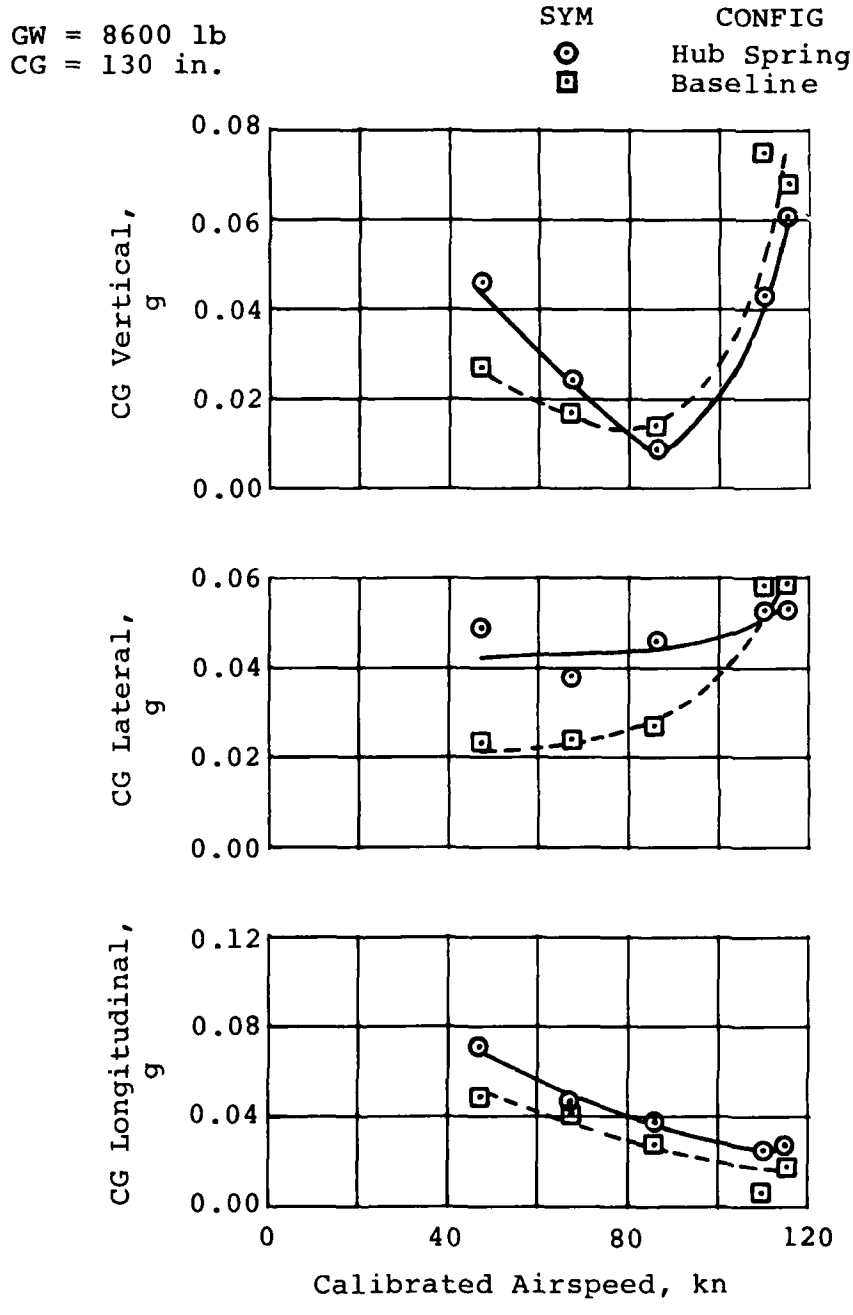

Figure 58. Concluded.

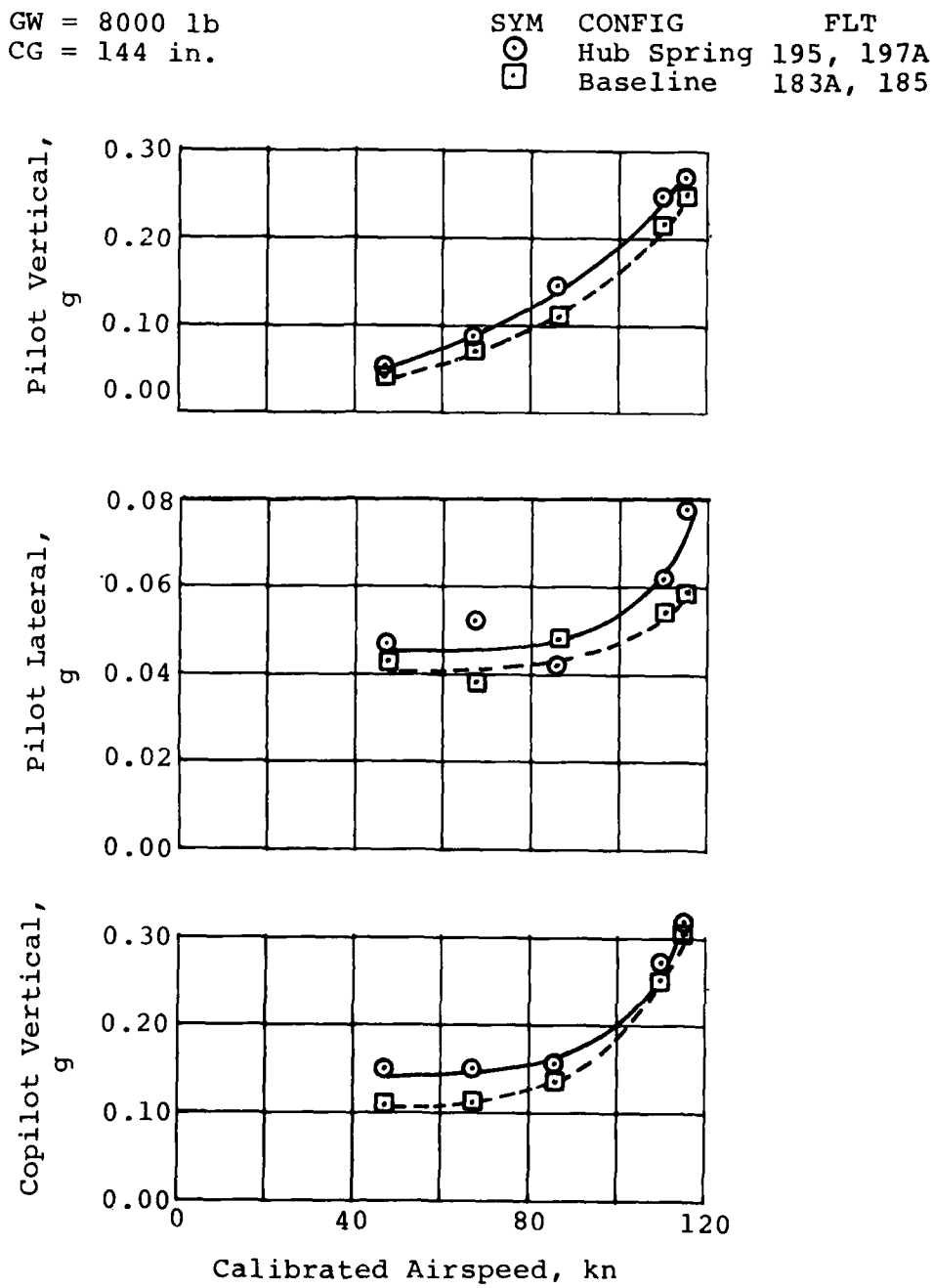

Figure 59. Effect of the hub spring on crew station 2-per-rev vibration acceleration in level flight.

GW = 8600 lb
CG = 130 in.

SYM	CONFIG	FLT
⊙	Hub Spring	195, 197A
⊡	Baseline	183A, 185

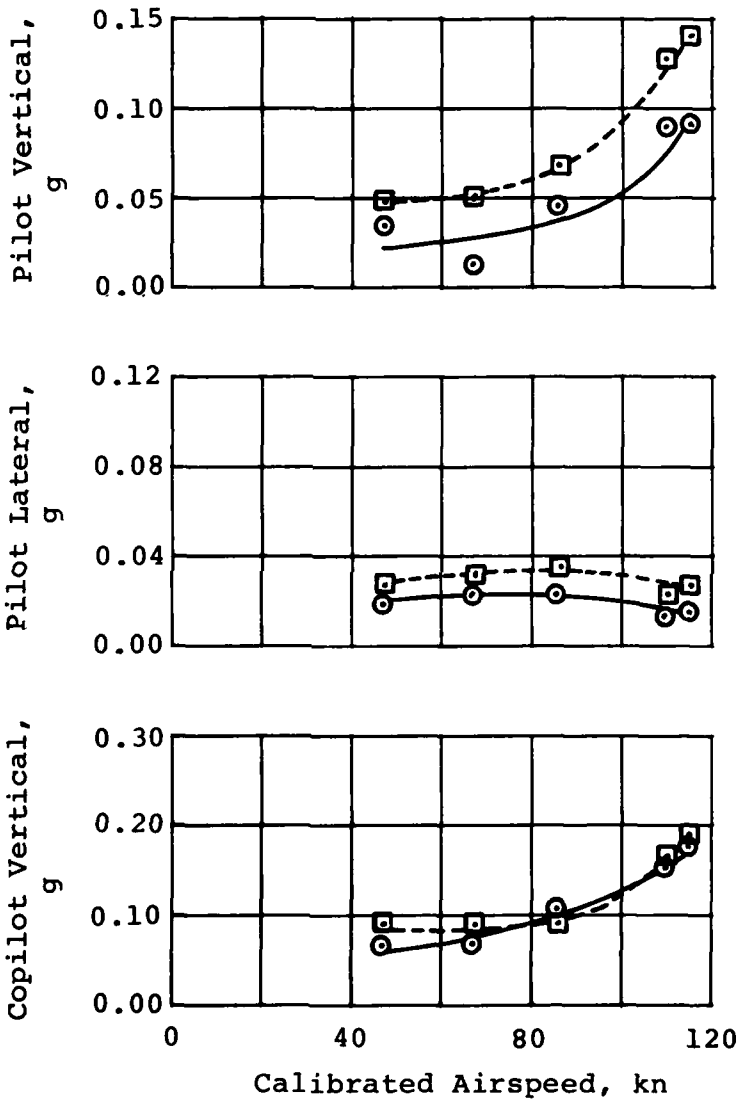

Figure 59. Concluded.

As stated by the test pilot, the helicopter exhibited some tendencies to wallow around during start-up when the main rotor was below 130 rpm. In any case, the increased vibration was not significant or objectionable to the pilot.

As expected, the stiffness of the hub spring used during this test program is not great enough to introduce significant changes to the vibration levels of the UH-1H helicopter.

7.5 EFFECT OF HUB SPRING ON MAIN ROTOR COMPONENT FATIGUE LIVES

During the flight test program of the nonlinear hub spring on a UH-1H aircraft, several loading parameters in the main rotor system were measured and recorded. These data are presented as fatigue damage summary tables for conditions where flight loads exceeded their respective endurance limits during the test program.

For the purpose of vibration evaluation, wind-up turns were flown during this investigation. These maneuvers are considered aerobatic in nature and would therefore not be within the operating manual limits prescribed for the UH-1H aircraft. Also, to generate maximum flapping, certain flight conditions were flown outside the gross weight/center-of-gravity envelope and are not representative of normal UH-1H flight conditions.

Considering the nature of these "extreme" conditions, they are not considered in the evaluation of the effect of the hub spring on component retirement intervals; however, they are used to assess the damage accumulated by each component during the flight test program. Paragraph 7.5.1 presents the fatigue evaluation for normal operation. Paragraph 7.5.2 gives the fatigue evaluation for the complete program, including retirement time adjustments as required to account for accelerated damage accrual.

7.5.1 Fatigue Damage During Normal Operation

Fatigue damage calculations were performed for the following components: main rotor, yoke, mast, and pitch horn. The results are presented in Tables 11 through 13. No summary was needed for the main rotor yoke, since no damage was incurred on this part during the normal flight conditions. In these tables, the cycles per hundred hours are the total per flight condition regardless of gross weight, center of gravity, or altitude from the appropriate fatigue life determination table in Reference 1.

TABLE 11. SUMMARY OF MAIN ROTOR BLADE FATIGUE DAMAGE DURING FLIGHT WITHIN OPERATIONAL ENVELOPE

Flight Condition	Cycles/100 Hours	Osc. Stress in Trailing Edge Sta. 192.0, psi	Cycles To Failure	Damage Fraction
Forward Level Flight				
0.2 V_{NE}, 317 rpm	19,133	±6226	908,000	.000116*
Cyclic Pull-ups				
0.9 V_H	957	±5641	1,786,000	.000023*
Normal Test Program Total				.000139
Fatigue Life Report Comparable Total				.001721

*Damage calculated from measured load frequencies

TABLE 12. SUMMARY OF MAIN ROTOR MAST FATIGUE DAMAGE DURING FLIGHT WITHIN OPERATIONAL ENVELOPE

Flight Condition	Cycles/ 100 Hours	Osc. Stress Sta. 49.75, psi	Cycles To Failure	Damage Fraction
Sideward Flight to Right	4783	±40,981	428,000	.001336*
Rearward Flight	4783	±39,365	725,000	.000415*
		Total =		.001751
		Life =		57,110 Hours

*Damage calculated from measured load frequencies

TABLE 13. SUMMARY OF ROTOR PITCH HORN FATIGUE DAMAGE DURING FLIGHT WITHIN OPERATIONAL ENVELOPE

Flight Condition	Cycles/ 100 Hours	Osc. M/R Red Pitch Link Loads, lb	Cycles To Failure	Damage Fraction
Sideward Flight to the Right	4783	±845	18,754,000	.000255
Cyclic Pull-ups				
0.6 V_H	3827	±773	58,515,000	.000065
0.9 V_H	957	±935	6,664,000	.000144
Normal Test Program Total				0.000464
Fatigue Life Report Comparable Total				.001721

7.5.1.1 Main Rotor Blade. As shown in Table 11, there were only two flight conditions within the normal flight envelope that produced stresses that exceed the endurance limit. The summation of damage for these two conditions during operation with the hub spring is 0.001721. Since this is less than the total for these two conditions in Table 12 of Reference 8 for the basic aircraft, no reduction in the main rotor blade retirement interval should be required for aircraft operating with the nonlinear hub spring.

7.5.1.2 Main Rotor Mast. During the flight test evaluation of the hub spring within the normal envelope, only two flight conditions produced stresses greater than the mast endurance limit. The damage fraction total for these two conditions is 0.001751. In Reference 1, the mast is substantiated for an unlimited fatigue life with no stress greater than the endurance limit. Therefore, the only damage expected for the mast is that shown in Table 12. From this damage fraction, a fatigue life of 57,110 hours was calculated. Since the life is greater than the recognized 25,000-hour service life, an unlimited fatigue life would be predicted for the main rotor mast during normal operation with the nonlinear hub spring.

7.5.1.3 Main Rotor Pitch Horn. An evaluation of the main rotor pitch horn was conducted, since its endurance limit is the lowest in the rotating control system in terms of pitch link axial load. The damage summary in Table 13 shows a total of 0.000464 for the conditions where measured loads exceed the endurance limit. Since this total is less than the 0.001721 total for the basic aircraft (Table VII of Reference 8), no reduction in the retirement intervals for the main rotor controls is anticipated.

7.5.2 Fatigue Evaluation of Complete Test Program

Tables 14 through 17 present fatigue damage summaries for the main rotor blade, yoke, mast, and pitch horn. The flight loads used are the top of scatter loads where maneuvers were flown more than one time. The fatigue damage is the real-time cycle-counted total using each measured cycle as it occurred with no projected spectrum. Where conditions were repeated,

---

[8]Orr, P., McLeod, G., Goodell, W., FATIGUE LIFE SUBSTANTIATION OF DYNAMIC COMPONENTS FOR THE UH-1D HELICOPTER EQUIPPED WITH THE 48-FOOT DIAMETER ROTOR, BHT Report Number 299-099-135, Bell Helicopter Textron, Fort Worth, Texas, June 1964.

TABLE 14. SUMMARY OF MAIN ROTOR BLADE FATIGUE DAMAGE DURING HUB SPRING TEST PROGRAM

Flight Condition	Damage Fraction/ Occurrence	Occurrences	Total
0.9 V_H Cyclic Pull-up	.000001	10	.000010
Bob-up	.000005	4	.000020
Dash	.000002	4	.000008
Lateral Dash-Rt	.000020	7	.000140
Lateral Dash-Lt	.000006	7	.000042
Quickstop	.000001	4	.000004
Zigzag - L/R	.000002	4	.000008
Zigzag - R/L	.000006	3	.000018
Roller Coaster @ .5g	.000001	7	.000007
Roller Coaster @ .2g	.000001	5	.000005
Wind-up Turn - Rt 1.7g	0	2	
Wind-up Turn - Lt 2.0g	.000670	5	.003350
Wind-up Turn - Rt @ 2.0g	.000203	4	.000812
Roll Step - .5 inch	.000001	5	.000005
Roll Step - .75 inch	.000001	2	.000002
Roll Step - .25 inch	.000001	2	.000002
Level Flight - .2 V_{NE}	.000008	3	.000024
			.004457

Fatigue damage = .000338/normal flight hour per Reference 8.

Therefore, test total (.004457) is equivalent to 13 hours of normal operations.

TABLE 15. SUMMARY OF YOKE FATIGUE DAMAGE DURING HUB SPRING TEST PROGRAM

Flight Condition	Damage Fraction/ Occurrence	Occurrences	Total
Lt Wgt @ 2.0g	.000005	5	.000025
			.000025

Fatigue damage = .000068/normal flight hour per Reference 8.

Therefore, test total (.000025) is equivalent to less than one hour of normal operation.

TABLE 16. SUMMARY OF MAIN ROTOR MAST FATIGUE DAMAGE DURING HUB SPRING PROGRAM

Flight Condition	Damage Fraction/ Occurrence	Occurrences	Total
Rt Sideward - 30 kt	.001117	4	.004468
Rearward - 30 kt	.000504	7	.003528
Lateral Dash - Rt	.000096	7	.000672
Lateral Dash - Lt	.000009	7	.000063
Quickstop	.000003	4	.000012
Zigzag - Lt/Rt	.000001	4	.000004
Sideward Flt - 10 kt	.000013	2	.000026
Sideward Flt - 20 kt	.000027	2	.000054
Rearward - 10 kt	.000009	2	.000018
Rearward - 20 kt	.000006	2	.000012
			.008857

Since no fatigue damage occurs during normal operation as stated in Reference 8, damage rate per hour does not apply to this component.

TABLE 17. SUMMARY OF MAIN ROTOR PITCH HORN FATIGUE DAMAGE DURING HUB SPRING PROGRAM

Flight Condition	Damage Fraction/ Occurrence	Occurrences	Total
Cyclic Pull-up	.000001	10	.000010
Lateral Dash-Lt	.000049	7	.000343
Quickstop	.000003	4	.000012
Roller Coaster @ .5g	.000013	7	.000091
Roller Coaster @ .2g	.000024	5	.000120
Wind-up Turn - Lt @ 2.0g	.000147	5	.000735
Wind-up Turn - Rt @ 2.0g	.000055	4	.000220
Wind-up Turn - Lt @ 1.7g	.000001	2	.000002
Wind-up Turn - Rt @ 1.7g	.000004	2	.000008
Roll Step @ .5 inch	.000017	5	.000085
Roll Step @ .75 inch	.000016	2	.000032
Roll Step @ .25 inch	.000022	2	.000044
Rt Sideward - 30 kts	.000935	4	.003740
Rearward - 30 kts	.001307	7	.009149
			.014591

Fatigue damage = .000141/normal flight hour per Reference 8. Therefore, test total (.014591) is equivalent to 104 hours of normal operation.

the damage fraction is raised in multiples of occurrences. The damage fractions shown in the tables are expressed as an accrual rate per flight hour during the 20-hour flight program. These rates were then compared with the hourly rates predicted by the retirement intervals presented in Reference 8. The main rotor pitch horn showed a damage rate that would indicate an equivalent flight time of 104 hours during the 22-hour test program.

Since the main rotor mast had no damaging conditions during normal operation without the nonlinear hub spring, it is considered that if returned to normal use in the standard UH-1H configuration, it would accumulate no further fatigue damage. Therefore, the .008857 damage fraction in Table 16 is considered to be the total to date and, as stipulated above, the total for future operation unless new test programs are accomplished. Since this total is far less than the 0.5 total at which retirement would be recommended, it is considered that the main rotor mast on this aircraft would retain its unlimited retirement interval.

7.5.3 Fatigue Evaluation Summary

There is no noticeable trend for variations in loads during forward level flight with the nonlinear hub spring versus baseline loads for the same conditions. Also, as stated in Paragraphs 7.5.1 through 7.5.1.3, the fatigue damage on the critical components during operation with the nonlinear hub spring is within the values established in Reference 7 for the basic aircraft. Under these considerations, it is therefore concluded that the nonlinear hub spring can be installed on UH-1H aircraft without lowering the present retirement intervals, as long as the operational flight limits specified in the operating manual are observed.

7.5.4 Recommendation

As stated in Paragraph 7.5.2, certain dynamic components did accumulate fatigue damage at an accelerated rate per flight hour compared to normal operation. It is therefore recommended that the retirement intervals for all time-life components on the test aircraft be lowered by 100 hours as calculated for the main rotor pitch horn in Table 17. This adjustment is considered necessary on all components due to the lack of measured flight loads on certain aircraft systems during the test programs. It is emphasized that this action is applicable to UH-1H test aircraft, U.S. Army S/N 73-21805 (BHT S/N 13493) only, and does not apply to all such aircraft.

7.6 PROBLEMS ENCOUNTERED AND SOLUTIONS

During the course of the flight test program and as a result of inspection of the hub spring after removal from the test helicopter, several design deficiencies and problem areas were found. Further analysis also yielded a problem concerning the transmission main case. The transmission case was not, however, instrumented during this flight test program. For all design deficiencies or problem areas, possible solutions have been identified below.

7.6.1 Structural Bond Failure

During the flight test program, the structural bond between one of the elastomeric shear pads and the side frame of the hub spring failed. This particular failure would not occur on a production hub spring. In the case of the experimental hub springs, the elastomeric shear pads were bonded to metal shims during the molding process. These shims were then cemented to the side frames, after the parts had cooled, following molding. It was this cemented bond that failed. In the production hub spring, the side member is incorporated into the mold and the elastomer bonded during the molding process. This is a much stronger bond and will not fail during operation.

7.6.2 Abrasion and Tearing of Elastomerics

Inspection of the elastomerics during the flight test program and following removal from the test aircraft showed abrasion loss of material on the snubber face and a tear of the elastomer of the shear pads. Abrasion of the snubber was caused by relative motion of the snubber following contact with the mast. It was determined that the snubber face and mast contact point were not parallel when snubber-mast contact was made and was the cause of this motion.

This problem will be eliminated by:

- Modification of the snubber mold to insure that mast contact point and the snubber face are parallel;
- Increased width of the mast contact point to insure that the compressed snubber does not wrap around the mast; and
- Using an abrasion-resistant elastomer for the snubber face.

Tears in the elastomer at the upper inside corners of all shear pads were found to have started at an unrelieved stress concentration. The stress at this location can be relieved by modification of the mold to extend a fillet and by changing the mold parting line.

7.6.3 Excessive Stress in Side Member

The stresses in the side member of the hub spring were such that fatigue damage was occurring at a rate that would make the part unacceptable as production hardware. These damaging stress levels were present for all flight conditions when flapping was greater than 4.5 degrees. A modification that increases the material cross area of the side member in order to reduce stresses below the endurance level will be required for this part. This modification can be accomplished without introducing interference problems. Additionally, correcting the angle of the snubber face will reduce the side member stress.

7.6.4 Fretting of Mast and Yoke

Inspection of the mast and yoke following flight test showed that there might be a problem with fretting of the mast and yoke under the clamps. The possibility of fretting can be eliminated by use of bluecoat or scrim buffers, or redesign of hardware to eliminate motion of the clamps.

7.6.5 Transmission Structural Analysis

During the post-flight analysis of the loads introduced by the hub spring, it was determined, by analysis, that the main case of the UH-1H could no longer be shown to have a positive margin of safety with hub spring installed.

This is a result of a combination of several factors. First, the revision downward of stress allowables for magnesium, from which the transmission main case is cast, found in MIL-HDBK-5, "Metallic Materials and Elements for Aerospace Vehicle Structures." Secondly, the new casting factors to be used for Class 1A castings that are found in AMCP 706-203, "Helicopter Engineering, Part Three, Qualification Testing" (Section 7-4 paragraph 7.4.2.2.1.6), and the additional stresses resulting from hub moments produced by installation of the hub spring. When all factors are considered, the transmission is calculated to be static strength limited. A fatigue analysis of the transmission under hub spring loading has not been performed. A solution to this problem would be to replace the magnesium main case with an aluminum one similar to that found on the Bell Model 212 helicopter. Another approach would be

to attempt to qualify the transmission by a static proof test that subjects the transmission to the maximum stresses introduced by the hub spring in addition to the maximum stresses encountered during the structural demonstration flight program.

7.7 SUMMARY OF FLIGHT TEST RESULTS

The flight test program demonstrated that the nonlinear hub spring did, in fact, reduce main rotor flapping and therefore improved the UH-1H mast bumping margin of safety. As shown, main rotor flapping was reduced at all conditions tested, and lateral control power was increased at low-g flight conditions by installation of a nonlinear hub spring in the test aircraft.

As expected, handling quality characteristics of the UH-1H helicopter were either improved or unchanged by installation of the hub spring. As an example, control power was increased approximately 15 percent in the pitch and roll axis, and static longitudinal stability increased at the aft center-of-gravity configuration. Also, improved control margins were demonstrated.

Although higher stresses were measured in the main rotor mast and hub at main rotor flapping angles greater than 4 degrees during flights with the hub spring installed, there would not be a requirement to decrease mast, hub, or blade retirement or overhaul intervals.

8. CONCLUSIONS AND RECOMMENDATIONS

8.1 CONCLUSIONS

A nonlinear hub spring was successfully designed and flight tested for the UH-1H helicopter. This design met the retrofit criteria as well as the additional load constraint that no main rotor component time-between-removal interval would be changed. Flight testing of the nonlinear hub-spring-equipped UH-1H helicopter proved the concept of the nonlinear hub spring as a method for improving the mast bumping safety margin. Flapping was reduced in all flight conditions with the greatest reduction being recorded when baseline flapping was above 5 degrees. The nonlinear hub spring also greatly improved the low-g control power of the UH-1H helicopter.

Following an analysis of helicopter tactical instruction manuals and observation flights over the UH-1H NOE instruction course at Fort Rucker, Alabama, it is concluded that current tactics do not cause excessive flapping if normal operating procedures are followed. There were flight conditions, however, during which main rotor flapping exceeded 8 degrees. It is concluded that if the loading condition is heavy and forward, 30-knot rearward and right sideward flight and right lateral dashes will result in main rotor flapping exceeding 8 degrees.

The comparison of main rotor flapping as predicted by the hybrid version of C81 with rigid rotor blades and digital C81 with elastic rotor blades shows that the main rotor flapping predictions are not greatly altered by elastic blades.

Simulation of mast loads during conditions of in-flight flapping stop contact can be satisfactorily accomplished utilizing a modified version of the rotor pylon hybrid computer program (ARHF01). An aeroelastic model rotor was satisfactorily tested on a whirl stand providing additional flapping and mast contact loads data. Comparison of data obtained from the aeroelastic model rotor and test helicopter measured data with that predicted by ARHF01 demonstrate excellent correlation.

A main rotor design criterion is suggested for teetering rotor helicopters. Using ARHF01 results, mast loads were predicted with a simplified method that will allow contact loads to be included in the structural design of rotor concepts.

8.2 RECOMMENDATIONS

The nonlinear hub spring has been demonstrated to be a feasible concept for increasing the mast bumping safety margin for the UH-1H. The problems identified during these tests can be eliminated while designing for production articles to retrofit the UH-1H fleet. The nonlinear hub spring should be subjected to qualification testing. The shortcomings of the nonlinear hub spring identified during this test should be corrected and the additional flight testing and fatigue testing conducted. Also, user tests of the nonlinear hub spring equipped UH-1H helicopter should be conducted. The application of the nonlinear hub spring as a hub flapping restraint mechanism on other helicopters with teetering main rotor systems should be studied.

A proof test of the current transmission should be conducted in order to determine if adequate structural safety margins exist with the additional loads introduced by the hub spring. If positive margin cannot be demonstrated, further effort is needed to qualify a stronger transmission assembly.

Additional testing and analysis is required to fully establish the design criteria for various pylon configurations, rotor thrust levels, and rotor blade designs.

9. REFERENCES

1. Dooley, L. W., ROTOR BLADE FLAPPING CRITERIA INVESTIGATION, Bell Helicopter Textron, USAAMRDL Technical Report 76-33, Eustis Directorate, U.S. Army Air Mobility Research and Development Laboratory, Fort Eustis, Virginia, December 1976, AD A034459.

2. Dooley, L. W., and Ferguson, S. W. III, EFFECT OF OPERATIONAL ENVELOPE LIMITS ON TEETERING ROTOR FLAPPING, Bell Helicopter Textron, USARTL Technical Report 78-9, Applied Technology Laboratory, U.S. Army Research and Technology Laboratories, Fort Eustis, Virginia, July 1978.

3. VanGaasbeek, James R. and Landry, L. Matthew, Jr., HYBRID COMPUTER PROGRAM ARHF02, Technical Data Report 699-099-015 to be published by Bell Helicopter Textron, Fort Worth, Texas.

4. Van Gaasbeek, James R., ROTORCRAFT FLIGHT SIMULATION COMPUTER PROGRAM C81, WITH DATAMAP INTERFACE, Volume I - User's Manual, to be published by the United States Army Research and Technology Laboratories, Applied Technology Laboratory, Fort Eustis, Virginia.

5. Bonham, D. G., and Hollifield, P. J., UH-1 HUB SPRING INSTRUMENTATION TEST PLAN, BHT Report Number 699-099-095, Bell Helicopter Textron, Fort Worth, Texas, June 1978.

6. Hollifield, P. J., UH-1 HUB SPRING TEST PLAN, BHT Report Number 699-099-099, Bell Helicopter Textron, Fort Worth, Texas, August 1978.

7. Harris, F. D., ARTICULATED ROTOR BLADE FLAPPING MOTION AT LOW ADVANCE RATIO, Journal of American Helicopter Society, January 1972.

8. Orr, P., McLeod, G., Goodell, W., FATIGUE LIFE SUBSTANTIATION OF DYNAMIC COMPONENTS FOR THE UH-1D HELICOPTER EQUIPPED WITH THE 48-FOOT DIAMETER ROTOR, BHT Report 299-099-135, Bell Helicopter Textron, Fort Worth, Texas, June 1964.

10. LIST OF ABBREVIATIONS AND SYMBOLS

B_0	Coning angle, deg
B_1	Longitudinal cyclic feathering, deg
B_2	Lateral cyclic feathering, deg
D	Drag force, lb
F_s	Factor of Safety
H	Hub longitudinal inplane shear force, lb
IL	Inplane shear force, lb
K_{EFF_T}	Theoretical effective spring rate, ft-lb/deg
K_{FS}	Flapping stop (mast) spring rate, ft-lb/deg
K_L	Hub restraint linear spring rate, ft-lb/deg
K_{NL}	Hub restraint nonlinear spring rate, ft-lb/deg
K_T	Effective spring rate due to rotor thrust, ft-lb/deg
KTAS	Knots True Airspeed, knots
L	Lift, lb
M	Mast bending moment, ft-lb
$M_\perp$	Mast perpendicular bending moment, ft-lb
$M_\parallel$	Mast parallel bending moment, ft-lb
M_{FS}	Bending moment due to flapping stop contact, ft-lb
M_{TOT}	Total bending moment due to flapping restraint, ft-lb
r	Order of nonlinearity
S	Mast shear force, lb
T	Thrust, lb
T_c	Thrust coefficient

V_H	Level flight airspeed requiring maximum continuous power, knots
V_{NE}	Never exceed airspeed, knots
WUT	Wind-up turn
X	Distance from teetering axis to a point at which a mast moment is computed, ft
XLFS	Distance from teetering axis to the flapping stop contact point on the mast, ft
Y	Hub lateral inplane shear force, lb
β	Hub flapping angle, deg
β_o	Coefficient representing flapping angle independent of blade azimuth angle, deg
β_{1_s}	Coefficient representing amplitude of pure sine flapping motion, deg
β_{1_c}	Coefficient representing amplitude of pure cosine flapping motion, deg
β_B	Flapping angle at which nonlinear hub spring is engaged, deg
β_s	Hub flapping at flapping stop contact, deg
β_x	Commanded hub flapping beyond flapping stop, deg
β^*	Value of hub flapping beyond flapping stop
δ_3	Pitch-flap coupling angle, deg
Ω	Main rotor rotational speed, rad/sec
ψ	Main rotor azimuth angle, rad
θ	Angular deflection, deg
θ_{75}	Blade collective pitch angle at 3/4 radius, deg

APPENDIX A

TABULATION OF ARHF01 INPUTS FOR THE UH-1H WITH NONLINEAR HUB SPRING

Description	Name	Value	Units
LIFT CURVE SLOPE	A	5.70000	ND
ROTOR PRECONE ANGLE	A0	0.4800E-01	RAD
SAME AS BBETA	B	10.72	FT
VH TO BLADE MASS(CON	BBETA	10.72	FT
FLAPPING STOP	BFS	0.2007	RAD
VH TO BLADE MASS (IP	BZETA	9.973	FT
SKID GEAR DAMPING	CG	500.0	ND
PYLON CONTROL COUPLING TERMS			
LAT TO PYLON ROLL	DA1DPP	0.0	ND
LAT TO PYLON PITCH	DA1DPT	0.0	ND
F/A TO PYLON ROLL	DB1DPP	0.0	ND
F/A TO PYLON PITCH	DB1DPT	0.0	ND
CONING VH OFFSET	E	3.240	FT
CONING VH OFFSET	EBETA	3.240	FT
IP VH OFFSET	EZETA	6.000	FT
FLAT PLATE AREA	F	18.35	FT**2
GRAV. ACCELERATION	G	32.17	FT/SEC2
LOCK NUMBER	GAMMA	6.293	ND
HUB UNDERSLING	HU	0.4333	FT
FLAPPING INERTIA	IBETA	1181.	SLUG-FT2
FUSELAGE PITCH INERT	IF	0.1108E 05	SLUG-FT2
FUSELAGE ROLL INERT	IR	3162.	SLUG-FT2
IP VH BLADE INERTIA	IZETA	515.3	SLUG-FT2
HUB SPRING	KBETA	0.1891E 05	FTLB/RAD
SOUTH. COEFF (CON)	KBETAP	1.229	ND
FLAP STOP SPRING	KFS	0.1300E 06	FTLB/RAD
SKID VERT SPRING	KG	3500.	FTLB/RAD
PYLON STOP SPRING	KP	3700.	FTLB/RAD
CONTROL SYS SPRING	KTHETA	0.3300E 05	FTLB/RAD
IP VH SPRING	KZETA	0.5963E 06	FTLB/RAD
SOUTH. COEFF (IP)	KZETAP	0.3736	ND
BLADE MASS	MB	4.010	SLUGS
ENGINE TORQUE	ME	0.0	FTLB
FUSELAGE MASS	MF	248.7	SLUGS
LANDING GEAR FRICTN	MU	0.8000	ND
PYLON ROLL STOP	PP0	0.3500	RAD
PYLON PITCH STOP	PT0	0.3500	RAD
3/4 BLADE RADIUS	R	18.00	FT
BLADE RAD GYR.(IP,CG	RG	5.391	FT
AIR DENSITY	RHO	0.2233E-02	SLUG/FT3
CONING FREQ SQUARED	WBETA2	154.4	(R/SEC)2
IP FREQ SQUARED	WZETA2	1157.	(R/SEC)2
FUS CG UNDER HUB	ZCG	7.312	FT
HUB MASS	MH	0.0	SLUGS
BLADE CONING INERTIA	IBETA0	770.1	SLUG-FT2
	DELTA3	0.0	RAD
INDUCED VEL TIME CON	TAU1	0.2500	SEC
XDIST CG TO PILOT	XPT	0.0	FT
ZDIST CG TO PILOT	ZPT	0.0	FT
ROTOR RPM	RPM	324.0	RPM
PITCH-LAG COUPLING	ALPHAJ	0.0	DEG
LAT TO PYLON VERT	DB1DPZ	0.0	ND
F/A TO PYLON VERT	DA1DPZ	0.0	ND
PITCH TO PYLON VERT	DTHDPZ	0.0	ND
PITCH TO PYLON PITCH	DTHDPT	0.0	ND
INPLANE MODE DAMPING	ZZETA	0.4000E-01	PCT
MAST TILT ANGLE	THTI	-0.8727E-01	RAD
PIN TO FLAP STOP ARM	XLFS	0.6083	FT
	X1LFS	1.333	FT
	X2LFS	3.896	FT
SPRING CONTACT ANGLE	BBRK	0.6981E-01	RAD
SPRING CONSTANT	KBBRK	4.363	FTLB/DEG
SPRING EXPONENT	EXPBRK	3.000	ND

APPENDIX A (Concluded)

LANDING GEAR DATA

DESCRIPTION	NAME	VALUE	UNITS
FWD GEAR DIST TO CG.	XGF	10.00	FT
AFT GEAR DIST TO CG.	XGA	10.00	FT
FWD GEAR SPRING	KGF	1000.	LB/FT
AFT GEAR SPRING	KGA	1000.	LB/FT
FWD GEAR DAMPER	CGF	10.00	LBSEC2/FT
AFT GEAR DAMPER	CGA	10.00	LBSEC2/FT
NO. FWD GEARS	NFG	2	-
NO. AFT GEARS	NAG	2	-
Z DIST. CG TO GEAR	ZLG	3.000	FT
GEAR TILT ANGLE	THFG	-0.0	RAD

GEOMETRY

DESCRIPTION	NAME	VALUE	UNITS
X DIST CG TO ROTOR	XCG	-0.9550	FT

AERO
RIGIDBODY FUSELAGE AERODYNAMIC COEFFICIENTS

FLATPLATE LIFT	CLOF	1.00000	FT**2
LIFT(ALPHA)	CLAF	10.0000	FT2/DEG
LIFT(DALPHA)	CLDAF	0.100000E 00	FT2/DEGS
FLATPLATE DRAG	CDOF	3.00000	FT**2
DRAG(ALPHA)	CDAF	10.0000	FT2/DEG
DRAG(DALPHA)	CDDAF	0.100000E 00	FT2/DEGS
DRAG(ALPHA2)	CDA2F	0.100000E-01	FT2/DEG2
PITCHING MOMENT	CMOF	0.200000	FT**3
PITCH(ALPHA)	CMAF	2.00000	FT3/DEG
PITCH(DALPHA)	CMDAF	0.200000	FT3/DEGS
PITCH(ALPHA**2)	CMA2F	0.100000E-01	FT3/DEG2
X-CENTER OF PRESS.	XAC	0.500000	FT
Z-CENTER OF PRESS.	ZAC	1.00000	FT
X-DOWNWASH FACTOR	DWNSX	0.100000E 00	
Z-DOWNWASH FACTOR	DWNSZ	0.100000E 00	
X-FREE-STREAM-VEL	XFSD	116.300	
Z-FREE-STREAM-VEL	ZFSD	-9.62380	

NORMAL MODE DATA

MODE UH1H NASTRAN MODES WITH PARTIAL HUB MASS SET MH TO 0.0 (01-22-80)

		MODE 1	2	3	4	5	6
FREQUENCY	W1	20.3823	23.9744	43.9107	-0.0	-0.0	-0.0
MASS	M1	26.3679	18.1293	9.2954	-0.0	-0.0	-0.0
DAMPING	Z1	0.0500	0.0500	0.0500	-0.0	-0.0	-0.0
HUB X	DELX1	0.0114	-1.0000	0.0062	-0.0	-0.0	-0.0
HUB Y	DELY1	1.0000	0.0054	-0.0047	-0.0	-0.0	-0.0
HUB Z	DELZ1	-0.0039	0.0722	-0.0933	-0.0	-0.0	-0.0
MAST PITCH	DELT1	-0.0022	0.2171	-0.0039	-0.0	-0.0	-0.0
MAST ROLL	DELP1	0.2332	0.0015	-0.0023	-0.0	-0.0	-0.0
PYLON PITCH	DELPT1	0.0	-0.0	-0.0	-0.0	-0.0	-0.0
PYLON ROLL	DELPP1	0.0	-0.0	-0.0	-0.0	-0.0	-0.0
PYLON Z	DELZT1	0.0	-0.0	-0.0	-0.0	-0.0	-0.0
CG X	DXCG1	0.0	-0.0	-0.0	-0.0	-0.0	-0.0
CG Z	DZCG1	0.0	-0.0	-0.0	-0.0	-0.0	-0.0
PILOT STA X	DXPT1	0.0	-0.0	-0.0	-0.0	-0.0	-0.0
PILOT STA Z	DZPT1	0.0	-0.0	-0.0	-0.0	-0.0	-0.0

LOADS SAMPLE MODULE

STATION NO. 123

MODE	1	2	3	4	5	6
X	1.20000	2.20000	0.32000	0.44000	0.88000	0.01000
Y	1.20000	2.20000	0.32000	0.44000	0.88000	0.01000
Z	1.20000	2.20000	0.32000	0.44000	0.88000	0.01000

APPENDIX B

QUALITATIVE PILOT FLIGHT REPORT ON THE UH-1 NONLINEAR HUB SPRING

GENERAL

During our flight testing, two helicopter configurations were tested: (1) the baseline, standard UH-1H helicopter, and (2) the UH-1H helicopter with hub spring installed:

This qualitative report will addresss only flight profiles that appear to me to be signficantly different from standard configuration UH-1H and UH-1H with hub spring installed.

FLIGHT TEST BASELINE

The flight tests to obtain the baseline data were completed without any major problems; however, the following should be mentioned.

(1) During rearward flight at 30 knots with center of gravity adjusted to 129.5, a 9-degree (80 percent) main rotor flapping was demonstrated. It should be noted that the cyclic was on the aft cyclic stop to achieve the 9-degree flapping.

FLIGHT TEST HUB SPRING INSTALLED

(1) During start up when main rotor speed was below 130 rpm, the helicopter exhibited some tendencies to wallow around. This condition was not serious but different from the standard UH-1H configuration.

(2) An increase of two-per-rev vibration in all flight conditions was noted.

(3) During high Tc turn maneuvers at V_{NE}, collective fixed, when 1.7g's or above was obtained, vertical vibration level increased with noted cyclic feedback. This information was validated by our telemetry which showed high pitch change link loads.

(4) In rearward flight at 30 knots with center of gravity adjusted to 128.88, the maximum main rotor flapping never exceeded 7 degrees. The cyclic at no time made positive aft cyclic stop contact. Telemetry indicated high loads in hub spring parts and main rotor mast during this maneuver.

(5) Low-g investigation did not exhibit any abnormal qualities. Control response appeared the same as baseline flight test. During baseline, .4g was obtained and during flight test with hub spring installed, .25g was obtained.

SUMMARY

The UH-1 nonlinear hub spring appears to do the job for which it was designed. It improves the UH-1 by giving the helicopter a new safety margin to keep it out of mast bumping. I feel that more testing is necessary to determine flight limits and serviceability.

/S/ J. Honaker
Experimental Test Pilot
22 March 1979